



# Development of a customizable digital tool for assessing aircraft passenger discomfort and fatigue

Léo Savonnet

## ► To cite this version:

Léo Savonnet. Development of a customizable digital tool for assessing aircraft passenger discomfort and fatigue. Biomechanics [physics.med-ph]. Université de Lyon, 2018. English. NNT : 2018LYSE1032 . tel-01838797

HAL Id: tel-01838797

<https://theses.hal.science/tel-01838797>

Submitted on 13 Jul 2018

**HAL** is a multi-disciplinary open access archive for the deposit and dissemination of scientific research documents, whether they are published or not. The documents may come from teaching and research institutions in France or abroad, or from public or private research centers.

L'archive ouverte pluridisciplinaire **HAL**, est destinée au dépôt et à la diffusion de documents scientifiques de niveau recherche, publiés ou non, émanant des établissements d'enseignement et de recherche français ou étrangers, des laboratoires publics ou privés.

N°d'ordre NNT :  
2018LYSE1032



**THESE de DOCTORAT DE L'UNIVERSITE DE LYON**  
opérée au sein de  
**l'Université Claude Bernard Lyon 1**

**Ecole Doctorale** N° accréditation  
**MEGA**

**Spécialité de doctorat :**  
**Discipline** : Mécanique

Soutenue publiquement le 09/03/2018, par :  
**Léo Savonnet**

---

**Développement d'un outil numérique personnalisable pour l'évaluation de l'inconfort et de la fatigue du passager d'avion**

---

Devant le jury composé de :

M. Aissaoui Rachid	Professeur, ETS de Montreal	Rapporteur
M. Payan Yohan	Directeur de recherche CNRS, (TIMC-IMAG)	Rapporteur
Mme. Ronel Sylvie	Professeur des Universités, UCBL- LBMC	Examinateuse
M. Obadia Jean Marc	Ingénieur, ZSFR	Examinateur
M. Wang Xuguang	Directeur de Recherche, IFSTTAR - LBMC	Directeur de thèse
Mme. Duprey Sonia	Maitre de conférence UCBL- LBMC	Co-directrice de
thèse		
M. Roy Philippe	Directeur R&D, ZSFR	Invité

N°d'ordre NNT :  
2018LYSE1032



**PhD of UNIVERSITE DE LYON  
at  
Claude Bernard University Lyon 1**

**Doctoral School  
MEGA**

**Discipline:** Mechanics

Publicly defended on the 09/03/2018, by:  
**Léo Savonnet**

---

**Development of a scalable digital tool  
for the discomfort and fatigue  
assessment of the aircraft passenger**

---

In front of the following jury:

M. Aissaoui Rachid	Professeur, ETS de Montreal	Rapporteur
M. Payan Yohan	Directeur de recherche CNRS, (TIMC-IMAG)	Rapporteur
Mme. Ronel Sylvie	Professeur des Universités, UCBL- LBMC	Examinateuse
M. Obadia Jean Marc	Ingénieur, ZSFR	Examinateur
M. Wang Xuguang	Directeur de Recherche, IFSTTAR - LBMC	Directeur de thèse
Mme. Duprey Sonia	Maitre de conférence UCBL- LBMC	Co-directrice de
thèse		
M. Roy Philippe	Directeur R&D, ZSFR	Invité

## UNIVERSITE CLAUDE BERNARD - LYON 1

### **Président de l'Université**

Président du Conseil Académique  
Vice-président du Conseil d'Administration  
Vice-président du Conseil Formation et Vie Universitaire  
Vice-président de la Commission Recherche  
Directrice Générale des Services

### **M. le Professeur Frédéric FLEURY**

M. le Professeur Hamda BEN HADID  
M. le Professeur Didier REVEL  
M. le Professeur Philippe CHEVALIER  
M. Fabrice VALLÉE  
Mme Dominique MARCHAND

### ***COMPOSANTES SANTE***

Faculté de Médecine Lyon Est – Claude Bernard  
Faculté de Médecine et de Maëutique Lyon Sud – Charles Mérieux  
  
Faculté d'Odontologie  
Institut des Sciences Pharmaceutiques et Biologiques  
Institut des Sciences et Techniques de la Réadaptation  
Département de formation et Centre de Recherche en Biologie Humaine

Directeur : M. le Professeur G.RODE  
Directeur : Mme la Professeure C. BURILLON  
  
Directeur : M. le Professeur D. BOURGEOIS  
Directeur : Mme la Professeure C. VINCIGUERRA  
Directeur : M. X. PERROT  
Directeur : Mme la Professeure A-M. SCHOTT

### ***COMPOSANTES ET DEPARTEMENTS DE SCIENCES ET TECHNOLOGIE***

Faculté des Sciences et Technologies  
Département Biologie  
Département Chimie Biochimie  
Département GEP  
Département Informatique  
Département Mathématiques  
Département Mécanique  
Département Physique  
  
UFR Sciences et Techniques des Activités Physiques et Sportives  
  
Observatoire des Sciences de l'Univers de Lyon  
Polytech Lyon  
Ecole Supérieure de Chimie Physique Electronique  
Institut Universitaire de Technologie de Lyon 1  
Ecole Supérieure du Professorat et de l'Education  
Institut de Science Financière et d'Assurances

Directeur : M. F. DE MARCHI  
Directeur : M. le Professeur F. THEVENARD  
Directeur : Mme C. FELIX  
Directeur : M. Hassan HAMMOURI  
Directeur : M. le Professeur S. AKKOUCH  
Directeur : M. le Professeur G. TOMANOV  
Directeur : M. le Professeur H. BEN HADID  
Directeur : M. le Professeur J-C PLENET  
  
Directeur : M. Y.VANPOULLE  
Directeur : M. B. GUIDERDONI  
Directeur : M. le Professeur E.PERRIN  
Directeur : M. G. PIGNAULT  
Directeur : M. le Professeur C. VITON  
Directeur : M. le Professeur A. MOUGNIOTTE  
Directeur : M. N. LEBOISNE

## Remerciements

Je tiens tout d'abord à remercier mon équipe d'encadrement. Merci A Xuguang pour m'avoir guidé, orienté tout au long de cette thèse. Merci pour toutes les choses que tu m'as enseigné, en particulier cette rigueur scientifique qui te caractérise et l'éternelle remise en question qui font les qualités d'un bon scientifique. J'ai beaucoup apprécié les longues discussions techniques que l'on a pu avoir durant ces 3 ans, cela m'a beaucoup apporté. Un grand merci à Sonia pour m'avoir encadré avec une grande pédagogie durant cette thèse. Ce fut vraiment un plaisir de travailler avec toi, tu es toujours de très bon conseils et as toujours les bons mots pour que l'on se sente soutenu. Je garderai de très bons souvenirs de ces moments partagés, en particulier les différents voyages que nous avons pu partager grâce à cette thèse. Je remercie également Jean Marc qui m'a permis de garder un œil sur les besoins industriels et ainsi de me faire redescendre sur terre un certain nombre de fois. J'ai beaucoup apprécié ton ouverture d'esprit et ton enthousiasme pour toute nouvelle idée. Merci également à Philippe Roy pour le suivi de cette thèse et la confiance qu'il m'a accordé dans ce travail de recherche.

Je souhaite également remercier les membres du jury, Yohan Payan, Rachid Aissaoui et Sylvie Ronel. Merci d'avoir accepté d'évaluer ce travail de thèse.

Un grand merci au directeur du laboratoire, David Mitton, pour ton accueil et pour ton accompagnement au cours de ces 3 années. Merci pour ta gentillesse et ton sens de la gestion des relations humaines.

Un grand merci également à Michelle Cardoso avec qui j'ai partagé beaucoup de temps durant ma deuxième année. Ces moments étaient remplis de gaieté grâce à ta joie de vivre et ton extraordinaire énergie. Ton sourire rayonnant et ton rire éclatant ont permis de faire passer ces longues heures d'expérimentations pour de très bons moments tout en gardant un très grand sérieux dans le travail.

Je remercie également Richard qui a beaucoup fait pour la réalisation des expérimentations. Beaucoup de choses n'auraient pu être possibles sans ton incroyable ingéniosité et ton efficacité. De plus tu as toujours su être à l'écoute et garder un sourire communiquant même quand on te demandait l'impossible. Merci également à Leila qui nous a accompagnés durant les expérimentations et qui est d'une gentillesse incroyable et avec qui la compagnie est très agréable. Merci à toute l'équipe support, Yves, Stéphane, Jean-Luc pour tous les conseils et l'aide qu'ils ont pu m'apporter.

Un merci tout particulier à mes trois compagnons de bureau avec qui j'ai partagé ces heures de d'énervernement, de joie, de désespoir, de satisfaction... Tout d'abord Junfeng qui m'a beaucoup appris sur ce qu'étais être doctorant, tu es un peu mon grand frère de doctorat. Tu as toujours été de très bon conseil. J'ai partagé pleins de très bons moments avec toi et j'espère que nous garderons contacts pour longtemps, et qu'un jour je te battrais au tennis. Ensuite Agathe qui fut un peu aussi comme ma grande sœur de doctorat. Merci de m'avoir montré l'exemple, je resterai toujours impressionné par ta rigueur dans le travail, rigueur que j'ai essayé d'imiter (je suis loin d'avoir réussi). Tu as également été de bonne compagnie et tu as toujours su me rassurer sur les quelques doutes que j'ai pu avoir. Enfin Julia avec qui j'ai partagé la dernière moitié de ma thèse. Cela a été un grand plaisir de partager ce bureau avec toi, comme tu l'as dit toi-même, tu es un peu ma maman de doctorat. Entre les thés anglais, le chocolat allemand et les gâteaux de tous les pays, tu m'as beaucoup trop gâté. Heureusement que tu

m'as emmené faire du sport pour me faire perdre les kilos que tu venais de me faire prendre. Et puis grâce à toi, j'ai pu me sentir fort à la course à pied, un peu moins au tennis. J'espère que nous garderons contact pour partager encore pleins de bons moments.

Merci à tous les autres doctorants avec qui j'ai partagé du temps au labo. Merci à Romain de m'avoir poussé à continuer l'escalade et de m'avoir permis d'améliorer mon niveau en me poussant à vouloir t'égaler. Je peux faire le même compliment à Thomas, sauf que je suis moins sûr d'atteindre son niveau un jour. Merci à mes deux comparses, Remy et Anicet, avec qui j'ai pu me vider la tête et partager les vrais plaisirs dignes d'un étudiant. Merci à Mehdi pour tous les voyages et découvertes que nous avons effectués ensemble. Merci pour tes conseils et ta motivation qui m'ont poussé à avancer. Je te souhaite tout le meilleur pour cette fin de thèse. Et merci à tous les chercheurs du labo pour les connaissances et expertises qu'ils ont pu m'apporter.

Merci aux stagiaires, Jing, Aurore et tout particulièrement Amal, avec qui travailler fût un réel plaisir. Vous m'avez permis de comprendre le sens du mot pédagogie.

Le plus grand merci à ma Solveig qui a dû supporter mes doutes et mes inquiétudes durant ces durs derniers mois. Merci de m'avoir transmis ta force. Merci du fond du cœur pour ton soutien et pour tout le bonheur que tu m'apportes.

Merci à tous mes potes qui m'ont encouragés au cours de ses derniers mois, Octave, Bastien, Fleur, Romain, Donald, Geraud, Bertrand, Dono, Florian, Guillaume, Adeline, Aurélien, Petrus, Torto, Hugo, Anna et en particulier Jean-Noé et Rafaële qui m'ont soutenus jusqu'aux dernières minutes.

Enfin merci à ma famille, mes parents et ma sœur adoré, sans qui rien de tout cela n'aurait été possible ! Merci pour tout !

# Table of contents

Remerciements.....	4
Table of contents .....	6
Abstract .....	10
Résumé .....	11
Introduction: Context and objectives .....	12
1.    Context: sitting discomfort in aircraft seats.....	12
2.    Comfort/Discomfort .....	12
3.    Scope of the thesis .....	14
4.    Objectives.....	15
Chapter 1: State of the art of discomfort factors and models dedicated to discomfort assessment	16
1.    Biomechanical sitting discomfort factors .....	16
1.1    Soft tissue compression.....	16
1.2    Muscle activity .....	18
1.3    Spinal disc compression .....	19
1.4    Conclusion.....	20
2.    State of the art of existing models dedicated to simulate passenger-seat interactions .....	20
2.1    FE models.....	21
2.2    MB models .....	31
3.    Conclusion.....	34
Chap 2: Finite element model development and sensitivity analysis.....	36
1.    Finite element model development .....	36
1.1 MRI .....	37
1.2 Segmentation.....	38
1.3 Mesh.....	39
2.    Sensitivity analysis .....	41
Geometry.....	41
1.    Mesh composition .....	41
2.    Muscles – adipose tissues proportions .....	44
2.2 Material properties .....	46

3. Conclusion.....	52
Chapter 3: A parametric geometric model of the buttocks-thighs complex based on 3d scan data: development and validation.....	53
Introduction.....	53
1. Part 1: A parametric skin shape model of the buttocks-thighs complex based on 3d scan data	
55	
1.1 Method.....	55
1.2 Results .....	61
1.3 Discussion .....	64
2. Part 2: Prediction of bones surface from bones landmarks .....	66
2.1 Method.....	66
2.2 Results .....	66
2.3 Discussion .....	68
3. Part 3: Parametric FE model and its validation .....	70
3.1 Introduction .....	70
3.2 Personalized finite element model creation.....	70
3.3 Comparison of the interface pressure predicted by the parametric FE model and experimental data .....	71
3.4 Results .....	75
3.5 Discussion .....	78
4. General conclusion.....	79
Chap 4: Coupling rigid multi-body and finite element models.....	80
1. Introduction .....	80
2. Coupling Method.....	80
2.1 MB Model personalization.....	80
2.2 MB model positioning.....	82
2.3 Contact and muscles forces estimation.....	82
2.4 Coupling the MB and FE modeling approaches.....	83
3 Validation.....	84
3.1 Simulations conditions .....	85
3.2 Coupling method convergence .....	86
3.3 Comparison between simulation cases and experimentation .....	87
4. Discussion / Conclusion.....	91
Chapter 5: Comparison of simulated tissue deformations with experimental MRI data .....	93
1. Introduction .....	93
2. Data collection on MRI .....	94

2.1	Unloaded configuration.....	94
2.2	Reference (rigid) configuration .....	95
2.3	Foam configuration .....	95
2.4	Shear configuration .....	96
3.	Finite element model development .....	97
3.1	Geometry .....	97
3.2	Material .....	98
4.	Simulation of experiments.....	98
4.1	Model positioning.....	98
4.2	Loading conditions .....	100
5.	Responses definition.....	102
5.1	Landmarks displacement.....	102
5.2	Hausdorff distance.....	103
6	Results .....	103
6.1	Tissue deformation .....	103
6.2	Simulation comparison.....	105
5.	Discussion/Conclusion .....	109
	Conclusion .....	111
6.	Main results .....	111
7.	Limitations and perspectives .....	112
	Bibliography.....	114
	Appendices.....	124
1.	Cabin environment discomfort factors .....	124
1.1	Cabin Pressure.....	125
1.2	Motion and vibrations .....	125
1.3	Cabin air quality .....	126
1.4	Noise.....	126
1.5	Temperature.....	126
2.	Regressions between distances from landmarks to hip joint (HJC) and lumbosacral joint (LSJC) and pelvis dimensions (pelvis width PW, pelvis depth PD, pelvis height PH, (see Figure 102)	127
3.	Regressions between PCs and predictors .....	128
4.	Local predictors .....	128
5.	Profile pressure measured (blue) and simulated (red) .....	129
6.	Comparison of measured (left) and simulated (right) pressure map .....	131
7.	Comparison between elastic linear and hyperelastic law .....	132

Comparison between bones scaled by kriging or by PCA model .....	133
9. Muscular activity and disc load estimation.....	133
8.    Muscular activity.....	134
9.    Disk load.....	135
French Abstract.....	137
1.    Intro .....	137
1.1    Contexte.....	137
1.2    Confort/inconfort.....	137
1.3    Objectifs .....	138
2.    Chapitre 1 : Etat de l'art des facteurs d'inconfort et des modèles dédiés à l'évaluation de l'inconfort.....	138
2.1    Facteurs biomécanique menant à l'inconfort.....	139
2.2    Etat de l'art des modèles.....	139
3.    Chapitre 2 : Développement du modèle FE et analyse de sensibilité.....	141
3.1    Modèle développement .....	141
3.2    Analyse de sensibilité .....	142
4.    Chapitre 3 : Un modèle paramétrique du complexe fessiers-cuisse basé sur des données scan 3d : développement et validation.....	143
4.1    Un modèle paramétrique de l'enveloppe.....	143
4.2    Prédiction de la surface des os.....	145
4.3    Modèle EF paramétrique .....	145
5.    Chapitre 4 :Couplage modèle multi-corps et modèle EF .....	146
5.1    Méthode de couplage.....	147
5.2    Validation .....	148
6.    Chapitre 5 : Comparaison des déformations internes simulées avec des données IRM.....	149
6.1    Collecte de données IRM .....	150
6.2    Développement du modèle EF .....	150
6.3    Simulations.....	150
6.4    Résultats .....	151
7.    Conclusion.....	155
7.1    Principaux résultats .....	155

# **Abstract**

## **Development of a scalable digital tool for the discomfort and fatigue assessment of the aircraft passenger**

**Keywords:** Discomfort, seat, finite element model, multibody model, coupling, soft tissue, pelvis, femur, anthropometry, deformations, MRI

The sitting position could be a source of discomfort, in particular in a long haul flight. This discomfort comes partially from mechanical factors linked to the interaction between the passenger and the seat. Having biomechanical models which can simulate this interaction and estimate these factors would allow optimizing the seat design in its conception phase to improve its ergonomic quality and reduce the passenger discomfort. The objective of this thesis is to develop a digital tool allowing estimating the mechanical factors leading to discomfort and fatigue of the passenger. This tool assembles two kinds of models, a finite element model allowing to simulate the sub dermal tissue deformation and a multibody model allowing to estimate the muscular and joint forces. A coupling method of the two models has been developed allowing simulating a position from where all discomfort factors are estimated. A finite element model has been developed after having done a sensitivity analysis on the different model parameters (mesh, geometry, material law). A multibody model developed by Anybody was used to be associated with this finite element model. This iterative coupling method between the two models allowed realizing an adjustment of the initial posture in the seat. To simulate the whole population and its large morphological diversity, a parametric shape model was developed from 3d experimental data, this shape model allowing to obtain a finite element model representing any kind of anthropometry. Different validation processes have been realized with experimental data and subject-specific model. The simulated external pressures were compared to experimental data. An experimental study done in an open MRI allowed to measure the different subcutaneous tissue to compare it to the simulated data. A digital tool is consequently now available to simulate the impact of the seat on the passenger, however future studies should focus on the one hand on the models studying the internal morphological variations between people, the person positioning in the seat, the time influence on the soft tissue and on the other hand on the discomfort and fatigue criteria.

# Résumé

## Développement d'un outil numérique personnalisable pour l'évaluation de l'inconfort et de la fatigue du passager d'avion

Mots clefs : Inconfort, siège, modèle éléments finis, modèle corps rigide, couplage, tissus mous, bassin, fémur, anthropométrie, déformations, IRM

La position assise peut être source d'inconfort, particulièrement en avion lors des vols long-courriers. Cet inconfort provient en partie de facteurs mécaniques liés à l'interaction entre le siège et le passager. Disposer de modèles biomécaniques pouvant simuler cette interaction et estimer ces facteurs permettrait d'optimiser le design du siège d'avion lors de sa phase de conception afin d'améliorer son ergonomie et réduire l'inconfort du passager. L'objectif de cette thèse est de développer un outil numérique permettant d'estimer les facteurs mécaniques menant à l'inconfort et la fatigue des passagers. Cet outil combine deux différents types de modèles. Un modèle éléments finis permettant de simuler la déformation des tissus sous-cutanés et un modèle corps rigides permettant d'estimer les efforts musculaires et articulaires. Une méthode de couplage des deux modèles a été développée permettant ainsi de simuler une position à partir de laquelle l'ensemble des facteurs d'inconfort sont estimés. Un modèle éléments finis a été développé après avoir fait une étude de sensibilité sur les différents paramètres de modélisation (maillage, géométrie, lois matériau). Un modèle corps rigides développé par Anybody a été utilisé pour être couplé avec ce modèle éléments finis. Cette méthode de couplage itératif entre les deux modèles a permis de réaliser un ajustement de la posture initiale dans le siège. Afin de simuler l'ensemble de la population et sa grande diversité morphologique, un modèle surfacique paramétrique a été développé à partir de données 3d expérimentales, ce modèle surfacique permettant ainsi d'obtenir un modèle éléments finis représentant tout type d'anthropométrie. Différents processus de validation ont été effectués à l'aide de données et d'un modèle « sujet-spécifique ». Les données de pression externe simulées ont été comparées à des données expérimentales. Une étude expérimentale sous IRM ouvert a permis de mesurer les déformations des différents tissus sous-cutanés afin de les comparer aux données simulées. Un outil numérique est donc aujourd'hui disponible pour simuler l'impact du siège sur les passagers, cependant de futures études devraient se concentrer d'une part sur les modèles en étudiant la variation morphologique interne inter individus, le positionnement dans le siège ainsi que l'influence du temps sur les tissus mous et d'autres part sur la définition de critères d'inconfort et de fatigue (inconfort considéré sur des temps longs représentatifs d'un vol long-courrier).

# **Introduction: Context and objectives**

## **1. Context: sitting discomfort in aircraft seats**

In modern societies, people spend a large amount of time sitting. For instance, it was reported that North Americans spend on average 10 hours a day sitting (Holmes et al. 2015): in a chair, in a car or in a plane, for leisure or occupational activities or due to mobility impairments and handicaps. However, inappropriate seating could lead to musculoskeletal problems (Vink & Hallbeck 2012a). It could be a risk factor for low back pain (Lis et al. 2006) and could even lead to pressure sores in the case of persons confined to a bed or wheelchair (Olesen et al. 2010).

In an airplane, reducing seating discomfort is a major concern for airline companies because it is a way to gain the loyalty of customers. This concern is all the more important if the duration of the flight is long. Many progresses in this domain have been achieved over the last decades. A study in 2007 by (Blok M et al. 2007) have shown that people perceive the new aircrafts (A330 and Boeing 737 Next Generation) more comfortable than the previous ones (A300, A310, Boeing 737-300 and 737-400). However, further improvements are expected especially in the economy class cabin. A recent survey performed by Air France (Zodiac company internal enquiry) has shown that people in business class give an averaged comfort rating of 7/10 whereas people in economy class gives an average of 5/10.

This work is performed in collaboration with Zodiac Seats France, a renowned aircraft seat manufacturer. The company is interested in seat improvement to reduce discomfort and improve ergonomic quality. They have two main objectives, producing a seat which minimizes the feeling of discomfort and developing a lighter weight seat. In order to this, they need tools which assess the impact of the seat on passenger discomfort. By evaluating the seat discomfort impact, its design can be modified until the seat gives few or no discomfort to the passenger. Consequently, this PhD project will focus on the physical interactions between the passenger and the seat, and on their biomechanical interactions.

## **2. Comfort/Discomfort**

First of all, it is important to distinguish comfort and discomfort: while, in the past, comfort and discomfort were considered as two levels on the same scale (Richards et al. 1980). It is now well accepted that they are two separate entities (Zhang et al. 1996; Helander et al. 1997). According to Zhang et al. (1996), the absence of discomfort does not necessarily mean comfort. Discomfort is related to biomechanical factors whereas comfort is associated to well-being and aesthetic factors. People rate a situation as comfortable when they get something more than expected like a luxury, safety, or refreshment.

**Table 1: Factors for comfort or discomfort (Zhang et al., 1996)**

Discomfort related factors:	Comfort related factors:
Fatigue	Luxury
Pain	Safe
Posture	Refreshment
Stiffness	Well-being
Heavy legs	Relaxation

So the following definitions are used by Vink & Hallbeck (2012b): “comfort is seen as a pleasant state or a relaxed feeling of a human being in reaction to its environment” and “discomfort is seen as an unpleasant state of the human body in reaction to its physical environment”.

Several conceptual models of comfort and discomfort have been proposed. In the model proposed by De Looze et al. (2003), both comfort and discomfort result from the interaction between person, product and environment. Discomfort is related to physical interaction while comfort is linked to human emotion and expectation.

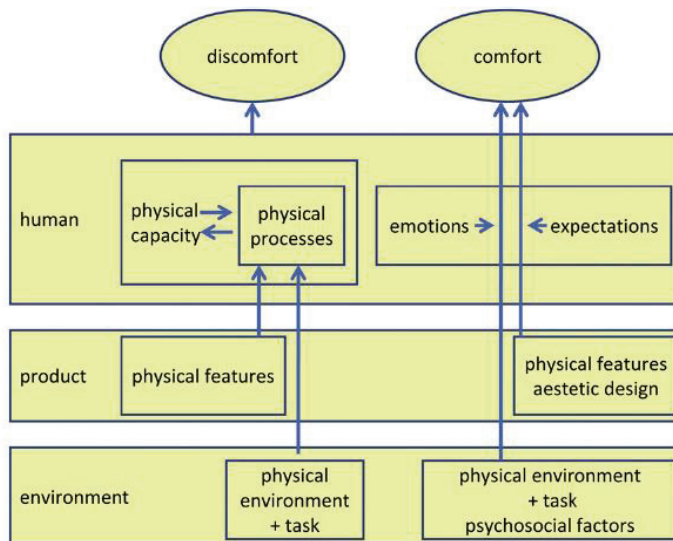


**Figure 1: Discomfort/comfort model from De Looze et al. (2003)**

The model by Moes N (2005) take only the discomfort into account. The model is a succession of 5 chronological phases leading to discomfort where each phase depends on the person without considering human expectation.

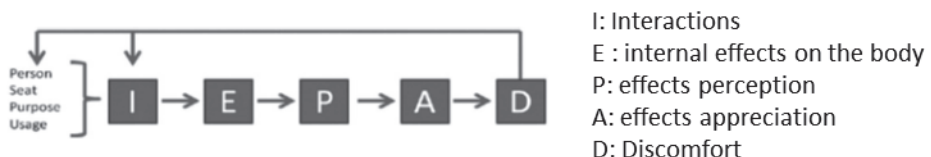


**Figure 2: Discomfort model from Moes et al. (2005)**

Vink & Hallbeck (2012) proposed a new model combining the two previous ones. The new one is linear like Moes’ model but contains the human expectation present in the De Looze’s model. This model gives the possibility to explain the feeling of comfort, discomfort or nothing. It shows the

distinction between objective parts (I: Interaction, H: Human body effects) and subjective parts (after H). Furthermore, between the levels of perceived comfort (C : comfort, N : nothing or D : discomfort) and the physical effects (H), appears the expectation. This factor depends on the habits of the person, which level of comfort he/she is used to (this point highlights the discrepancies between target groups such as business or economy class passengers) and his/her psychological state at the moment of the flight. According to Vink and Hallbeck, a person's expectation affects not only comfort but also discomfort, though comfort is more related to initial expectation.

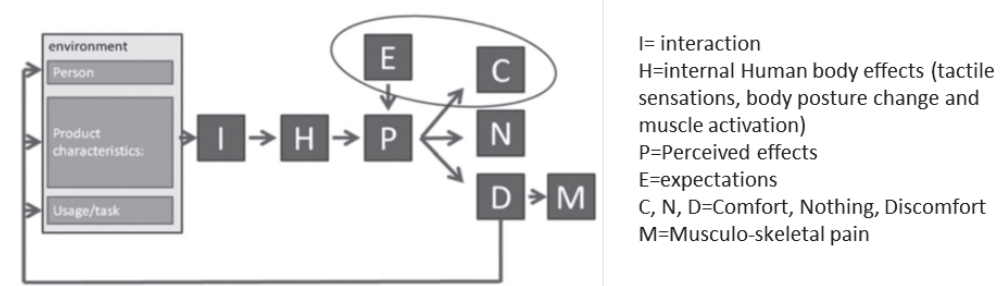


Figure 3: Discomfort/comfort model from Vink et al. (2012)

In this thesis, we will focus on the discomfort generated by the physical interactions between the body and the environment.

Fatigue is, as defined in the Oxford dictionary (Stevenson 2010): an “extreme tiredness resulting from mental or physical exertion” or “a reduction in the efficiency of a muscle or organ after prolonged activity”. The fatigue can be physical or mental and is due to a situation maintained during a certain period of time. Indeed, fatigue appears with time. It is generally assumed that an initially uncomfortable seating will lead to a state with more fatigue along the time.

### 3. Scope of the thesis

As will be explained later, two kinds of biomechanical models can estimate the mechanical factors of discomfort: Finite Element (FE) models and musculoskeletal (MSK) models. These models estimate complementary biomechanical factors (Figure 4). The deformable FE model is appropriate for estimating contact pressure distribution and soft tissue compression, whereas the MSK model is more suitable to estimate muscle forces and internal joint loads such as inter-disc pressure. Consequently, these two modeling approaches will be associated in the present work.

What causes discomfort and fatigue ?

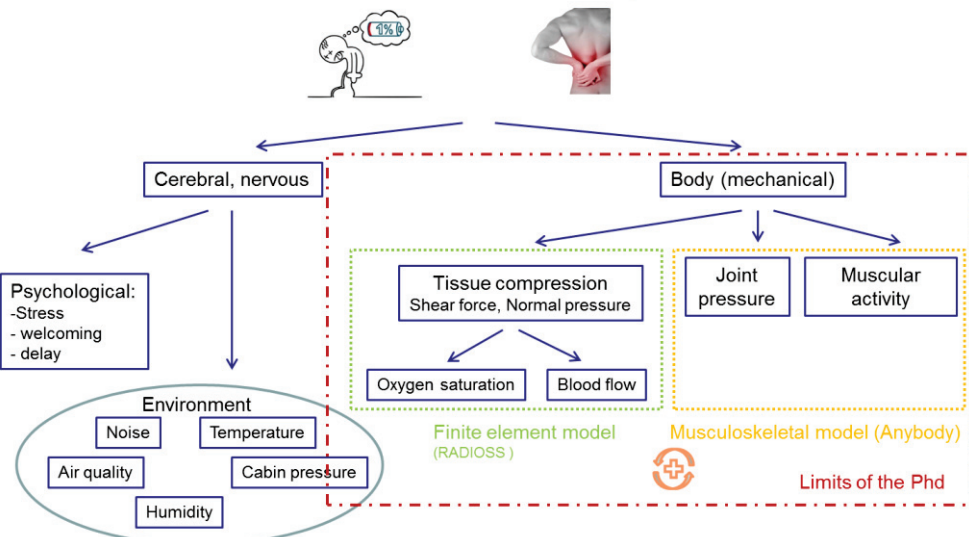


Figure 4: Scope of the thesis

## 4. Objectives

The main objective of this thesis is to develop a computational tool to assess the sitting discomfort of an aircraft seat during its design phase. This tool, based on biomechanical human body models will allow us to estimate the discomfort impact of the seat on the passenger by predicting discomfort factors. Furthermore, this tool will enable us to estimate the impact of the seat on the passenger by using existing discomfort criteria.

To achieve this goal, the following subsidiary objectives were formulated:

- to establish a state of art of the factors of sitting discomfort and a state of art of the existing models developed for the assessment of this discomfort (Chapter 1),
- to develop a buttock-thigh FE model dedicated to sitting simulations (Chapter 2),
- to develop a parametric model enabling the representation of various morphologies and validate it by comparing the outputs with experimental data on several subjects (Chapter 3),
- to develop a methodology coupling both the FE and MSK modeling approaches (Chapter 4),
- To study the soft tissue deformations estimated with the buttock-thigh FE model by comparison with MRI data (Chapter 5).

# **Chapter 1: State of the art of discomfort factors and models dedicated to discomfort assessment**

To develop a tool assessing the ergonomic quality of a seat, it is first necessary to know what are the factors implied in the mechanisms leading to discomfort. As mentioned earlier, we will solely focus on sitting biomechanical discomfort factors. They will be described in a first section (cabin environment discomfort factors were detailed in Appendix 1 though). The second section of this chapter will consist of a state of the art of all the existing models dedicated to the assessment of the discomfort induced by a seat by simulating the person-seat interaction.

## **1. Biomechanical sitting discomfort factors**

### **1.1 Soft tissue compression**

The biomechanical impact of sitting has been studied for years and different mechanical factors of discomfort are widely detailed in the literature. The source of discomfort the most cited in the literature is the compression of the buttock-thigh soft tissues (De Looze et al. 2003; Mergl et al. 2005; Kamijo et al. 1982; Kolich 2004; Oudenhuijzen et al. 2003). Indeed, during sitting, the human soft tissues are compressed at specific locations (e.g. the ischial tuberosities or the sacrum). This compression leads to large deformation of the different layers of soft tissues, particularly under the two prominence of the pelvis called ischial tuberosities (Al-Dirini et al. 2015; Linder-Ganz et al. 2007a), thus limiting the blood circulation and reducing the quantity of oxygen in the tissue (Olesen et al. 2010). These physiological phenomena would then induce discomfort to the sitting person (Sember J 1994; Reed et al. 1994; Al-Dirini et al. 2015b).

These compressions can be studied easily by measuring the pressure at the interface between the seat pan and the body. A lot of studies conducted experimental work to find correlation between seat contact pressure and discomfort. De Looze et al. (2003) wrote a literature review on experimental studies correlating discomfort and objective measurements (pressure map, body movements, muscle activation, foot/leg volume change...). They showed that pressure distribution was the objective measure that best correlates with discomfort ratings. In their literature review, three of seven studies on pressure measurement at the seat interface (Yun et al. 1992; Thakurta et al. 1995; Vergara M & Page A 2000), reported significant correlations between pressure and discomfort, and two others (Kamijo et al. 1982; Tewari & Prasad 2000) reported link between pressure and discomfort. Gossens (Goossens 1998) found a strong correlation ( $r>0.80$ ) between the peak pressure at the interface on the buttocks and the perceived discomfort. As reported in another literature review (Mastrigt et al. 2017), several studies reported significant correlations between discomfort and percentage of the load, maximum pressure, mean pressure (Porter et al. 2003; Mergl et al. 2005; Kyung & Nussbaum 2008a),

or the contact area (Carcone & Keir 2007; Kyung & Nussbaum 2008b; Liu & Wang 2011) or the center of pressure at the seat interface(Søndergaard et al. 2010).

If all these studies found a correlation between pressure at the seat interface and discomfort, very few proposed criteria for assessing the discomfort. A few studies defined a maximum external pressure value as discomfort threshold based on physiological observations. Ciaccia et al. (1994) and Conine et al. (1994) suggested thresholds of respectively 4.25 kPa and 7.8 kPa. These values correspond to the limits above which capillaries could be obstructed and a deprivation of oxygen in the tissues could result. These limits are a bit lower than the one found previously by Kosiak (Kosiak 1961): he found that a constant pressure of 4.7 kPa produced no ischemic changes for up to 4h, whereas a constant pressure of 9.3 kPa for 2h produced irreversible cellular changes. Sember J (1994) showed from in vivo experimentations that a pain threshold is reached after 30 minutes with a pressure of 55 kPa, whereas a discomfort feeling appears after 15 minutes with a pressure of 6.9 kPa. He also explained that capillaries obstruction can lead to skin cell death (necrosis) above 6.89 kPa. Jackson et al. (2009) found that the maximum pressure under which no discomfort appears without moving was 8.8 kPa. The location of the pressure is of course important, because of the capacity of the tissue to support the load. For example, Kamijo et al. (1982) found different pressure thresholds depending on the location (<5.8 kPa under the ischia; 2.9 kPa elsewhere under the thighs). It is in accordance with Chen, J. et al. (2007) who said that the pressure should be highest underneath the central sitting bones i.e. ischial tuberosity and should dissipate toward the thighs and sides. Most of the studies preferred considering the whole pressure distribution on the seat pan as discomfort criterion (Kamijo et al. 1982; Kolich 2004; Oudenhuijzen et al. 2003). However some studies divided the seat pan into different parts like the front high, the middle thigh and buttocks. Thresholds in terms of load for different parts of the thighs and buttocks were experimentally defined by Hartung (2006) and Mergl (2005) based on in vivo experimentations on 20 participants. For example, according to Mergl, the buttocks should bear between 50% and 65% of the total load, the middle of the thigh should support less than 14% of the total load and the front of the thigh less than 6% (Figure 5). Mergl also studied the pressure gradient and found that, it should not be up to 5.6 kPa/mm under the buttocks, 1.6 kPa/mm under the thighs and 0.5 kPa in front of the thighs. In terms of maximal pressure at the seat interface, the limit of acceptance was 20 kPa under the buttocks and 7 kPa under the thighs.

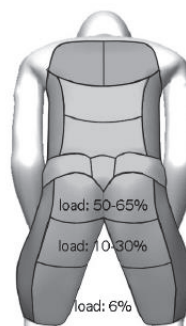


**Figure 5: Ideal pressure distribution (Hartung 2006)**

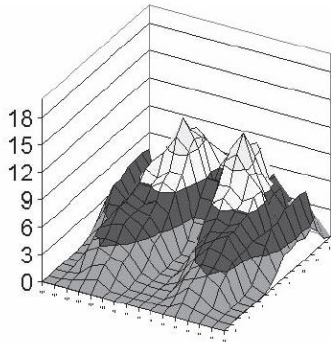


**Figure 6: Ideal pressure distribution at the seat-person interface (Mergl 2005)**

Although the seat pressure distribution has been widely used due to the fact that it can easily be measured, it cannot reveal what are the sub-dermal tissue conditions. It has been shown that the pressure in the sub-dermal tissue can be much higher than the one at the interface (Oomens et al. 2003). Furthermore, the location of the maximal pressure differs a lot between the interface and the sub-dermal tissues (Silber & Then 2009). This can be explained by the fact that the internal strains are also influenced by the interface shear stresses (Goossens et al. 2000). Goossens et al. (2000), Ming Zhang and Roberts (1993) explained that shear forces have a role as important as normal forces in the genesis of internal pressure.

Indeed, shear forces were shown to limit the blood flow and lead to a lack of oxygen in the tissue (Reichel 1958; Chow & Odell 1978; Krouskop et al. 1978; Bennett et al. 1979; Scales 1982; Bader & Hawken 1990; Goossens et al. 1994a; Goossens 2009). Ming Zhang & Roberts (1993) and Goossens et al. (1994) showed that blood flow decreases linearly with the augmentation of shear forces. Goossens et al. (1994) also measured the oxygen tension of the skin and they showed that shear forces of 3.1 kPa could reduce it by half. Because of the difficulty to measure these forces, a discomfort threshold has not been determined. However, a minimization of these forces can be searched (Rasmussen et al. 2007).

## 1.2 Muscle activity

A constant muscular activity, even low but maintained during a long time, can lead to muscular fatigue and discomfort. Several studies (Bendix et al. 1996; Ferrari et al. 1999; Lueder 2004) have shown that moving during long-term static tasks and exercising higher muscular activities to allow blood circulation might reduce discomfort. However, most of the experimental studies considered muscular activity as a factor of discomfort (Andersson et al. 1977; Hosea 1986; Bush et al. 1995; De Carvalho & Callaghan 2011a). A certain number of studies found a relation between muscle activation and discomfort feeling or perception of fatigue. Michida et al. (2001) measured level of muscle activity of different muscle groups and correlated it with the subjective perception of fatigue. Neck, shoulder, abdomen, thigh, leg and spine muscle groups were found to be the key contributors to long-distance driving fatigue perception. Lee et al. (1988) found a strong correlation between the increase of muscle activation on the shoulders and back and the increase of discomfort when using a microscope. Later, Lee et al. (1993) found that a seat was rated comfortable when the lower neck and the medial hamstrings muscle activations were the lowest. On the contrary, some studies found that a higher muscle activity in the shoulder (Graf et al. 1993) or even in the whole body (Udo et al. 1999)

corresponds with less discomfort in the back. There isn't any consensus on the relationship between the muscular activity and discomfort feeling. However, numerical studies considered that muscular activity had to be minimized (Rasmussen et al. 2007; Grujicic et al. 2010; De Carvalho & Callaghan 2011).

### 1.3 Spinal disc compression

While the disc pressure varies depending on the studies, most experiments showed that the intra disc pressure is higher when sitting than when standing (Claus et al. 2008). Nachemson & Elfström (1970) and (Andersson et al. 1977) showed with experimental measurement that the spinal disk compression during the sitting posture is much higher than during the standing (30% lower) or lying postures (50% lower). Furthermore, the load on the spine also vary with the sitting posture : it can vary from one to three times the value between relaxed sitting and flexing forward sitting (Wilke et al. 2001).

This disc compression leads to a lack of nucleus irrigation and may cause discomfort and what is called low back pain (Andersson & Ortegren 1974). Bendix (1987) explains that an excessive lumbar curvature can lead to increase compression in the lumbar vertebrae which contribute to pain. He also explains (Bendix T 1994) that the load, which can be high when sitting, combined with the duration of the maintained position increase the risk of low back pain injury.

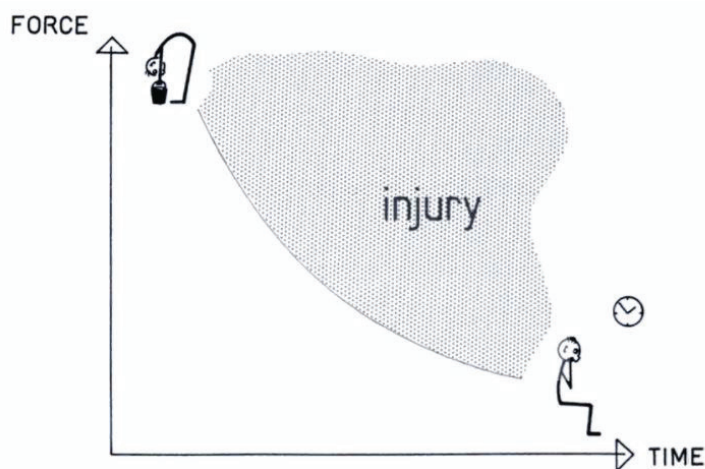


Figure 7: Relation between discs load, time and injury (Bendix 1994)

Franz (2010) carried out *in vivo* measurements of this compression to observe the influence of the thigh and buttock pressure on it. It reveals that for the best preconize pressure distribution, the spinal disk pressure was 0.5 bar whereas it could increase up to 1.5 bar for a non-optimal posture. These values confirmed those found by Wilke (1999) during experimental measurement on a person in an automotive seat.

If it is clear that pain increases with loads in the disk, because of the difficulty to experimentally measure the inter-disk load, there is no consensus on the optimal posture the seater should adopt to reduce this load. As described by Harrison et al. (Harrison et al. 1999), “the vast majority of authors have favored a lordosis (Figure 8) lumbar spine, whereas a few have advocated a flexed posture when sitting”.

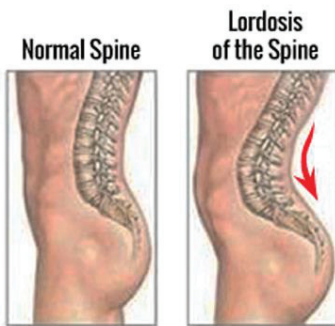


Figure 8: Lordosis of the spine

However, by synthesizing the studies of the literature review, Harisson concluded that the optimum seat (i.e. minimising the disc pressure) would be as follow : a seat-back angle would be of 120 degrees, the seat pan angle would be between 0 and 10 degrees and the lumbar support optimum would be 5 cm of protrusion from the seat back.

#### 1.4 Conclusion

All these mechanical factors allow estimating in an objective way the seat discomfort. Measuring these data is expensive and time-consuming and requires sometimes very intrusive process (measuring spinal disk pressure). Because of the improvements in hardware and software combinations, numerical human models have become a very efficient way to calculate mechanical data. Some human models are used by engineers for ergonomic seat design and others are used by researchers to investigate the data that can't be experimentally measured. Significant research has been conducted to achieve models allowing estimating seating discomfort, mostly for the automobile industry. They will be detailed in the following section.

## 2. State of the art of existing models dedicated to simulate passenger-seat interactions

The aim of the following review is to analyze the human models ever developed for assessing comfort by simulating passenger-seat interaction. As mentioned in the introduction, two main kinds of models exist in the biomechanical field.

Finite Element (FE) models were firstly developed for automobile safety applications and are recently also used for comfort applications. These models are deformable and are mainly used to simulate the deformation of the soft tissues during sitting. They are made up of meshes divided in different parts representing different anatomical parts of the body. Mechanical properties of each part are set from experimental data. After applying boundary conditions, FE simulations can provide the stress and strain of each element.

The second modeling approach used to assess seat discomfort is based on multibody (MB) systems. MB models are composed of rigid segments modeling the bones connected with perfect joints. They can also include lineic (1D) muscles. This kind of model is mainly used in motion analyses. Based on MB models and on the experimental position of their anatomical segments, inverse kinematics and inverse dynamics can provide the kinematics and joint reactions during the movements. Then from the joint reactions, optimization methods can permit to estimate muscular activities. Thus, MB models can't predict the strain or stress in the tissue but can estimate joint reactions and muscular activities.

These two kinds of models are both relevant in discomfort assessment applications since they can both calculate specific mechanical data linked to discomfort. The following section will include a review of these models (FE and MB) focusing on passenger-seat interaction.

## 2.1 FE models

### 2.1.1 Literature search

A systematic literature review has been performed in 3 databases: Science direct, Web Of Knowledge and PubMed. These databases were chosen for their comprehensiveness in the scientific and clinical fields. The review has been performed with the following keywords in the title: (finite element OR model) AND (\*comfort OR pressure ulcer OR seat OR sitting) and the following keywords in the topics: finite element AND \*comfort AND seat.

The search returned a total of 178 results (including repetitions). The returned articles were then reviewed to remove irrelevant articles, papers that did not include any details on the model development and duplicate articles. Finally, the references were searched for additional articles to complete the initial search.

Finally 27 papers were selected after the review process; they are all listed in Table 2.

Table 2 : Geometry of the FE models (the star (\*) indicates when this is a full-body model and the double star (\*\*) indicates when the geometries are coming from different sources)

	Study	D/3D	Composition	Source of geometry	Number of elements	Population category	Application
1	Todd Thacker, (1994)	D	-Bones: tuberosity -Soft undifferentiated	Ischial tissues: MRI	1008 hexahedral elements	One 58-kg female and one 74-kg male	Internal stress estimation for clinical purpose
2	Brosh Arcan, (2000)	D	-Bones: Pelvis -Soft undifferentiated	CT-scan**	//	//	Internal stress estimation for seat design
3	Moes, N. C. C. M., and Horvath ,(2002)	D	-Bones: femur, sacrum and pelvis -Soft undifferentiated	Pictures of slices (Visible Human)**	Hexahedral elements	77-kg male	Contact Pressure estimation for seat design
4	Mergl et al., (2004)	D	-Bones: femur, sacrum and pelvis -Soft undifferentiated	CT-scan**	53510 tetrahedral elements	50 <sup>th</sup> percentile male	Contact Pressure AND internal stress estimation for seat design
5	Verver et al., (2004)	D	-Bones: femur, sacrum and pelvis -Soft undifferentiated	Pictures of slices (HUMOS)	158 310 elements (tetrahedral elements for soft tissues and triangular shells for skin and bones)	HUMOS subject (173 cm, 80 kg)	Contact Pressure estimation for seat design
6	Lin et al. (2004a)	D	-Soft tissues: Epidermis, dermis, fat and muscle	CAO element	Hexahedral element	//	Internal stress estimation for clinical

7	Kuroda and Akimoto, (2005)	D	2	-Soft undifferentiated tissues:	CAO elements	576 Hexahedral		Internal stress estimation for clinical purpose
8	Choi et al., (2007)	D*	3	-Bones: head, neck, full spine, thorax, pelvis with sacrum, -Soft tissues : Skin and flesh	CT-scan**	Tetrahedral elements	One 5 <sup>th</sup> , one 50 <sup>th</sup> and one 95 <sup>th</sup> percentile	Contact Pressure estimation for seat design
9	Cheng et al., (2007)	D	3	-Bones: femur, sacrum and pelvis -Soft tissues: Skin and flesh	3d Scan**	//	50 <sup>th</sup> percentile male	Contact Pressure estimation for seat design
10	Pankoke and Siefert, (2007a)	D*	3	-Bones: Pelvis, femur, tibia, cervical spine, head and arms -Soft tissues: flesh in contact regions (around thigh and pelvis) and abdominal and dorsal musculature	Pictures of slices (Visible Human)	Tetrahedral elements	5 <sup>th</sup> , one 50 <sup>th</sup> and one 95 <sup>th</sup> percentile	Contact Pressure estimation for seat design
11	Linder-Ganz, et al. (2007)	D	2	-Bones: pelvis -Soft tissues: fat and skin together, gluteus muscle and other muscles	MRI	2894 8-node hexahedral elements for gluteus muscle 488 8-node hexahedral elements for other muscle 3688 8-node hexahedral elements for fat and skin	6 subject around 50 <sup>th</sup> percentile	Internal stress estimation for clinical purpose

12	Makhsous et al. (2007)	D	3	- Bones: femur and pelvis, - Soft tissues: skin, fat and five muscle groups	MRI	453 502 tetrahedral elements	4-node solid	24 years, male 165 cm, 70 kg	Internal stress for purpose estimation clinical
13	Wagnac, Aubin, and Dansereau,(2008a)	D	3	- Bones: pelvis -Soft tissues: undifferentiated	CT-scan**	29 292 tetrahedral elements	24 years, 75 kg, 180 cm	Internal stress for purpose estimation clinical	
14	Grujicic et al. (2009a)	D*	3	-Bones: pelvis -Soft tissues: skin and flesh	3deadbrowse r database**	Skin: 60 000 node shells Soft tissues: 135 000 tetrahedral elements Bones:30 000	3- 4-node tetrahedral elements 3-node shell	Contact Pressure AND internal stress estimation for seat design	
15	Chak Yin Tang, Chan, and Tsui, (2010)	D	2	-Bones: Femur and ischial tuberosity -Soft tissues: undifferentiated	CAO		50 <sup>th</sup> percentile	Internal stress for purpose estimation clinical	
16	Wenyu, Chenqi, and Lindong, (2013)	D	3	-Bones: Femur and ischial tuberosity -Soft tissues: undifferentiated	CAO	//	95 <sup>th</sup> percentile	Contact Pressure estimation for seat design	
17	Li, Zhang, and Wang, (2013)	D	2	-Bones: pelvis -Soft tissues: muscles and fat	MRI**	Bones and muscles: tetrahedral elements 10-node Fat: hexahedral elements 8-node	50 subject-specific models	Internal stress estimation for seat design	

18	Oomens et al., (2013)	D	2	-Bones: pelvis, -Soft tissues: muscles and fat	skin,	MRI	//	3 female models: (159 cm, 49 kg)(172 cm, 68 kg)(168 cm, 77 kg)	Internal stress for purpose	Internal stress for purpose
19	Levy, Kopplin, and Gefen, (2014)	D	2	-Bones: pelvis, -Soft tissues: muscles and fat	skin,	MRI	Tetrahedral elements	Male: years, 90 kg	27	Internal stress for purpose
20	Mohanty and Mahapatra, (2014)	D	2	-Bones: tuberosity -Soft undifferentiated	ischial tissues:	MRI	//	55 kg male for purpose	Internal stress for purpose	Internal stress for purpose
21	Luboz et al., (2014)	D	3	-Bones: pelvis, -Soft tissues: muscles and fat	skin,	CT-scan	45374 hexahedral elements, pyramids, tetrahedral elements	100 kg, 190 cm male	100 kg, 190 cm male	Internal stress for clinical purpose
22	Xiaoming et al., (2013)	D*	3	-Bones: pelvis femur -Soft tissues: skin and flesh	and Poser database	Bones tissue: 436 590 solid Skin: 38 204 shell	50 <sup>th</sup> percentile male (173 cm, 68 IMC)	Chinese Pressure estimation for seat design	Contact	Internal stress for seat design
23	Mircheski, Kandikjan, and Sidorenko, (2014)	D	3	-Bones: femur, sacrum and pelvis -Soft undifferentiated	Human Builder database	//	One 50 <sup>th</sup> and one 80 <sup>th</sup> percentile	50 <sup>th</sup> percentile	Contact	Pressure estimation for seat design
24	Volpe, Govanni, and Furieri, (2015)	D	3	-Bones: femur, sacrum and pelvis	CAO	//	Parametric model	Parametric model	Contact	Pressure

			-Soft tissues: undifferentiated					estimation for seat design
25	Huang et al., (2015)	D*	3	-Bones: femur, sacrum and pelvis -Soft tissues: undifferentiated	Based on Hybrid dummy	Tetrahedral elements for soft tissues	50 <sup>th</sup> percentile American male	Contact Pressure estimation for seat design
26	Guo, Dong, and Zhang, (2016)	D*	3	-Bones: femur, sacrum and pelvis -Soft tissues: undifferentiated	Poser Database	//	50 <sup>th</sup> percentile Chinese male	Contact Pressure estimation for seat design
27	Al-Dirini et al., (2016)	D	3	-Bones: femur, sacrum and pelvis -Soft tissues: Skin, 28 muscles, inter-muscular fat and subcutaneous fat	MRI	1 293 241 tetrahedral elements	44 years, 73 kg, 171 cm male	Internal stress estimation for clinical purpose

### 2.1.2 FE models' applications

Most models (15 over 27) have been developed for industrial purposes, in particular in the automobile applications (13 over 15). Other models (12 over 27) were developed for clinical applications. Due to the context and the needs, FE models dedicated to clinical applications were mainly generated from medical images. Furthermore, the models generated from MRI images usually integrated detailed soft tissues (muscles separated from the fat and skin) were (Table 2).

### 2.1.3 FE models' composition and geometry

Among 3D models, a few (6 over 27) represented the whole human body (8, 10, 14, 22, 25, 26), while 8 models were limited to the upper leg and buttocks (3, 4, 5, 9, 12, 17, 21, 27). As for 2DFE models (10/27) representing an anatomical slice of a few centimeters thickness in the frontal plane (1, 6, 11, 12, 13, 15, 18, 20, 21).

Regarding the models' composition in terms of soft tissues, 14 models merged all the soft tissues together, 4 dissociated the skin from the other tissues (muscles and fat) and 11 differentiated muscles and fat (Table 2).

Regarding their geometries' origin, 8 models have been created from MRI images, 5 from CT-scan images, 3 from pictures of human slices (from the Visible Human Project or the European HUMOS project), 5 from geometric databases (3dcadbrowser, Poser and Human Builder), 1 from 3D laser scan data and 5 basic geometries have been generated with design softwares (Poser software or the human builder module of Catia). Most of the models represented 50<sup>th</sup> percentile males and only 4 studies developed 2 or more models representing various anthropometries (Table 2). Most of the time, all the anatomical parts of a model came from the same source (1, 5, 10, 11, 17, 18, 20, 21, 22, 23 and 24). For a few models, the soft tissues and bones came from different sources. The bones were either obtained by CT-scans (4) or MRI (1, 11, 12, 17, 18, and 20). Then the skin derived from a CT-scan of another subject (3, 4, 8) or from the same person (13) or from a database like CEASAR (9) or 3dcadbrowser ([www.3dcadbrowser.com](http://www.3dcadbrowser.com)). To position the bones inside the soft tissues, anatomical bony landmarks located on the skin were mostly used (3, 8, 9, 13), while Mergl et al. (2004) used CT images.

MRI images from a seated subject (2, 11, 17, 19, 20, 27) or from a subject in a posture close to sitting (4, 12, 21) were sometimes used. However, most of the studies used images of a lying subject and adapted the model posture afterwards (5, 9, 10, 14, 22, 23). Finally, we can notice that most of the models with detailed soft tissues (muscles separated from the fat and skin) were generated from MRI images (Table 2), while less detailed models were generated based on anthropometric data only. It can also be noticed that the models integrating detailed soft tissues are mainly dedicated to clinical applications while the others focus on automotive discomfort applications.

### 2.1.4 Material properties

In the listed FE models, bones were considered as rigid bodies (3, 4, 5, 8, 10, 11, 12, 14, 15, 20, 21, 23) or their behavior is set as linear elastic with a large Young Modulus (2, 9, 17, 19, 22, 24, 25, 26) with a Poisson ratio of 0.3 or 0.49 (Li et al. 2013).

Within a given model, the soft tissues, muscles and fat (being merged together or differentiated) have the same material law. In models differentiating muscles and fat, specific law parameters are set for each part. Regarding soft tissues, 5 different laws are used in the listed models: a Mooney Rivlin law (9/27), a Neo-Hookean law (7/27), a generalized Mooney Rivlin law (2/27) an Ogden law (3/27) and an elastic linear law (5/27), (Table 3).

The Mooney Rivlin law (Mooney 1940; Rivlin 1948), is a hyperelastic isotropic material law expressed by the following strain energy function (Equation 1), where  $J_1$ ,  $J_2$ ,  $J_3$  are the invariants of the right Cauchy-Green strain tensor and the material parameters  $A_3$  and  $A_4$  are functions of the coefficients  $A_1$  and  $A_2$ .

#### Equation 1

$$W = A_1(J_1 - 3) + A_2(J_2 - 3) + A_3(J_3^{-2} - 1) + A_4(J_3 - 1)^2$$

Verver et al. (2004) proposed values for the  $A_1$  and  $A_2$  coefficients from a range of values proposed in prior FE models ((Chow & Odell 1978; Bosboom et al. 2001; Oomens et al. 2003). Then, the following models relied on these parameters proposed by Verver et al. (9, 10, 12, 14, 22, 23, 25, 26). Grujicic et al. (2009b) is the only one to have checked the values of these parameter by an optimization procedure (inverse method) based on experimental indentation test data (Zhang et al. 1997).

The generalized Mooney Rivlin law is a polynomial hyperelastic law (Equation). It was used at the second order by Tang et al. (2010) and (Mohanty & Mahapatra 2014) with parameters determined by indentation tests (Tang & Tsui 2006).

#### Equation 2

$$W = \sum_{i,j=0}^n C_{ij} (I_1 - 3)^i (I_2 - 3)^j + \sum_{k=1}^m D_k (J - 1)^{2k}$$

The Neo-Hookean law is a special case of the Mooney Rivlin law with  $C_{01}=0$ ,(Equation).

#### Equation 3

$$W = C_1(I_1 - 3)$$

In the listed FE models to model soft tissues, the  $C_1$  parameter was determined from various experimental dataset :

-Moes et al. (2002) used an inverse method to find  $C_1$  based on experimental Cauchy stresses

-Lin et al. (2004) used parameters based on an experimental study performed by (Larrabee 1986)

-Brosh et al. (2000) found parameters using indentation tests.

-Linder-Ganz et al. (2007) used also the parameters found by Brosh et al. (2000).

Levy used values from *in vitro* indentation tests performed on sheep (Gefen & Haberman 2007) for the skin and fat tissues and values from *in vitro* indentation tests on fresh porcines (Palevski et al. 2006) for muscles.

-Luboz et al. (2014) performed an inverse method based on the internal strain calculated in numerical studies (Linder-Ganz et al. 2009; Oomens et al. 2003).

The Ogden material property (Equation) is a hyperelastic law expressed by the following strain energy density where  $\lambda_i$  are the principal stretches.

#### Equation 4

$$W(\lambda_1, \lambda_2, \lambda_3) = \sum_{p=1}^N \frac{\mu_p}{\alpha_p} (\lambda_1^{\alpha_p} + \lambda_2^{\alpha_p} + \lambda_3^{\alpha_p} - 3)$$

It was used by (Li et al. 2013) at the second order for the fat tissue and by Oomens et al. (2013) and Al-Dirini et al. (2016) at the first order. Oomens et al. (2013) found the parameters by optimization method by fitting data from experiments (Ogden et al. 2004). Al-Dirini et al. (2016) found the parameters by doing a optimization on the model to fit his own experimental data, whereas Li et al. (2013) doesn't specify the parameters' origin.

Finally, a simple linear elastic law was used in a few models. Wagnac et al. (2008) obtained a Young Modulus value using indentation tests (Zheng & Mak 1999). (Kuroda & Akimoto 2005) used a 15 kPa-Young modulus without justifications. Mergl et al. (2004) defined 4 different regions in the thigh with 4 Young modulus of 1 kPa, 15 kPa, 20 kPa and 30 kPa found through indentation tests (Hartung et al. 2004). Todd and Thacker (1994) and Volpe et al. (2015) used different values of Young modulus depending on the gender: 64.8 kPa for male and 47.5 kPa for female based on experimental indentation test (Todd and Thacker 1994).

Furthermore, regarding soft tissue modeling, it can be noticed that the same Poisson coefficient of 0.49 was always used in order to simulate the incompressible aspect of the soft tissues. To model the skin, a linear elastic law is often used with a Young modulus of 0.15 MPa (Verwer et al. 2004; Grujicic et al. 2009a; Xiaoming et al. 2013) or 0.85 MPa (Cheng et al. 2007b).

**Table 3: Material properties for the soft tissues of the FE models**

Material law	Study	Parameters
Elastic linear	Wagnac (2008)	E=81.5 kPa
	Kuroda (2005)	E=15 kPa
	Mergl (2004)	E=1 kPa, E=15 kPa, E=20 kPa, E=30 kPa
	Volpe (2015), Todd (1994)	Male: E= 64.8 kPa Female: E=47.5 kPa
Neo-Hookean	Moes (2002)	E= 250 kPa G= 83 kPa
	Lin (2004)	E= 700 kPa (muscle) G=234 kPa E= 30 kPa (fat) G=1 kPa

	Luboz (2014)	$E = 30 \text{ kPa}$ (fat) $G = 10 \text{ kPa}$ $E = 100 \text{ kPa}$ (muscle) $G = 1 \text{ kPa}$
	Brosh (2000)	$G = 34.9 \text{ kPa}$
	Linder (2007)	$G = 25.33 \text{ kPa}$ (muscle) $G = 95 \text{ kPa}$ (fat and skin)
	Levy (2014)	$G = 31.9 \text{ kPa}$ (skin) $\mu = 3179.37 \text{ kPa}$ $G = 0.286 \text{ kPa}$ (fat) $\mu = 28.5 \text{ kPa}$ $G = 7.1 \text{ kPa}$ (muscles) $\mu = 707.6 \text{ kPa}$
Mooney- Rivlin	Verver (2004), Cheng (2007), Siefert (2007), Makhsoos (2007), Grujicic (2008), Xiaoming (2014), Mircheski (2014), Huang(2015), Guo (2016)	$A_1 = 1.65 \text{ kPa}$ $A_2 = 3.35 \text{ kPa}$
Generalized Rivlin (2 <sup>nd</sup> order)	Tang (2010), Mohanty (2014)	$C_{10} = 0.08556$ , $C_{01} = -0.05841$ , $C_{20} = 0.039$ , $C_{11} = -0.02319$ , $C_{02} = 0.00851$ , $D_1 = 3.65273$ , $D_2 = 0$
Ogden	Li (2013) (2 <sup>nd</sup> order)	Fat: $\alpha_1 = -0.107647$ , $\mu_1 = 0.118261e-2$ , $\alpha_2 = -0.318953$ , $\mu_2 = 0.643855e-7$ Muscle: $\alpha_1 = 0.1316402e+1$ , $\mu_1 = 0.10257e-2$ , $\alpha_2 = -0.1835933e+2$ , $\mu_2 = 0.145209e-6$
	Oomens (2013) (1 <sup>st</sup> order)	Skin: $\mu = 8 \text{ kPa}$ $\alpha = 5$ Fat: $\mu = 1 \text{ kPa}$ $\alpha = 5$ Muscle: $\mu = 0.3 \text{ kPa}$ $\alpha = 5$
	Al Dirini (2016) (1 <sup>st</sup> order)	Fat and skin: $\mu = 1.17 \text{ kPa}$ $\alpha = 16.2$ Muscles: $\mu = 1.91 \text{ kPa}$ $\alpha = 4.6$

### 2.1.5 Simulations boundary conditions

When performing a simulation, the boundary conditions were applied either by 1) applying the gravity on the body to reach the fixed seat (20/27) or by 2) applying a load or moving the seat to a fixed human model (7/27).

The first boundary condition was applied on whole body models, where the gravity was applied for moving the body from an initial position already close to the desired sitting position (8, 10, 14, 22, 25) or on models limited to the upper leg and buttocks. In this case the weight of the upper body was

estimated and applied on the ischial tuberosity of the pelvis (1, 15, 17, 24) or on the whole pelvis (5, 6, 13, 18, 20 23). The weight of the lower leg was applied on the femur (1, 5, 24). A displacement observed experimentally could also be imposed to the ischial tuberosity (2, 7, 19) to simulate the seat tissue crushing.

Regarding the second boundary condition, the load applied on the seat was either the body weight (3, 4) or directly measured pressures (6, 12, 21). The femur was usually fixed at its extremities in the frontal direction and the lower trunk was fixed in the vertical direction. Linder-Ganz et al. (2007) and Al-Dirini et al. (2016) applied a displacement measured on MRI images.

### 2.1.6 FE model validation

Very few studies described or included a validation process. Within the 13 studies focusing on pressure prediction, only 6 compared simulated peak or average pressure at the seat interface with experimental observations (Table 4). Among the models dedicated to internal strain prediction (14), only 4 studies estimated an error in deformation between simulations and experimental observations from MRI (1, 12, 27) or from X-ray images (13). Todd and Thacker (1994) calculated the soft tissues displacement under the ischial tuberosity of loaded buttocks. Wagnac et al. (2008a) measured the displacement of radio-opaque landmarks placed on the skin. Makhous et al. (2007) estimated the displacement of 30 regions of interest identified on the soft tissues. Al-Dirini et al. (2016) calculated the quadratic mean error between the deformed and non-deformed surface of the gluteus muscle.

**Table 4:Error percentage between simulated and measured pressure value from the studies by Mergl et al; Verver (2004); Mircheski (2014); Volpe (2014); Wagnac (2008); Li (2013)**

	Mergl (2004)	Verv er (2004)	Mirch eski (2014)	Volpe (2014)	Wagn ac (2008)	Li (2013)
P <sub>max</sub> (%err)	2%	37%	2%	9%	9%	5%
P <sub>mean</sub> (%err)	11%	44%		7%	31%	

## 2.2 MB models

### 2.2.1 General state of the art of the MB models

As mentioned above, MB models are composed of articulated rigid segments representing the bones linked with perfect joints. They can be equipped with muscular beams attached to the bones and enable the estimation of the muscular activity.

Lots of MB models including muscles were developed for gait analysis and included only the lower limbs (Delp et al. 1990; Hoy et al. 1990; Doriot & Cheze 2003; Al Nazer et al. 2008). Several entire body models have been developed for gait applications. Haze (1997) developed a quite basic model with 8 joints and 40 muscles, then Komura et al (Komura et al. 2000) created a more detailed

model with the muscles of the lower limbs (Figure 9), Hamner et al. (2010) developed a model with 92 muscles activating the lower limb and the torso.

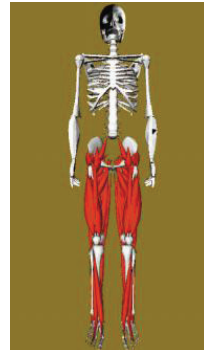


Figure 9: Komura model

Several models of the lumbar spine were created to study the joint loads in the back for diverse activities. Macintosh et al. (1993) developed a model of the back muscles with 29 fascicles of the lumbar multifidus and erector spinae. Bogduk et al. (1992) built a model of the lumbar back muscles incorporation 49 fascicles of the same muscles. McGill & Norman (1986) created a model of the low back with musculo-ligamentous-skeletal system in three dimensions. In this model, musculature was driven from surface EMG. Stokes & Gardner-Morse (1995) developed a model containing five lumbar vertebrae, the pelvis, the thorax and 66 symmetric pairs of multi-joint muscles. Van Dieën (1997) used a model with 114 muscles over the lumbosacral junction to compare prediction of individual muscle slips and surface EMG recorded. Finally Christophy et al. (2012) developed a model including the pelvis, five lumbar vertebrae, thoracic spine, ribcage and 238 muscles fascicles.

If a certain number of musculoskeletal model have been developed for gait study, for task ergonomic assessment (Chaffin 1987), or for spine load estimation, few were used for properly sitting discomfort assessment.

### 2.2.2 MB models used for sitting discomfort assessment

Kwang et al. (2009) developed a detailed spine model to simulate kinematic behavior of musculoskeletal forms and generate a human-wheelchair interface to offer effective design solutions for people suffering from long-term sitting. The LifeMOD software was used to build the model. This model was improved later by Huynh et al. (2015) by refining the three spine segments (cervical, thoracic and lumbar regions) into individual vertebra segments, using joints to represent the intervertebral discs, and creating additional ligaments, lumbar muscles and abdominal muscles. This MB model has already been used in preliminarily investigations of the effects of sitting posture on human body (Huang et al. 2012).

Hirao et al. (2006) created a 2D-model with 13 rigid segments and 63 muscles. He studied lumbar muscular activity for two seated postures.

Finally the most used model for comfort application is the one developed by Michael Daamsgard and John Rasmussen (Daamsgard 2006). The model (AAUHuman) developed in a specific oriented-object language is available with dedicated software, the *Anybody Modelling System* and will be detailed in the next subsection (3.2.2).

Anybody's research team carried out some research with their model on the seat comfort. They first studied the influence of the seat angle and seat friction coefficient on the shear forces and the muscular activity (Rasmussen et al. 2007b). The model was positioned in the seat by defining geometrical constraints between the subject and the seat. The seat reaction and tangential/friction forces were provided. In another study, they tried to find the optimum combination of seat and backrest angles by minimizing a comfort function depending on shear forces and muscle activity with normalization factors (Rasmussen & Zee 2008). They also studied the influence of friction coefficient and seat pan inclination on the internal forces (spinal joint forces) (Rasmussen et al. 2009). The influences of the seat pan inclination, back-rest inclination and pedal's spring stiffness on the different muscle group activity were investigated in a study by Majid et al. (2011). Grujicic et al. (2010b) used also the same model from Anybody to simulate the effect of four driver/seat interaction parameters (the back-rest inclination angle, the friction coefficient, the longitudinal-track seat-position and the presence/absence of lumbar support) on long-distance driving fatigue. With results from their simulations and findings in the literature, they defined a long-distance driving-fatigue function (LDDFF) depending on the cumulative muscle activity (CMA) representing the sum of activity levels of the muscle groups defining the muscle-activity envelope, the contact normal force (CNF) and the contact shear force (CSF).

#### **Equation 5**

$$\text{LDDFF} = 5.0 \left( \frac{\text{CMA}}{0.0045} \right)^2 + 1.0 \left( \frac{\text{CNF}}{1.0} \right) + 1.5 \left( \frac{\text{CSF}}{0.5} \right)^2$$

Finally, Li et al. (2015) created his own model with the Anybody Modelling System corresponding to the 95th percentile of the Chinese population for a dynamic automobile study. The simultaneous effects of backrest inclination and vibration frequency changes were investigated on several muscle groups (right leg, left leg, abdomen and lumbar). It was found that vibration frequency significantly affects the muscle activity of the lumbar area whereas backrest inclination affects right leg and abdomen activity.

The Anybody model is one of the most complete MB model and the most largely used for sitting discomfort application. We can consequently suppose that it will be adapted to our needs.

The whole-body AAUHuman model is composed of bones and muscles with geometry coming from different databases. It includes an arm/shoulder assembly containing 114 muscles; a spine model comprising the sacrum, all lumbar vertebrae and a rigid thoracic-spine section containing 158 muscles; a pelvis and the lower extremities containing 70 muscles. Anthropometric data (length of the segments, inertial data, origins and insertions of the muscles, centers and axes of rotations geometrical shapes) from specific studies were used for each part of the model. The arm and shoulder segments were built with data from a Dutch research group (<http://homepage.tudelft.nl/g6u61/repository/shoulder/overview.htm>). For the spine model, data of vertebrae dimensions and spine parameters were taken from the study by Nissan & Gilad (1986) and mechanical properties of the ligaments were taken from a study performed by (Pintar et al. 1992). The model of the lower extremity is based on anatomical datasets on muscle and joint parameters provided by Martin Klein-Horsman from the University of Twente in Netherlands (Klein Horsman et al. 2007). The entire model contains more than 500 individual muscles in total. This model corresponds to the 50th percentile European male but can be easily scaled to represent another population category or a specific subject.

To simulate the environment (i.e. the mechanical boundary conditions applied to the human body), several solutions exist within the Anybody software. The first one is to apply contact forces on the body model. The force value has to be known and consequently has to be experimentally measured. In the case of simulation where experimental data would not be available, a contact formulation can be used to calculate the contact force. Discrete points are defined on the body model where the contact with the seat can occur. A Coulomb friction contact is defined between this point and the seat surface. This contact formulation allows calculating discrete normal and shearing contact forces. The limit of this method is that discrete points have to be defined and to obtain biofidelic simulations and results, a very wide number of points have to be set. Furthermore, only rigid surfaces can be simulated because of the non-deformable characteristics of this approach.

Several validation tests have been performed on specific parts of the model. For example, the gait movement has been simulated and compared to experimental data. Several data sets have been investigated: the ground reaction force and moments, the hip flexion moment and knee flexion moment. In the study by Fluit et al. (2014), forces have been recorded on nine healthy subjects performing several Activities of Daily living. No significant differences were found ( $P>0.05$ ) between the mean predicted and measured ground force and moment reactions for almost all ADLs except for the transverse moment. Simulated knee reaction force has been compared to measured force during the “Grand Challenge” (<https://simtk.org/home/kneeloads>). After improvements in the model the predicted force fitted with the measured one ( $R^2= 0.80$  for medial contact force,  $R^2=0.93$  for total contact force). Preliminary validations of the lumbar spine model have also been done by comparing intradiscal pressure with experimental data, showing that model can give a good estimation (de Zee et al. 2007). In an upright position, the model estimated an axial force of 4520N and a shear force of 639 N in the L5/S1 disc at this maximum extension moment. It is in the range of axial forces between 3929 and 4688 N and the minimum shear forces of 650 N given by (McGill & Norman 1986).

A large number of musculoskeletal model have been developed since the beginning of the 90's, but most of them were used for gait or different activities analysis and some to study low back pain mechanism and very few were dedicated or used to analyze the link between muscular activities or discs load and discomfort. One of the most used for this application is the Anyody model, this model will be used in this project.

### 3. Conclusion

After a review of literature, three main biomechanical factors appear for sitting discomfort: 1/ the tissue compression and deformation due to both shear and normal forces on the seat, 2/ the muscular activity and 3/ the intervertebral discs compression. Since FE models can simulate the tissue compression and MB models can estimate the disc compression and the muscular activity, both of these models will be used in this project.

A state of the art of the existing FE model dedicated to sitting discomfort revealed that a wide variety of models exist. There is a need for a sensitivity analysis to determine what is the influence of each of the modeling options on the different output. It also revealed that most of the models didn't take into account the variation of anthropometry. There is a need for methods enabling to personalize models' geometry to represent any 'population's category. This literature review also revealed that

very few FE models are actually validated especially the models dedicated to the prediction of soft tissue internal deformations. There is a need to confront model results to experimental data.

A state of the art of the MB models revealed that very few were used to assess seat discomfort. The most used one was the Anybody model.

Finally here is a need to associate a FE model to a MB model to assess all the factors leading to discomfort. This would be innovative as no study proposing such a coupling could be found in the literature.

## Chap 2: Finite element model development and sensitivity analysis

The literature review on the existing FE models revealed the need to perform a sensitivity analysis on the different model parameters. To perform this sensitivity analysis, a template model of the thigh-buttocks complex was created, on which different parameters have been varied. Then, the impact of these parameters on several model outputs have been studied to determine how important each of them are for discomfort assessment. This chapter will first describe the development process of the FE model and then the sensitivity analysis and its results.

### 1. Finite element model development

As mentioned earlier, most of the models found in the literature aren't whole body models (21/27), they represent only the buttocks and thigh and sometimes only the buttocks. The reason is, as explained before, that the highest compression of soft tissue while sitting is located under the buttocks and more precisely under the ischial tuberosities. Consequently, the existing discomfort criteria are based on the contact pressure at the seat pan interface. Since this is the most interesting area regarding our application and most of the model focused on it, it has been decided to only model the buttocks and thigh with the FE approach. The anatomical zone concerned is between the top of the sacrum and the femur epicondyle (white zone Figure 10). Furthermore, a partial model is easier to morph and position than a full body model, as we will see later in this thesis.

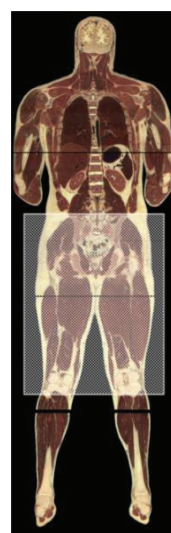


Figure 10: Anatomical zone of the model on Visible Human picture

## 1.1 MRI

MRI acquisition of the buttocks-thigh area of a healthy male subject (1m74 and 65 kg) was used to get the geometry of the concerned anatomical parts. The MRI technology was chosen because it has the advantage to be noninvasive. Furthermore the MRI allows having a good distinction of adipose tissues on the images which is mandatory to detect the different soft tissues. Since the model will be used for simulating a seated position, the subject had to be in a position close to sitting during the MRI acquisition. The seated position was not possible in the MRI system, thus the subject was lying on a side with the leg bent (Figure 11: Subject's position in the MRI). The trunk-thigh angle was calculated from the MRI images: an angle of  $130^\circ$  was obtained between the femur (line between the center of epicondyle and center of femoral head) and the pelvis (line between the center of femoral head and the top of the sacrum) in the sagittal plane (Figure 12).

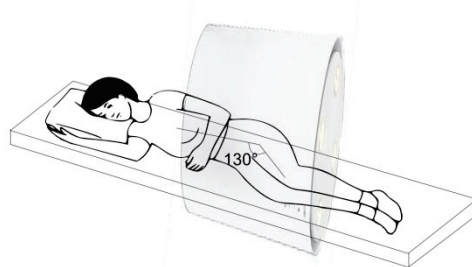


Figure 11: Subject's position in the MRI system

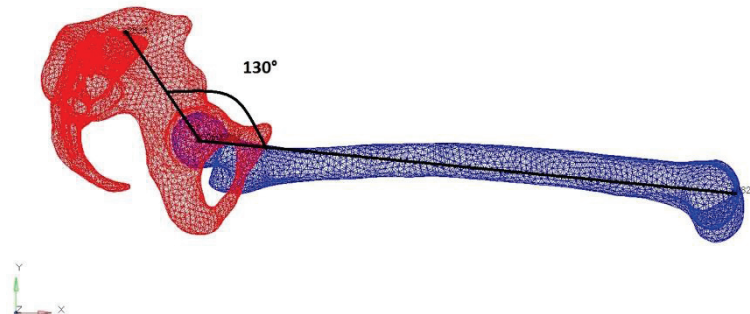


Figure 12: Bones orientations in the MRI images

The type of MRI sequence used was T1 weighted. The acquisition was conducted in 3D with a window of  $316*359*307\text{mm}^3$  and a resolution of  $0.853*1.1*1.0\text{ mm}^3$ .

Because of the limited MRI window size, two scans were realized to cover the whole region of interest, one centered on the pelvis and the other centered on the femur. The two regions were overlapping a bit each other in order to allow for a rigid registration.

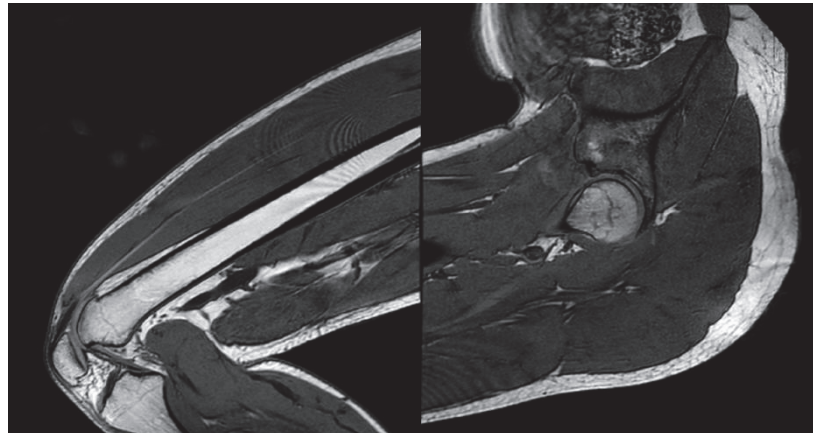


Figure 13 : Illustrations of 2 sagittal MR images of the two anatomical regions

The two acquisition regions (centered on the pelvis and on the femur) were associated by performing a rigid registration with the meshlab software (<http://www.meshlab.net/>). An ICP algorithm (Iterative Closest Point) was applied on the surfaces of the femur and the skin from the two acquisitions area to realize the superposition of the two acquisition regions.



Figure 14: Registration of the two acquisition regions

Once the two area were registered, it appeared that if the regions overlapped on the top of the thigh, there was however a gap of 15 mm below the thigh. This gap was due to a wrong orientation of the window by the MRI operator. This gap was filled by interpolation thanks to the continuity of the tissues in this area.

## 1.2 Segmentation

MR images were then segmented using the 3D slicer software (version 4.4.0). The segmentation was performed on each plane automatically and then manually adjusted.

Sacrum, pelvis and femur, were segmented so that each bone contains both cortical and cancellous tissues. Fat contour and skin were segmented together. All the organs located inside the

pelvis (bladder, prostate, rectum) were segmented in one block. Finally, all the muscles located between the pelvis and the femur epicondyles were segmented one by one.

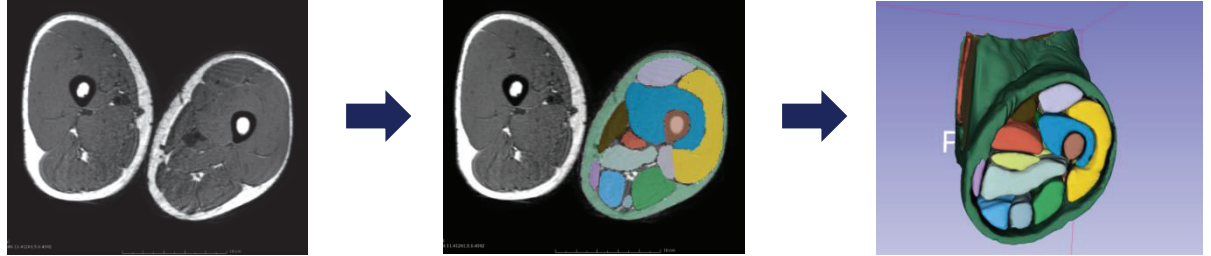


Figure 15: Images segmentation

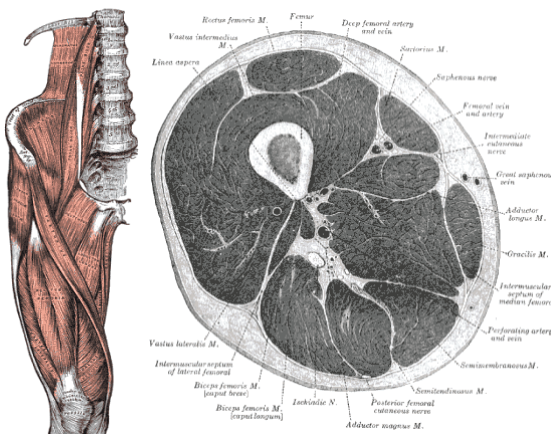


Figure 16: Anatomy of the leg ((H Gray 1918)

Twenty-three muscles of the leg were segmented. Two muscles, the vastus medialis and intermedius, were merged in one part because of the difficulty in distinguishing them. The geometry of each muscle and the location of their insertions were checked with the book of anatomy from H Gray (1918) as well as the data from the Visible Human project (<http://visiblehuman.epfl.ch/>) which allows visualizing segmented muscles.

Only one thigh and half of the pelvis were segmented assuming that the body is symmetric.

### 1.3 Mesh

The obtained surfaces had to be meshed to create a FE model. After the segmentation we got very detailed surfaces with a very large number of points. Meshing these surfaces could be done with a greater or lesser resolution. To determine what the best mesh resolution is, a mesh sensitivity analysis was performed using a basic mesh model without distinction of different soft tissues. The sacrum and the pelvis were tied in one part. A revolute joint between the pelvis and the femur was introduced at the center of the femoral head to model the pelvifemoral joint. To mesh the soft tissues, the volume between the bones and the outer surface was meshed with volume tetrahedron elements. The bones were assumed rigid and the soft tissues were modeled with an hyperelastic material law which will be described later (2.1).13 models were created with a range of mesh size between 3 mm and 15 mm.

A generic loading condition to simulating the action of sitting on a rigid plane was defined to test the different meshes. The model was loaded by the gravity above a rigid plane. The upper body weight was applied on the pelvis barycenter. The lower leg weight was applied on the knee at the center of the epicondyles. Due to the symmetry, the pelvis was also constrained in translation in the sagittal plane and in rotation along the axis perpendicular to the sagittal plane.

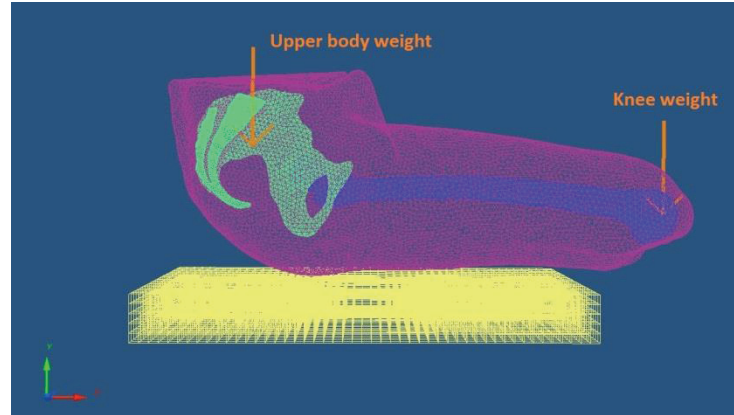


Figure 17: Boundary conditions

An explicit simulation was run with the Radioss solver (finite element solver developed by Altair Engineering ® for linear and nonlinear problems) and stopped when the model was totally in contact with the seat, *i.e.* the contact force was equal to the model weight.

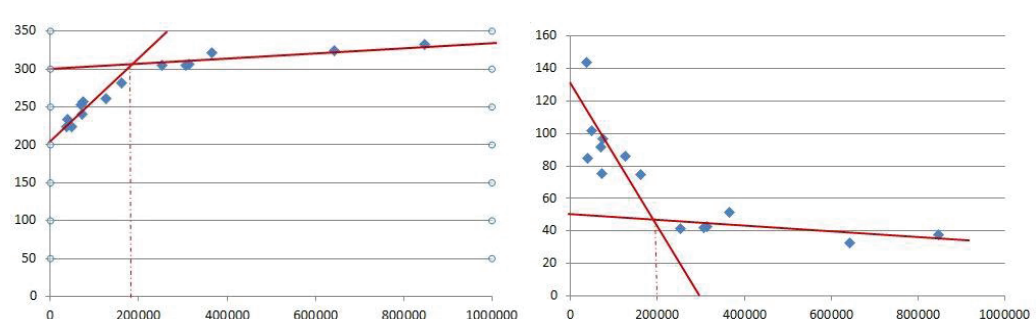
Simulations were performed with the 13 different mesh models. The model outputs were defined according to the applications of our model. As explained before, the FE model is dedicated to simulate soft tissue compression and deformation. The outputs which represent this compression are the pressure on the interface between the body and the seat and the internal stresses and strains. Consequently, the relevant model outputs taken into considerations were:

- The interface contact area (in cm<sup>2</sup>)
- The mean normal pressure (in kPa)
- The maximal normal pressure (in kPa)
- The maximal internal stresses (Von Mises) calculated under the ischial tuberosity (in kPa)
- The maximal internal strain

The maximal gradient pressure calculated by adding all the pressure cells of a row, *i.e.* a line parallel to the femus axis)

These outputs were studied in all the upcoming analyzes.

The influence of the mesh size was studied on these outputs. Results are shown respectively in Figure 18.



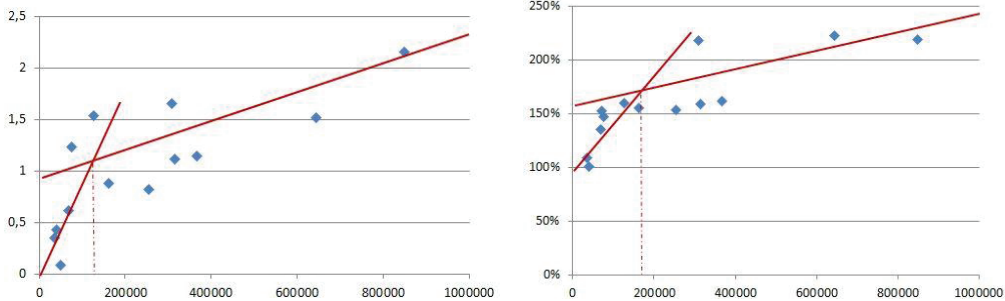


**Figure 18:** Surface in  $\text{cm}^2$  (top left), maximale pressure in  $\text{kPa}$  (top right), maximal stress in  $\text{MPa}$  (down left) and maximal strain in  $\%$  (down right) depending of the element number

It appears that under a certain number of elements, the outputs diverge, suggesting that the size of elements should be carefully selected. We can observe that the critical number of element would be around 200000. Models containing a number of elements close to and greater than 200000 elements have elements of a characteristic length of at least 5mm. More precisely, the model with 5mm-characteristic length elements has 253879 elements.

This mesh convergence study was performed with a specific FE model. However, we can make the assumption that the mesh resolution would be the same for identic loading cases (a person seating on a seat) but with slightly different models (other mesh composition and other material parameters in the same order of magnitude)..

## 2. Sensitivity analysis

The literature review on the existing FE model revealed a wide diversity among them. First, the mesh composition varies a lot between the models. Most simple models contain only bones and soft tissues in one layer. Some models dissociate soft tissues between adipose tissues and muscles, and some dissociate each muscle from each other. Secondly, a wide variety of material laws and material parameters are used in the different FE models. In the following paragraph, the influence of these two conditions, mesh composition and material law on the simulation outputs will be investigated.

### Geometry

#### 1. Mesh composition

To study the influence of the mesh composition, several meshes were developed to reproduce the variety found in the literature. The first mesh with the lowest detail level contained bones and soft tissues merged together (Figure 19).

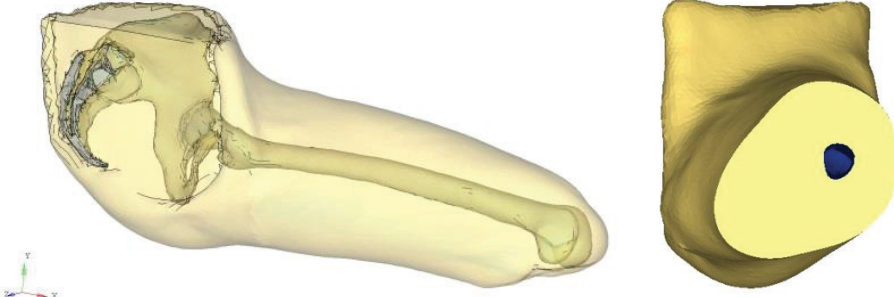


**Figure 19: Mesh 1 (soft tissues merged together)**

In the second mesh, a thin layer made of shells of 2 mm was added to model the skin layer. This layer was created on top of the soft tissue.

For the third mesh, a distinction between the adipose tissue and muscles layers was made. The soft tissues were divided in one block for all the fat tissues, one block containing all the muscles (Figure 20).



**Figure 20: Mesh 3 (orange=fat; purple=muscles, yellow=skin)**

Finally the more fourth mesh was composed of individualized muscles. It contains all the muscles described in the section 2.2 (Figure 21).



**Figure 21: Mesh 4 (various colors=muscles, purple=fat, yellow=skin)**

A contact was defined between the different muscles to avoid inter-penetration. This contact was defined without any friction between the muscles.

All the models were meshed with the element size determined in the mesh convergence study : a minimal characteristic length of 5 mm.

The material property of the soft tissues was defined as an hyperelastic incompressible Neo-Hookean law. The Neo-Hookean law was used because it was the only material law which has been used to model individualized and merged soft tissues in the literature. The material parameter found by (Brosh & Arcan 2000) using indentation tests was used,  $C_1 = 34.9$  kPa, when soft tissue were merged (mesh 1 & 2) and the two following parameters from Linder-Ganz et al. (2007) were used,  $C_1 = 25.33$  kPa for muscles and 95 kPa, when they were individualized.

As for the boundary conditions, the pelvis was fixed and half of the total body weight was applied to the seat on which the displacement was constrained to the vertical direction (perpendicular to the plane of the seat). Since the lower leg weight had a negligible impact, the leg was let free by introducing a revolute joint between the femur and the pelvis and the weight of the lower leg was applied on the center of the epicondyles.

Simulations were run with the three models and the outputs listed earlier (1.3) were analyzed.

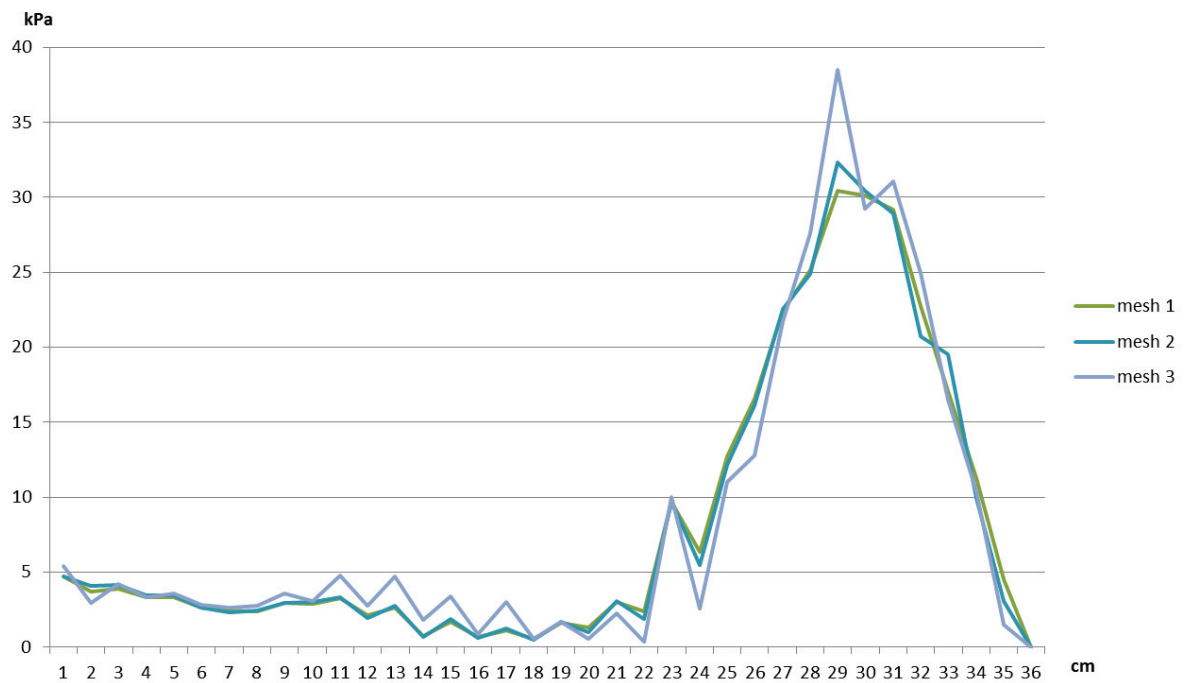


Figure 22: Profile pressure (summation of the whole pressure for each row) in kPa for the 3 meshes

Table 5: Simulations outputs for the 4 different meshes

M esh	Surface cm <sup>2</sup>	Pmea n kP	Pmax kPa	Max Grad kPa/cm	Max Stress kPa
1	247	13.4	63.5	7.4	55.1
2	253	13	66.47	7.8	57.8
3	240	13.75	77.74	10.9	112.5
4	381	8.66	256.9		157.9

The outputs of the simulations with the meshes 1 and 2 were very close (Table 5): the presence of the skin didn't impact much the results. The results of the simulations with the mesh 3 were also very

close to the results of the simulations with the meshes 1 and 2 except for the maximal stresses: modeling the fat increased this result of 104%. As for the mesh 4, simulations were somehow different for contact results (contact area, pressure...) up to 28% but large discrepancies were observed for the internal maximum stresses (up to 186%). Thus, for contact results (contact area and pressure at the seat interface), the mesh composition didn't show much influence, while for internal results having individualized soft tissues appear as paramount for internal stress and strain predictions.

## 2. Muscles – adipose tissues proportions

To fully study the impact of mesh composition and the necessity or not to distinguish the soft tissues, we varied the proportion of adipose tissues and muscles in the same leg. The goal was to investigate if the proportion of adipose tissues in the leg affected the outputs.

A first scaling of the leg was done to increase its volume to have more possibilities of variation of fat volume. The outer shape of the original model was scaled: the total leg volume was multiplied by 1.5 with an homogeneous scaling in the plane normal to the femur axis.. Then, the muscle volume was scaled in the same way, with 6 different scaling coefficients. Six meshes were created, with a volumic percentage of muscles varying from 36 % to 58 % of the total leg volume. This range was defined to represent realistic variation of fat proportion between healthy people and overweighed people. Indeed, Jeukendreup Asker & Gleeson Michael (2009) found that the fat percentage can vary of 15% in the whole body between athletic and obese persons, this variation is a bit more important in the thigh and buttocks. Kelley et al. (1991) found that healthy people must have 58.5 % of muscles in the leg in volume ( $65 \pm 5$  % of lean tissues from the total leg volume, considering that 90% of the lean tissues are muscles). .

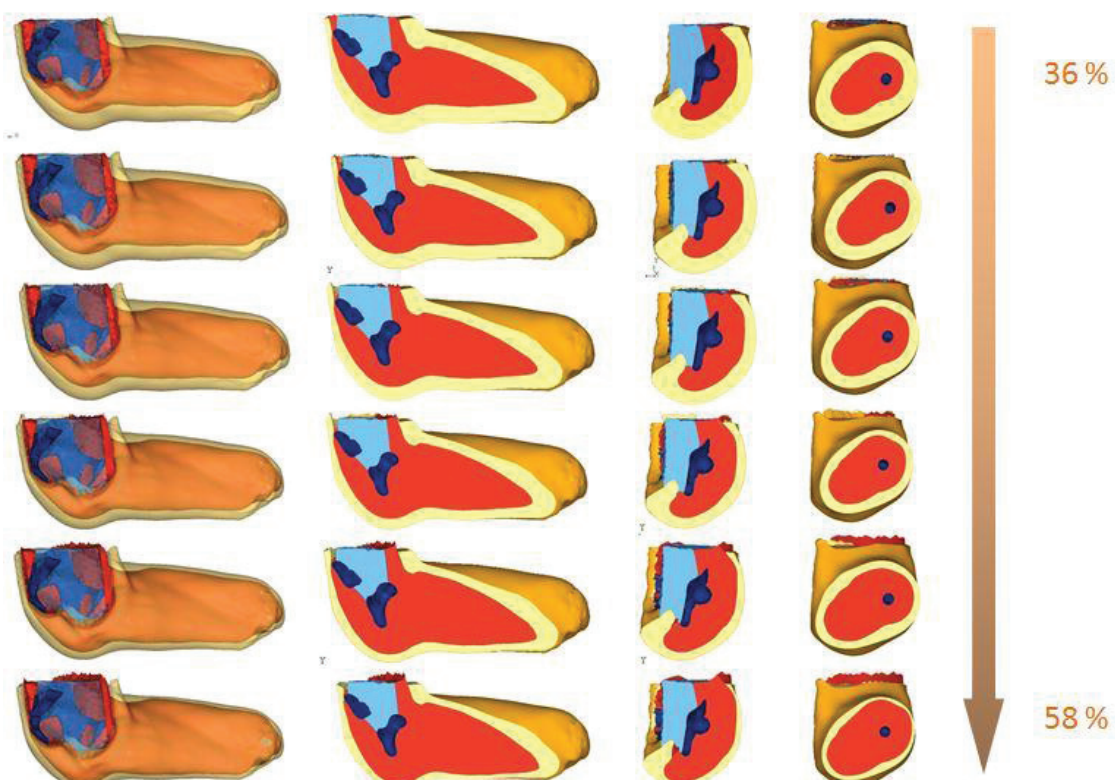


Figure 23: Muscle volume variation (in volume percentage of the leg)

The percentage of fat and muscles didn't affect at all the contact area. The curve representing the evolution of the contact area with the increase of muscle percentage (Figure 24) is totally flat. The same effect was logically seen for the mean pressure (Figure 24).

However, the fat proportion affected the maximal estimated pressure. The maximal pressure evolved linearly with the percentage of muscles. The maximal gradient also evolved linearly. While the pressure profile were very similar between the different muscle percentage (Figure 25), the peak of pressure was higher when the volume of muscle was smaller. When there are less muscles surrounding the ischial tuberosity, the pressure is less distributed.

Finally, it has to be noticed that these results may depend on the material parameters used (here we used the parameters proposed by Al Dirini).

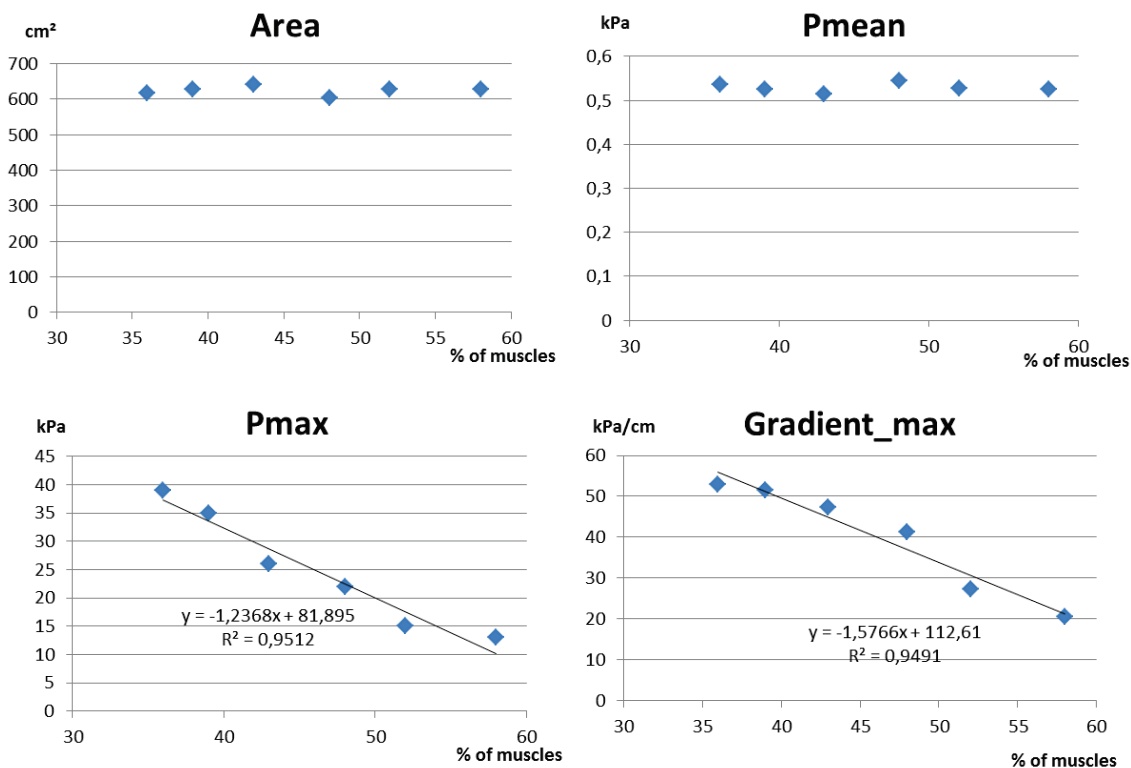
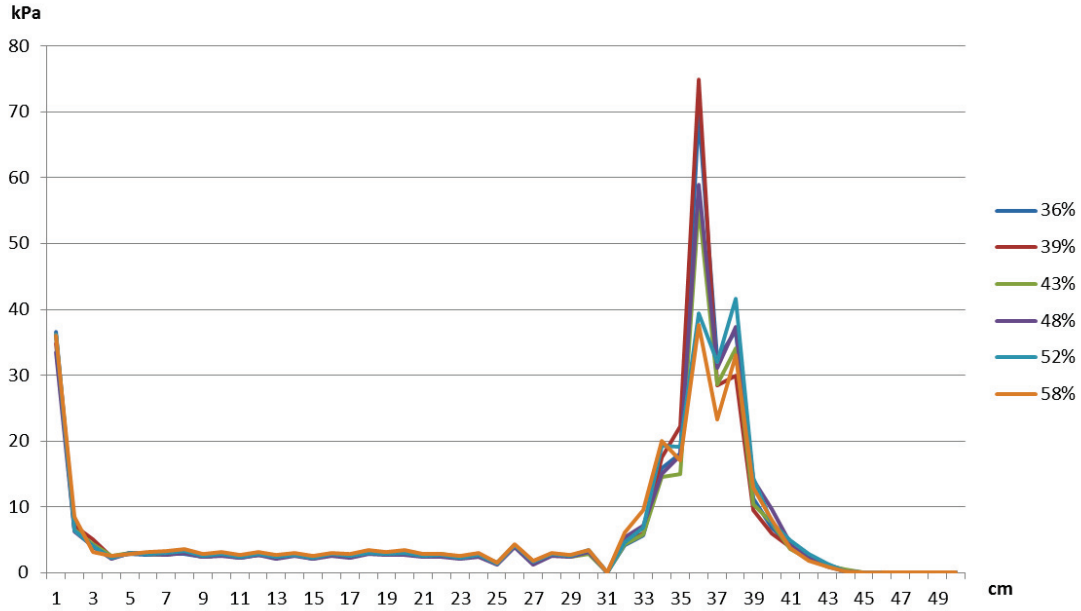


Figure 24: Area in cm<sup>2</sup> (top left); Mean pressure in kPa (top right); Max pressure (down left); Maximal gradient (kPa) function of the muscles volume



**Figure 25: Profile pressure (0cm : front of the seat, 50cm : back of the seat) in kPa for different muscles volume proportion**

## 2.2 Material properties

As explained before, a wide variety of material laws have been used to model the soft tissues. In most of the studies, the objective reasons of the choice of the law were not explained and the origins of the material parameters were not always detailed. This can be an issue if the material properties have an impact on the model outputs. This is why we chose to investigate the effect of these properties on the simulation outputs. First we tested several material laws from the literature with their associated parameters and then we compared some specific laws with adapted parameters.

### 2.2.1 Literature values comparison

The laws the most frequently used in the literature (22 models over the 27) were tested with their associated parameters: a linear law, a 1<sup>st</sup> order hyperelastic law (Neo-Hookean) and a 2<sup>nd</sup> order hyperelastic law (Mooney Rivlin). The generalized Rivlin and Ogden laws were excluded because they were unfrequently used and never used to model merged soft tissues (fat and muscles). The linear elastic law was defined with a Young modulus of 81.5 kPa determined by (Zheng & Mak 1999) using experimental indentations. The hyper elastic incompressible Neo-Hookean law was defined with one material parameter found by (Brosh & Arcan 2000) using indentation tests:  $C_1 = 34.9$  kPa.

The Mooney Rivlin hyper elastic incompressible law was defined with the material parameters provided by (Grujicic et al. 2009), and obtained by an inverse approach based on experimental indentation tests (Zhang et al. 1997):  $C_1 = 1.65$  kPa and  $C_2 = 3.35$  kPa.

The three laws were implemented with the mesh 1 described earlier. Bones were set as linear elastic with a Young modulus of 17 GPa (Li et al. 2013). The skin was modelled as linear elastic with a Young modulus of 0.15 MPa and nearly incompressible with a Poisson coefficient of 0.49 (Verver et al. 2004a; Grujicic et al. 2009; Xiaoming et al. 2013).

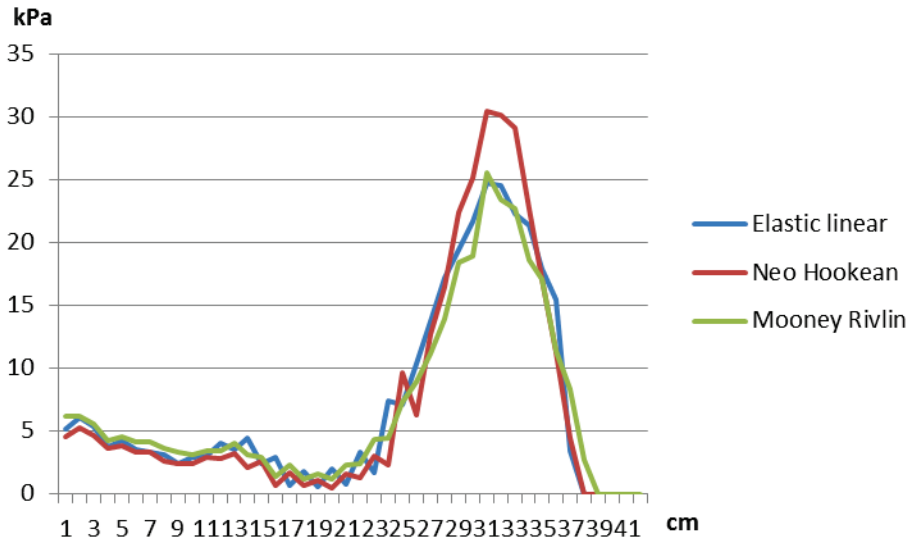


**Figure 26: Profile pressure (summation of the whole pressure for each row) in kPa for the three different material laws**

**Table 6: Simulation outputs for different material laws**

Model	Mesh	Law	Surface cm <sup>2</sup>	Pmean kP	Pmax kPa	Gradmax kPa/cm	Stress max kPa
1	1	Linear elastic	226	14.6	45.92	5.7	68.07
2	1	Neo Hookean	247	13.4	63.5	7.4	55.1
3	1	Mooney Rivlin	335	9.85	40.5	6.6	509.8

The material law has an important impact on the contact area and pressure (Table 6: Simulation outputs for different material laws). The difference of contact area was 9,3 % between the models 1 and 2 (See Table 5 for the models's description) , 48% between the models 1 and 3, and 35% between the models 2 and 3. The difference of maximal pressure was 38% between the models 1 and 2, 13% between the models 1 and 3 and 57% between the models 2 and 3. When looking at the pressure profile (Figure 26), it can be observed that the main difference concerns the peak value but not the distribution.

Regarding the internal stress, the material law affected a lot the values. The difference of maximal stress between models 1 and 2 is 23.5%, 649% between models 1 and 3 and 825% between models 2 and 3.

## 2.2.2 Parameters effect – Young Modulus

The more complex is the law, the higher is the number of its parameters. They can be determined by experimental mechanical tests or by inverse method through simulations. Since the parameters are subject-specific and may depend on the gender, BMI, age..., it is necessary to know their influence.

We decided to investigate first the effect of the variation of the Young Modulus of a linear elastic law on the contact pressure estimation. The Young modulus was made varied from 10 to 65 kPa.

A linear relationship was found between the maximal pressure and the Young modulus of the soft tissues (Figure 27). For an increase of the Young modulus of 20 kPa, the maximal pressure increased of almost 10 kPa. Thus the Young modulus has an important impact, and should be chosen wisely. (Figure 27).

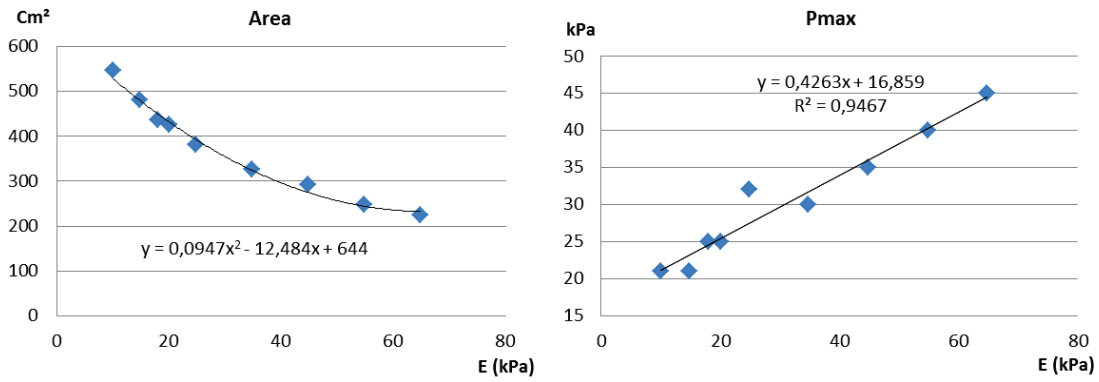


Figure 27: Contact area (in cm<sup>2</sup>) and maximal pressure depending on the Young modulus (in kPa)

## 2.2.3 Material property effect

To compare different material properties together, material parameters can be chosen so that they are equivalent in the two laws. We compared results from simulations with a Mooney Rivlin law and a linear elastic law. For the linear elastic law, the Young modulus was calculated so it would be equivalent to the Mooney Rivlin parameter. In uniaxial compression the Cauchy stress is equal to:

**Equation 6**

$$\sigma = 2C_{10} \left( \lambda - \frac{1}{\lambda^2} \right) + 2C_{01} \left( 1 - \frac{1}{\lambda^3} \right)$$

Or for small deformations, around  $\lambda = 1$ , the tangent modulus is :

**Equation 7**

$$E_{\varepsilon=0} = \frac{d\sigma}{d\lambda}_{\lambda=1} = 6(C_{10} + C_{01})$$

In the literature, the two material parameters  $C_{10}$  and  $C_{01}$  are respectively 1,65 kPa and 3,35 kPa, so the equivalent Young modulus was  $E = 30$  kPa. When we compared the results from the model with Mooney Rivlin and model with equivalent linear elastic law, results were very similar in terms of contact area and pressure (Table 7).

**Table 7: Simulations' outputs for models with a Mooney Rivlin law and an equivalent linear elastic law**

	Surface cm <sup>2</sup>	Pmean kP	Pmax kPa
Linear	332	9.93	34.1
Mooney			
Rivlin	335	9.85	40.5

Consequently, to estimate the contact pressure, a linear elastic model would be sufficient. However, since a linear elastic material property can't estimate correctly the stress and strains at high deformations, we also compared the results of these two models for different level of deformations. The weight of the person was made varied to expose the tissues to more deformations. The estimated Von Mises stresses differed a lot between the two models from a weight of 40 kg to a weight of 90 kg (Figure 28). This showed that above a given limit (about 40 kg), we aren't any more in the elastic domain, meaning that an hyper elastic law would be needed to simulate the internal conditions of the soft tissues.

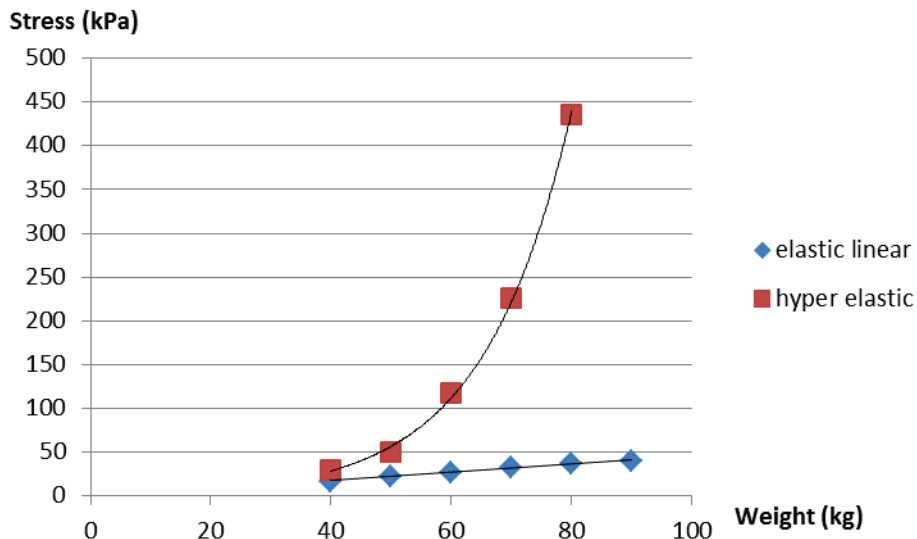


**Figure 28: Maximal stress (Von Mises in kPa) under the ischia depending on the person weight (in kg)**

#### 2.2.4 Parameters effect – hyperelastic parameters

We have seen that internal strain and stress are affected by the material law and the material parameters. To know the influence of each of the parameters, a sensitivity analysis has been conducted

on these parameters. We estimated the sensitivity of the outputs (here the tissue displacement) to the parameters. Soft tissues were modeled with a hyper elastic first order law, except the skin which was modeled with a simple elastic linear law. The nominal values for each parameters were taken from the literature: 0.15 MPa for the Young modulus of the skin (Verver et al. 2004b; Grujicic et al. 2009; Xiaoming et al. 2013), 1 kPa and 0.3 kPa for  $\mu$  of fat and muscles respectively and 5 for  $\alpha$  for fat and muscles. Then, a variation of  $\pm 50\%$  was applied to all the parameters.

**Table 1: Parameters variation for the sensitivity analysis**

	Lower Bound	No minal	Upper Bound
Skin Young Modulus	0.075	0.1 5	0.225
$\mu$ for fat	0.005	0.0 01	0.0015
$\alpha$ for fat	2.5	5	7.5
$\mu$ for muscles	0.00015	0.0 003	0.00045
$\alpha$ for muscles	2.5	5	7.5

We focused on the following simulations' outputs: the displacement of the two layers of soft tissues, *i.e.* adipose tissues and muscles. To calculate these displacements, a plane was defined by the two ischial tuberosities and the right and left anterior superior iliac spines of the pelvis. Then the vertical displacement of the two layers in this plane was calculated between the reference state and the end of the simulation (Figure 29).

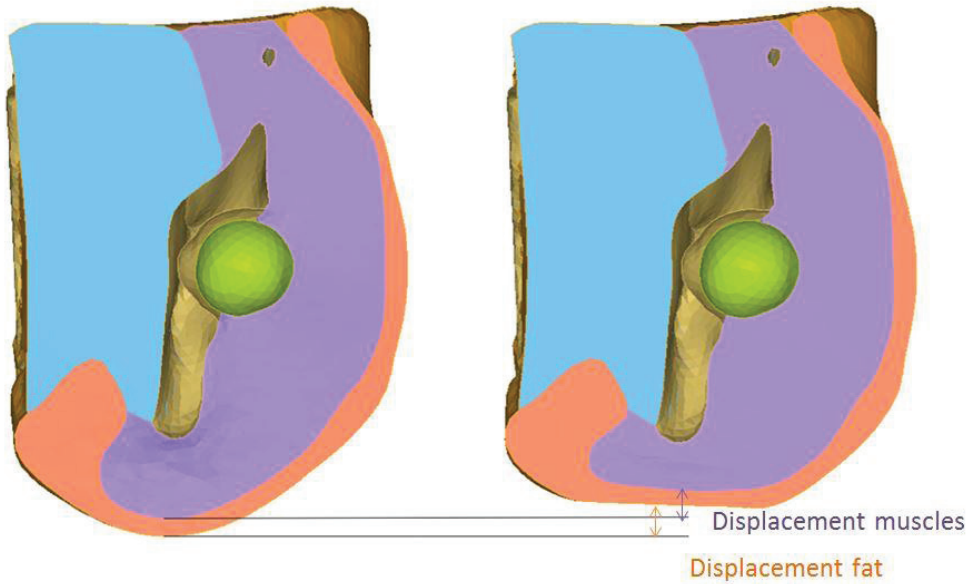


**Figure 29: Soft tissues displacement measures on the model**

Then, a design of experiment (DOE) was defined with the Hyperstudy software (Altair). A central composite design was defined (AltairKorea ). A total of 43 simulations were launched.

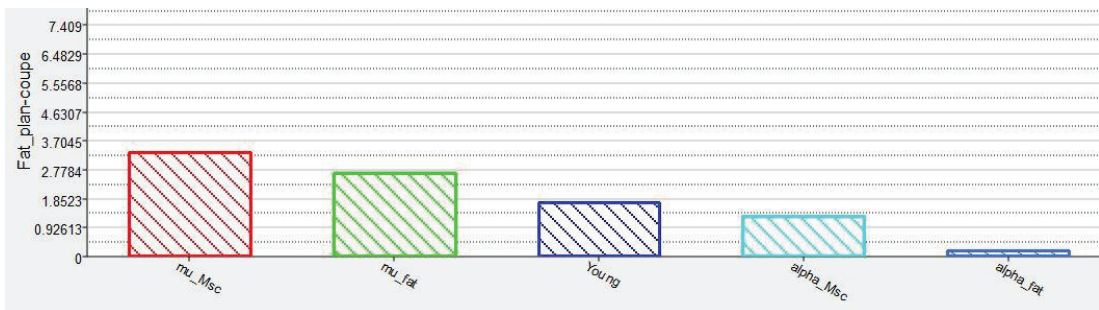


Figure 30: Pareto plot: percentage x 0.1 of the contribution of each parameter on the fat displacement

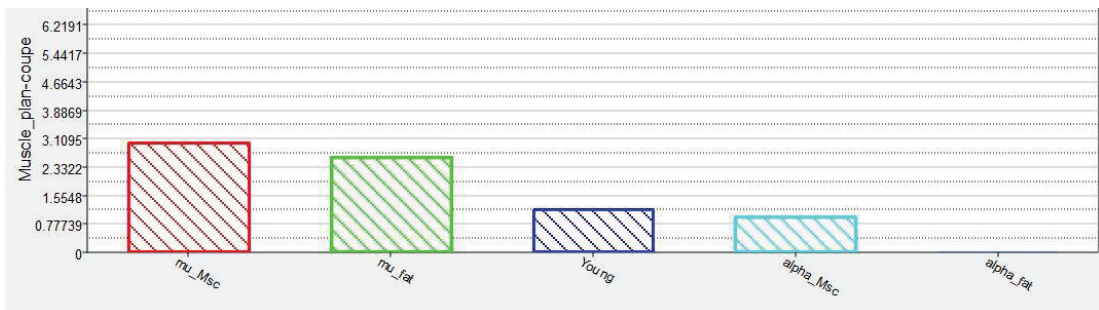


Figure 31: Pareto plot: percentage x 0.1 of the contribution of each parameter on the fat displacement

It appeared that most influential parameters were the  $\mu$  coefficients of the different material properties. The parameter with the less impact was the alpha coefficient of the fat. It can be seen on the pareto plots which showing the sensitivity of the fat displacement and muscle displacement to the different parameters (Figure 30 & Figure 31). Skin Young modulus appeared to be less important than the  $\mu$  parameters of the other soft tissues.

When looking at the principal component analysis (Figure 32), it appeared that the  $\mu$  parameters are strongly linked to the displacement in an opposite way. The larger are these coefficients, the smaller is the displacement of the soft tissues, i.e. the more rigid is the material.

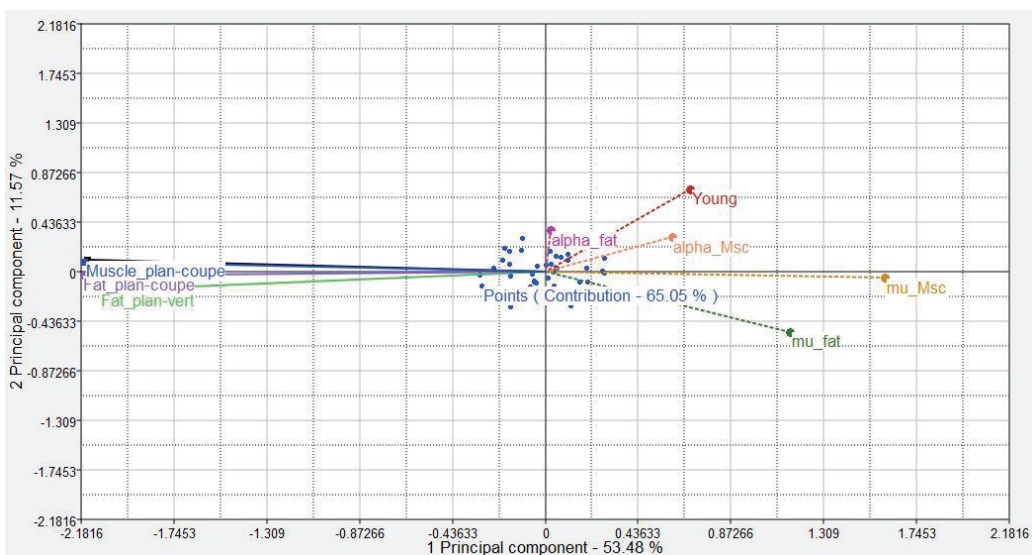


Figure 32: 2nd principal components versus the 1st principal components

### 3. Conclusion

A finite element model of the thigh-buttocks complex has been developed from MRI images. From this model, several sub-models were created to investigate the effect of the geometry (mesh composition and muscles-fat proportion) and the material properties. First, parameters from the literature were used and outputs, contact area, pressure and internal stress and strains, were compared. It has been observed that the mesh composition didn't affect much the contact pressure estimation. The variations of contact area or maximal pressure don't exceed 6% between models with different mesh composition. Even between different morphology and different proportion of muscles and fat, the contact pressure was not strongly affected. These results showed that there is no need to distinguish the different layers of soft tissue to estimate the contact pressure. However, different material properties used in the literature revealed important variations on the contact pressure estimation. The variations between models could reach more than 100% for the maximal contact pressure estimation. This effect was mainly due to the material parameters. For instance, we have seen that a linear elastic law with an equivalent Young modulus was sufficient to estimate the contact pressure (under a given limit corresponding to the elastic domain). Consequently, an optimal model to simulate the contact pressure could be defined as a mesh of 5 mm-characteristic length with undifferentiated soft tissue modeled with a linear elastic law. This model will be used in this thesis. If the model is dedicated to calculate internal strain and stress, it has been observed that a linear elastic law is not sufficient. Material law and material parameters have indeed a strong impact on the internal stress and strain estimation. Consequently to well estimate soft tissue stress and strain, a hyper elastic law should be used with a specific care on the choice of material parameters.

# **Chapter 3: A parametric geometric model of the buttocks-thighs complex based on 3d scan data: development and validation**

## **Introduction**

In the precedent chapter, it has been shown that a simplified FE model with rigid bones and undifferentiated soft tissue modeled with an elastic linear law is sufficient to estimate seat contact pressure. As reported in the first chapter, such a kind of model has been developed in several studies and is often used in the automotive field for seating discomfort evaluation. However, almost all of the existing models represent only one specific body size (predominantly, the 50<sup>th</sup> percentile male in stature) or two or three specific anthropometries (5<sup>th</sup>, 50<sup>th</sup> and 95<sup>th</sup> percentile (Choi et al. 2007; Pankoke & Siefert 2007)). These models cannot represent the large anthropometric variation of the sitters' population. The pressure on the seat pan surface is strongly dependent on the sitter's anthropometry (Kyung and Nussbaum 2008). Mastrigt et al. (2017) reported 9 studies about the relations between anthropometric variables, such as stature, weight gender, age, BMI, percentage of subcutaneous fat, somatotype (human body shape and physique type) and pressure related variables, such as contact area, mean pressure and peak pressure. Strong correlations were found between the anthropometric variables and pressure variables, particularly between BMI and contact area. It was observed that the contact area increased linearly with BMI, for example it can be multiplied by 1.4 for a person of 97 kg versus a person of 53 kg (Swearingen et al., 1962). A high linear correlation was also found between stature and contact area. Some also reported a correlation between buttock related anthropometric variables such as hip breadth and mean pressure (Gyi & Porter 1999). Hip breadth is highly variable amongst the population. As an example, the 95<sup>th</sup> female sitting breadth is much larger than the 95<sup>th</sup> male; they are respectively 432 and 412mm based from the Anthropometric Survey of US Army Personnel in 1988 (Gordon et al., 1988). Consequently to assess the ergonomic quality of a seat, the model used should be able to represent the large anthropometric variation of the population. Several methods have been used to take into account the anthropometry in past studies. The first is to create a family of models representing each a specific population category (5<sup>th</sup>, 50<sup>th</sup> and 95<sup>th</sup> percentiles for example) as developed by Choi et al. (2007) or Pankoke & Siefert (2007). Currently, the number of specific population category represented is very limited. A high number of models would be necessary to have a good representation of the anthropometric variations in a population. To be able to represent a wide variety of anthropometry, parametric models started to be developed first in the computer design field (Wang 2005; Hasler et al. 2009). The development of 3d body scanners helped to build parametric surface shape models which aim to predict 3d body skin surface from a few target anthropometric parameters such as stature, gender, obesity or even age. For example Baek & Lee (2012) developed a whole body parametric shape model based on scan data of 250 subjects selected by age, weight and stature. These kind of models have been then developed for ergonomic

purpose to take anthropometry and shape in consideration (Allen et al. 2003a). For example a parametric shape model of the shoulder was developed by Kim et al. (2016) to assess the ergonomic quality of a space suit. A whole-body shape parametric model was built from scan data by Reed & Parkinson (2008; Reed et al. 2014). (Park et al. 2017) developed a parametric model for the child population. Since these parametric models only focused on the external shape, they could not be directly used as a basis for a whole FE model for seating comfort assessment. However parametric FE model of intern organs or skeleton started to be developed for finite element simulations in diverse applications. University of Michigan Transportation Research Institute (UMTRI) has used this framework to develop children pelvis, thorax and scapula parametric model (Reed et al. 2009). Li et al. (2011) developed a parametric child head FE model containing the skull and brain based on statistical geometry model build from CT images. Bryan et al. (2010) developed a parametric FE model of the femur from the statistical analysis of CT scan in an orthopedic purpose. All these studies used the same methodology. They build a statistical shape model thanks to images of the organs or segment of several persons. They used a morphing method to adapt a baseline FE mesh to the wanted geometry.

This approach will be used in this work to develop a parametric shape model of the buttock-thigh complex containing both skin and bones (pelvis and femur). The shape of skin and bones will be predicted from anthropometric parameters such as BMI, stature and gender and posture parameter such as joint angles. As explained in the precedent chapter, the model is focused on the buttock-thigh because this is where tissues are the more compressed while seated. The parametric shape model will be then used to develop a parametric finite element mesh to enable further in simulations predicting occupant seat interaction for all kind of anthropometry.

This chapter will be divided in three parts: 1) development of a parametric model of the skin surface with body landmarks, 2) development of PCA models of the bones' surfaces including body landmarks, and 3) development of a finite element model based on this parametric model and the comparison with experimental pressure data.

# 1. Part 1: A parametric skin shape model of the buttocks-thighs complex based on 3d scan data

This part describes the development of a parametric model which could predict skin surface and bones landmarks of the thigh-buttocks complex from anthropometric and postures parameters. Surface data was collected to build the parametric shape model. A laser scan was used to get the skin surface and then estimate the bones landmarks by palpation. The data (skin surface and bones landmarks) was analyzed to build a statistical model of the external shape and bones landmarks. A principal component analysis (PCA) was used to reduce the data dimensionality. For each principal component, a multiple regression was used to predict how the associated PC score varied with the anthropometric and posture parameters (BMI, stature, gender and joint angles). Then outer surface and bony landmarks could be predicted from these anthropometric parameters.

## 1.1 Method

### 1.1.1 Data collection

Data was collected from 36 participants, who were selected to cover a wide range of anthropometry for both males and females (Table 8). Three stature groups were defined: short (5-15%ile), average height (around 50%ile) and tall (80-95%ile, based on an French population) with two BMI categories 18.5 - 25 and over 30 kg/m<sup>2</sup> for each stature group.

**Table 8: Summary statistics of stature, body mass index (BMI), age and hip width of the 36 participants**

	N		Average	SD	Minimu m	Maximu m	Range
Female	17	Stature (mm)	1639.41	75.48	1510	1760	250
		BMI (kg/m <sup>2</sup> )	27.75	7.99	18.98	44.26	25.28
		Age (y)	29.94	11.54	19	56	37
Male	19	Hip width (mm)	358.88	46.83	305	470	165
		Stature (mm)	1784.47	75.74	1680	1930	250
		BMI (kg/m <sup>2</sup> )	27.1	5.28	19.3	35.7	16.4
All	36	Age (y)	28	7.63	20	41	21
		Hip width (mm)	345.47	27.43	310	393	83
		Stature (mm)	1715.97	104.63	1510	1930	420
		BMI (kg/m <sup>2</sup> )	27.41	6.61	18.98	44.26	25.28
		Age (y)	28.92	9.58	19	56	37
		Hip width (mm)	351.81	37.89	305	470	165

For each participant, anthropometric data such as stature, thigh length, hip width, waist width, buttocks depth, thigh circumference, waist circumference were measured at first. Then, the participants were asked to take a sitting posture with help of a specific jig (Figure 33) which helped maintaining a torso-thigh angle of approximately 110°. Both the torso and the thighs were not supported, and could thus easily be scanned. The kneeling structure was adjustable to ensure that the same position could be adopted by every participant. The torso-thigh angle was checked using a goniometer. A hand laser scanner (Nikon ModelMaker MMCx) was used to scan the body area from the knees to the shoulders.

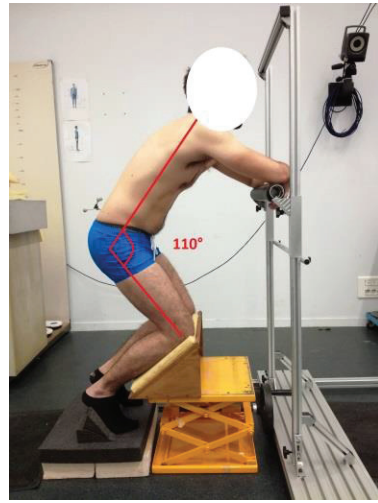


Figure 33: Scanning posture of a participant in the support device

A cluster with 4 reflective markers attached on the skin above the sacrum was used to estimate the position of the bony landmarks previously palpated. The palpation was previously performed with a manual palpator called “A-Palp” (Salvia et al. 2009) (Figure 36). The “A-Palp” consists of a gantlet with a cluster fixed on it (Figure 34) whose shape was adapted to the experimenter hand. The experimenter first calibrated the palpator by touching 4 known landmarks on a rigid plate. The position of the finger’s extremity in the gantlet cluster coordinate system was then calculated. The following bony landmarks were palpated (Figure 36): RIAS and LIAS (Right and Left Anterior Superior Iliac Spine), RIPS and LIPS (Right and Left Posterior Superior Iliac Spine), RICT and LICT (Right and Left Ilium Crest Tubercle) and IPJ (Ilium Pubic Joint) (Van Sint Jan 2007). The two epicondyles of each femur were located with reflective markers. We made the assumption that no movements occurred between the cluster and the pelvis between the palpation position and the scan position. All the palpated landmarks were expressed in the cluster reference system.



Figure 34: A-Palp and calibration plate

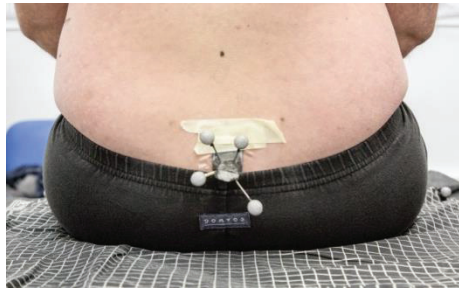


Figure 35: Pelvis cluster

The positions of the markers for the sacrum, the knees and A-palpator were recorded using the VICON optoelectronic system with 12 infrared cameras.

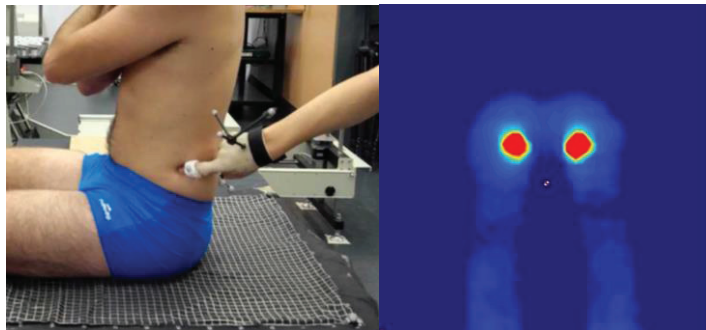


Figure 36: Bony landmarks palpation with the A-palp and pressure map

To obtain the position of the ischial tuberosity, a pressure pad (X3, XSensor, Calgary, AB) was used. The participant was sitting on a flat rigid surface and the locations of the centers of the two areas of maximal pressure on the pressure map were identified as the ischial tuberosity positions (Figure 36).

### 1.1.2 Data processing

#### *Generation of meshes and landmarks position*

The scan data for each participant were first cleaned by filling the holes and deleting the superimposed mesh parts. The surfaces were re-meshed to decrease the number of triangles to 20 000 using the MeshLab Software. The scans of all participants were then aligned in the pelvis local reference system with the help of the pelvis anatomical landmarks palpated previously. The pelvis reference system is defined by an origin at the midpoint between RIAS and LIAS, a z axis defined by the vector between RIAS and LIAS and an x axis defined by the vector going from the middle of RIPS and LIPS and the origin (Figure 37).

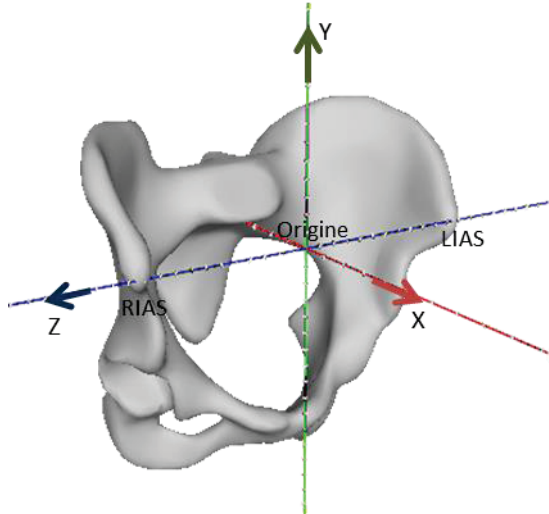


Figure 37: Pelvis reference system

The scans were then cut to keep only the thigh and the pelvic area as follows. The pelvic and thigh surfaces were delimited by three planes: 1) the plane defined by the two markers on the two epicondyles of the knee and a point located at the poplite (at the crease of the knee) (green plane on Figure 38), 2) the sagittal plane passing by the midpoints of PSIS and ASIS landmarks, and the normal direction by the two ASIS (purple plane on Figure 38), 3) plane formed by the two ASIS and midpoint of the two PSIS with an offset of 4 cm along the normal of this plane (red plane on Figure 38). The previously palpated bony landmarks were merged with the scan thanks to the common cluster reference system which was also scanned.

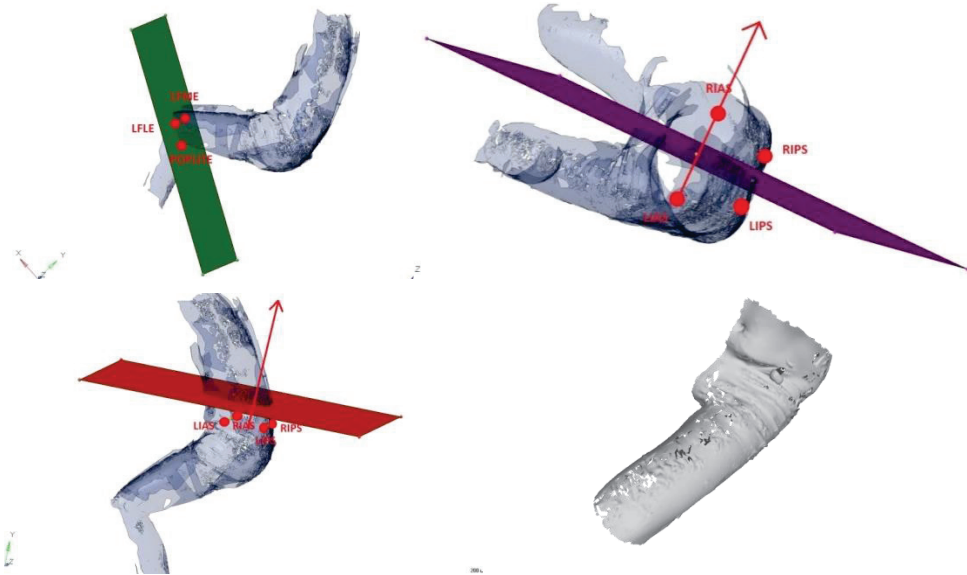
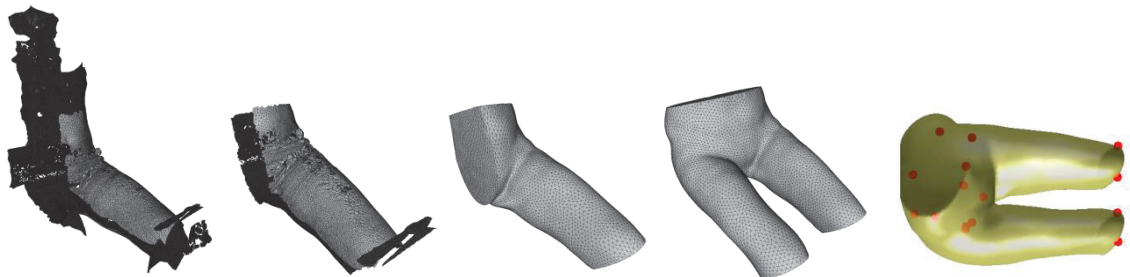


Figure 38: Cutting the mesh in 3 planes (top left: knee plane, top right: symmetry plane, bottom left: top plane, bottom right: segmentation results)

A generic template was created from the data of a subject. The mesh scan data of this subject was properly cleaned to create a regular mesh with triangles of 5mm side length. Mesh was enclosed at the three cutting planes. Cleaned meshes with vertices ordered identically for each subject were obtained by deforming this template towards the other subject's scans using mHBM software (Markerless Homologous Body Modeling Software, National Institute of Advanced Industrial Science and Technology, Digital Human Research Center). The template was matched to the scan point clouds

thanks to a variant of non-rigid ICP (Iterative Closest Point) algorithm described in the study by Yamazaki, S. et al. (2013).

Once the regular meshes corresponding to the scan data obtained, 16 landmarks were identified, including the 7 manually palpated bony landmarks, the two ischia estimated using the pressure map, the two epicondyles at the knee, the two hip joint centers and the lumbosacral (L5/S1) joint center in the same local reference system (pelvis reference system described previously). The joints centers were estimated from the anatomical landmarks using the regression equations provided by Peng et al. (2015) (Appendix 1).



**Figure 39: Mesh processing steps.** From the left to right show raw scan, raw surface after segmentation, deformed template after having matched with scan, full buttock thigh surface after symmetrization, landmarks association.

Additionally, local body dimensions were measured digitally on each scan. The thigh length was measured between the top of the knee and the more backward part of the bottom, the hip width was measured at the larger part of the hip, the waist section was measured in the segmentation plane (4 cm under the IAS) and the thigh section was measured at the middle of the femur in the plane with the femur axis as normal.

### Statistical Shape analysis

A Principal Component Analysis (PCA) was used (Jolliffe, 2002) to reduce the dimensionality of the data. The coordinates of the 9 923 mesh vertices from the 36 subjects were gathered in a matrix  $\Psi_{n \times p}$  with n corresponding to 36 subjects and p to 3\*9923 vertex coordinates. The q (= 3\*16) coordinates of the 16 bony landmarks were appended to  $\Psi_{n \times p}$  resulting in a matrix  $\Psi_{n \times (p+q)}$ . A smaller set of ordered variables, called principal component (PC) scores, was obtained with PCA, so that the first PCs retained most of the variation from the original dataset.

From the PCA, M main PCs  $\mu_j$  ( $j = 1, M$ ) were retained. Then for a subject, the vector  $\Psi$  containing coordinates of p vertices and q landmarks can be expressed:

**Equation 8**

$$\Psi(1:p+q) \approx \bar{\Psi}(1:p+q) + \sum_{j=1}^M c_j \mu_j(1:p+q)$$

where  $\bar{\Psi}$  is the average from the sample data sets and  $c_j$  is the jth PC score.

A linear regression was performed between the M PC scores  $[C]_{N \times M}$  and K predictors (Allen et al. 2003b).

**Equation 9**

$$[a]_{(k+1)*M} = \text{inv}([P]_{N*(K+1)}) * [C]_{N*M}$$

where  $[P]$  is the matrix containing the  $K$  predictors for the  $N$  subjects. Knowing the predictors from a new subject, the PC scores  $c_j$  could be obtained by

**Equation 10**

$$c_j = a_{0j} + \sum_i^k a_{ij} P_i$$

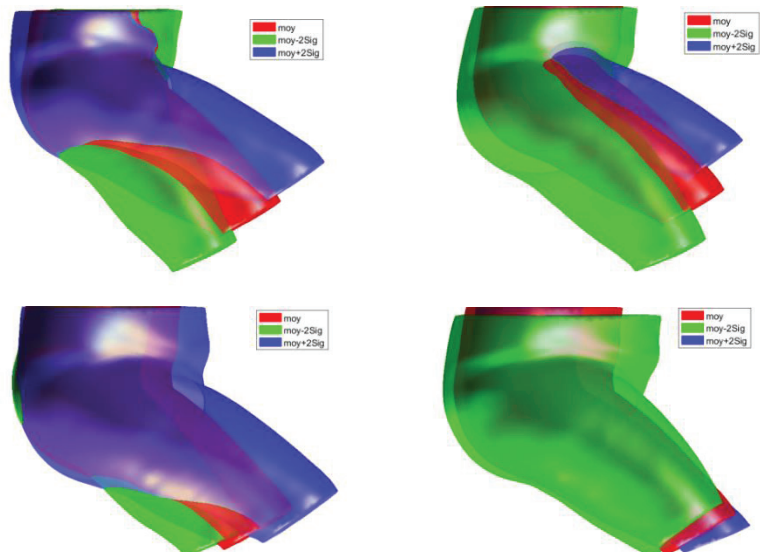
Then the external shape of the buttock-thigh complex and the bony landmarks of the pelvis and femur can be predicted thanks to (1).

## 1.2 Results

### 1.2.1 PCA model

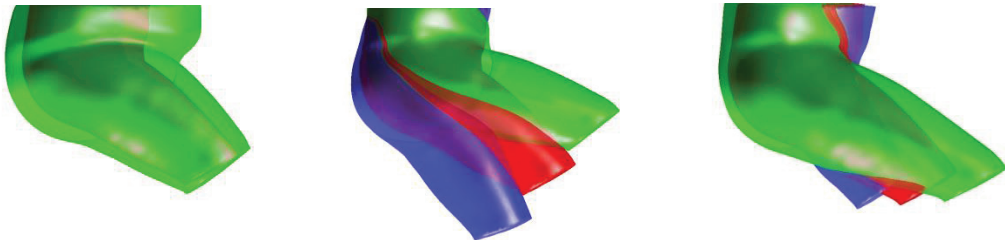
A PCA was performed on the 36 external thigh-buttock shapes placed in the pelvic reference system. The 9 first PCs accounted for 95% of the variance in data. Consequently, only the 9 first PC were kept to express the scan data.

Figure 40 shows the shape variation along the first 4 PCs which account for 88% of total variance. The shape variation along the 1st and 2nd PC could mainly be explained by trunk-leg angle and leg length. The 3rd and 4th components were mainly related to BMI.



**Figure 40:** Shape variation along the first 4 PCs (from 1st PC to 4th PC), red = average, blue = average +  $2\sigma$ , green = average -  $2\sigma$

Stature, BMI, gender and torso-thigh angle were selected as predictors. Figure 41 shows the effects of BMI, pelvis-femur angle and stature.



**Figure 41: Influence of BMI and Leg angle and stature as predictors. The predictions for the mean (red), mean + 2 standard deviations (blue) and mean – 2 standard deviation (green) are compared for each predictor**

### 1.2.2 Surface shape and bony landmarks prediction: leave-one-out validation

A leave-one-out procedure was performed using the meshes from the 36 subjects to evaluate the prediction of the external shape. The PCA regression was first built from  $n-1$  subjects, then the external shape and the bones landmarks of the  $n^{\text{th}}$  extra subject were predicted using this regression. This procedure was iteratively repeated until each subject had been considered as an extra subject once. To estimate the accuracy of the predicted surface, two errors were computed: distance between predicted and palpated landmarks, and distance between the predicted and scanned surfaces. Errors in anatomical landmarks are described in (Table 9: Means and standard deviations of the differences (in mm) between predicted and palpated distances from the 36 leave-one-out tests). The smallest errors were obtained for the two iliac landmarks (RIAS, LIAS) as they were used to align the scans. The two lateral femur epicondyle (LFLE, RFLE) had the largest errors.

**Table 9: Means and standard deviations of the differences (in mm) between predicted and palpated distances from the 36 leave-one-out tests**

	Mean $\pm$ Std
RIAS (Right Ilium Anterior Spine)	9.6 $\pm$ 8.6
IP (Ilium Pubic)	27.7 $\pm$ 15.9
RIPS (Right Ilium Posterior Spine)	20.2 $\pm$ 14.9
RICT (Right Ilium Crest Tubercle)	25.4 $\pm$ 15.5
RHJC (Right Hip Joint Center)	19.1 $\pm$ 13.4
LSJC (Lumbo Sacral Joint Center)	15.5 $\pm$ 7.7
RIIT (Right Ilium Ischial Tuberosity)	23.7 $\pm$ 13.4
RFLE (Right Femur Lateral Epicondyle)	30.2 $\pm$ 14.9
RFME (Right Femur Medial Epicondyle)	23.7 $\pm$ 12.3
All	21.7 $\pm$ 6.2

**Table 10: Means and standard deviations of the differences (in mm) between predicted and palpated distances from the 36 leave-one-out tests**

Lengths	Mean $\pm$ Std
Pelvis width between ASIS (L1)	19.2 $\pm$ 17.2
Pelvis width between Ischioms (L2)	10.2 $\pm$ 8.6
Pelvis height between mid of ASIS and mid of ischioms (L3)	11.6 $\pm$ 7.9
Pelvis depth between mid of ASIS and mid of PSIS (L4)	17.9 $\pm$ 15.3
Right Hip joint - mid of epicondyles (L5)	16.5 $\pm$ 14.6

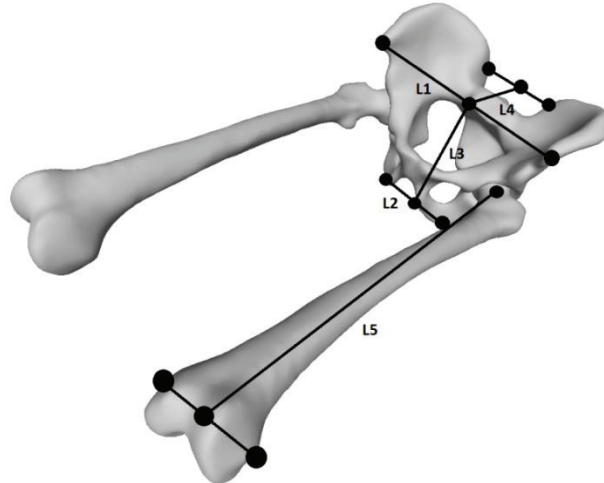


**Figure 42: Chosen distances between landmarks**

The distances characterizing the pelvis (width, height and depth) and femur (length) dimensions are summarized in Table 9. All dimensions had an error under 20 mm on average. The smallest error was found for the distance between the two ischial tuberosity, while larger errors were found for pelvis width and depth.

The distance between predicted and corresponding scanned vertices for each subject was also calculated. Then the distances of all the vertices over the entire surface was calculated. The average of the mean distances between the predicted and measured external shape was  $26.6 \pm 9.3$  mm (std of the all means) over the 36 subjects. Figure 43 shows the mean 3D distances between the predicted and scanned external shape over the 36 subjects on the template. The large error areas are mainly located on the groin, the belly and the knees.

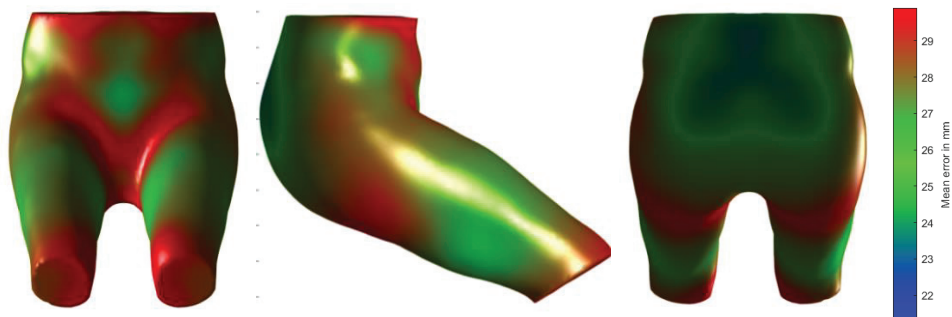


**Figure 43: Mean error between predicted and real shape over the 36 subjects**

To appreciate the prediction error in another way, sections of the shape were also compared. A first section was applied on the scan in the coronal plane (calculated with the pelvis landmarks) with the origin at the hip joint center (see Figure 44). A second section was applied in the sagittal plane with the same origin.

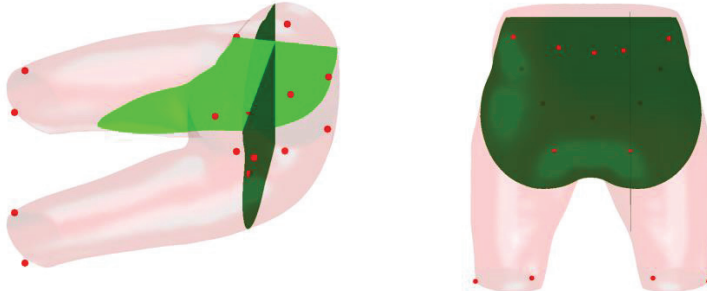


**Figure 44: Sagittal and coronal sections (in green) on a subject scan**

The areas of these two sections were calculated for the scan data and the predicted surface. Then an error percentage of the predicted area was calculated. The mean error percentage for the 36 subjects was  $9.17 \pm 7.41\%$  for the coronal section and  $8.67 \pm 9.14\%$  for the sagittal section. This percentage was greater than 20% for a few subjects; but it remained mainly under the 10%.

### 1.3 Discussion

The strong influence of anthropometry on the sitting contact pressure found in the literature implied that the model should consider the anthropometry variations. The developed parametric shape model of the thigh-buttock complex allows simulating the anthropometric variations. Its prediction of skin surface was evaluated with a leave-one-out process. A mean error of  $26.6 \pm 9.3$  mm was found for the shape prediction. This error was a bit high compared to other parametric models. For example, Kim et al. (2016) calculated an error between  $11.98 \pm 6.59$  mm and  $12.90 \pm 6.88$  mm depending on the position for their parametric shape model of the shoulder. Bd et al. (2017) found a root mean square error across the scan with their parametric seated child model of  $9.5 \pm 2.2$  mm and an error of  $17.35 \pm 3.43$  mm for the prediction of 95<sup>th</sup> percentile.

The local parameters (thigh section, waist section, hip width or thigh length) were also used as predictors instead of global ones. Surprisingly local parameters based models predicted similar or even worst results. A mean error of shape prediction of  $26.4 \pm 10.67$  mm was found with thigh section, waist section, hip width, thigh length and gender as predictors (see Appendix 4). These results can be explained by the strong correlations between the different parameters. Most of the local parameters are strongly linked to BMI or stature. For example, correlations coefficients between the waist section and the BMI, the thigh section and the BMI are respectively 0.72 and 0.87. It means that global shape is as far linked to the BMI or stature as to the local measurements such as hip width, thigh length, waist circumference or thigh circumference.

The developed parametric model contains skin shape but also bones landmarks of pelvis and femur. A leave-one-out validation was performed on these landmarks. An average error of  $21.7 \pm 6.2$

mm was found for the landmark prediction over the 36 subjects. This error was a bit higher than the one found by Nerot et al. (2016) who predicted the internal spine skeleton from the external body shape. The average of the residual distances between predicted and real points found by Nerot et al. (2016) were between 12.5 mm and 14.7 mm depending on the method. However, in our case, the predictors were global (stature, BMI, gender) whereas they were local (external shape) in Nerot study. Predicted distances between landmarks were also compared to measured distances. For example a mean error of pelvis width prediction of  $19.2 \pm 17.2$  mm was found. This prediction was better than in the study of Reed et al. (2009) who found an error of 27 mm in the pelvis width for the prediction of 6 years old child.

One of the main limitations of this study was the limited number of subject. A larger sample would allow developing specific model for each gender. Indeed, the shape variation can differ depending on the gender. Our model contains data from the two genders mixed. Nevertheless, thanks to important variability between subjects, regressions with high correlation between the principal components of the model and the anthropometric parameters have been found, allowing to represent the anthropometric variability accurately.

## 2. Part 2: Prediction of bones surface from bones landmarks

The previous part described the development of a parametric model which can predict the skin shape of the thigh-buttocks complex and bones landmarks of the pelvis and femur. However, to develop a FE model of the buttock-thigh complex, bones shapes are also needed. Consequently, surface of a template has to be deformed thanks to the bone landmarks. Two methods were tested to adjust bone shape to the landmarks: a kriging method which deforms a template geometry and a method based on a PCA model of the bones geometry. These two methods will be described. The objective is to finally obtain a method to predict both bones surfaces and skin surface from external predictors (anthropometric and posture parameters).

### 2.1 Method

#### 2.1.1 Kriging

Kriging was applied to a template with landmarks digitally palpated on the scan of the 41 cadaveric pelvis used as control points. Then for each pelvis, the surface of the deformed template and the surface of the scan were compared. To compare the meshes, the same template was deformed towards the scan using the same methodology as for the skin with the mHBM software. Then, surfaces can be compared vertex per vertex. Finally the average of the mean distances between the scaled bones and the scan was  $12.53 \pm 3.22$  mm over the 41 subjects.

#### 2.1.1 PCA model based on CT data

The second method was based on the PCA of 41 pelvic and femur surfaces extracted from CT scans from the ULB (Université Libre de Bruxelles) (Peng et al. 2015). PC models were obtained from the 3d data, processed as described in the previous section (Valgalier, 2016) and were used to predict the pelvis shape from the 12 pelvis landmarks and the femur shape from the 3 femur landmarks (two epicondyles and joint center).

## 2.2 Results

### 2.2.1 Kriging method

Kriging was applied to a template with landmarks digitally palpated on the scan of the 41 cadaveric pelvis used as control points. Then for each pelvis, the surface of the kriged template and the

surface of the scan were compared. To compare the mesh, the same template was deformed towards the scan using the same methodology as for the skin with the mHBM software. Then, surfaces can be compared vertices per vertices. Finally the average of the mean distances between the scaled bones and the scan was  $12.53 \pm 3.22$  mm over the 41 subjects.

## 2.2.2 PCA method

The method using PC model developed with the 41 scans to predict the bones surfaces from the landmarks was evaluated by a leave-one-out process. The PCA model was first built from n-1 subject, and then the pelvis shape of the n<sup>th</sup> extra subject was predicted using the digitally palpated bones landmarks. Then for each subject, the error between the palpated and predicted landmarks was computed. The error between the original surface and predicted surface was also computed. Figure 45 shows original bone of one subject (in grey) compared to the predicted bone (in yellow).

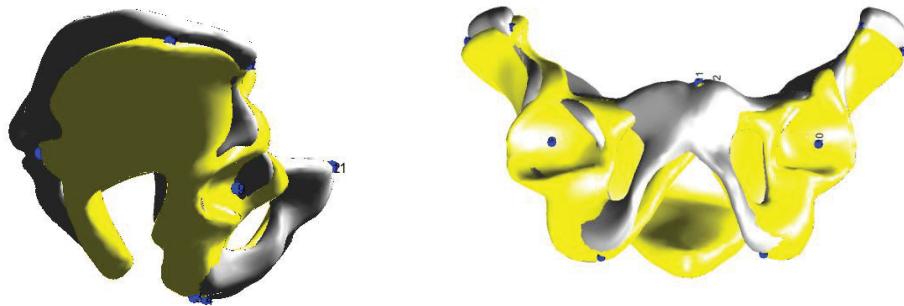


**Figure 45:** Scaled bone (yellow) compared to the original scan (grey)

The PCA model was built with 9 principal components, which explained 95% of the variance. This permits to have a reduced size of dimensions, while keeping an accurate representation of the possible variations. The error prediction for each landmark with 9 PCs is summarized in Table 11. The average of the mean error for the 6 landmarks over the 41 subjects was  $5.7 \pm 1.6$  mm.

**Table 11: Means and standard deviations of the distances (in mm) between predicted and digitally palpated bones landmarks**

	Mean $\pm$ Std
RIAS (Right Ilium Anterior Spine)	$2.5 \pm 1.9$
IPJ (Ilium Pubic Joint)	$5.9 \pm 3$
RIPS (Right Ilium Posterior Spine)	$6.3 \pm 3.3$
RICT (Right Ilium Crest Tuberclle)	$7.4 \pm 4.1$
RHJC (Right Hip Joint Center)	$5.7 \pm 2.6$
RIIT (Right Ilium Ischial Tuberosity)	$6.7 \pm 3.2$
All	<b><math>5.7 \pm 1.6</math></b>

The error between the original and predicted surfaces was also computed with 9 PCs. The average of the mean distances between the scaled bones and the scan was  $9.4 \pm 3.7$  mm over the 41 subjects.

A similar error was found when using the kriging method (see Appendix 8).

To assess the accuracy of the pelvis shape prediction from palpation, the predicted shape of one subject was compared to the real surface of his pelvis segmented from MRI images (Figure 46). The mean distance between each vertex of the two surfaces was  $20.48 \pm 12.48$  mm.

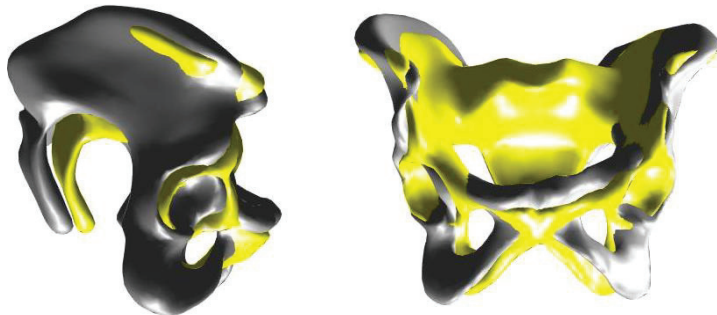


**Figure 46:** Predicted surface from palpated landmarks (grey) and original pelvis from MR images (yellow)

To estimate the accuracy of the parametric model, the real pelvis shape of this subject was also compared to the surface predicted by the parametric model with the anthropometric parameters (Stature, BMI, gender). The mean distance between each vertex of the two surfaces was  $6.52 \pm 4.22$  mm.

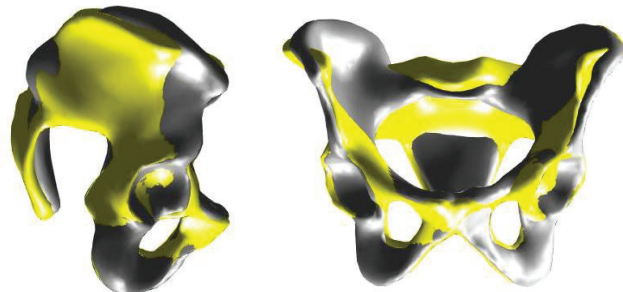


**Figure 47:** Predicted surface from anthropometric parameters (grey) and original pelvis from MR images (yellow)

## 2.3 Discussion

Two methods were tested to estimate the bones shape from the landmarks and it appeared that the methods based on the statistical analysis of data from CT scans gave better results. The average of the mean shape prediction error was of  $9.4 \pm 3.7$  mm with the PCA method, instead of  $12.53 \pm 3.22$  mm with the kriging method. Consequently the PCA method will be used to predict the bones shape. In the literature, very low errors were also found with this approach, for example (Bryan et al. 2010) found a mean Euclidian distance error of 1 mm for the femur prediction. The validity of the shape prediction

from landmarks was evaluated but the prediction of the shape from the anthropometric parameters was not evaluated because no data were available on the subject bones geometry.

Two approximations could be a source of error for the bone prediction. First manual palpation of the bony landmarks may reduce the level of accuracy, especially for people having an important thickness of adipose tissue. Secondly, bones on which the PC model was based didn't cover the anthropometry variety of the subject used for this study. Consequently, bones shape prediction can be sometimes based on extrapolation. To evaluate the bone shape prediction of the parametric model, it should be compared to the pelvis shape obtained by medical imaging. This has been done with only one subject. The mean shape error for this subject was only  $6.52 \pm 4.22$  mm. Clearly validation should be continued with more subjects.

Finally the main limitation comes from the fact that the bones geometry of the subjects could not be acquired simultaneously. Bones geometry was indirectly estimated from palpated bones landmarks and then combined by using the PC models previously developed with another data set. Merging two datasets from two different samples may be an issue.

### 3. Part 3: Parametric FE model and its validation

#### 3.1 Introduction

In the precedent sections, a method to predict bones (pelvis and femurs) from a few predictors like gender, stature, BMI and posture have been detailed. From this prediction, the goal was to develop a FE model to simulate the human body seat interaction in particular the contact pressure on the seat. This chapter presents the method to create the FE model from the predicted surfaces. To validate the FE model, pressure data was collected from 13 differently sized persons chosen among the 36 participants of the skin surface data collection. The simulated pressures with the parametric FE models were compared to the measured ones.

#### 3.2 Personalized finite element model creation

##### 3.2.1 Mesh creation

From the target values of the predictors for a person, the bones and skin surfaces were predicted by the statistical shape model previously described. A volumic mesh has to be built between the two surfaces to represent the soft tissues. A template mesh was developed from one subject (female, 25 year old, 1.70m, 60 kg). This template contained the bones meshed with triangular shells of 5 mm-length and the soft tissues meshed with tetrahedronelements of 5mm-length . All the vertices of the predicted surfaces were the target landmarks for kriging the volume mesh. Then, the FE mesh of a specific person was generated by deforming the template through a kriging approach. For this, all the nodes of the surface mesh (bones and skin surfaces) were used as control points. All the vertices of the predicted surfaces were the target landmarks for kriging the volume mesh. At the end, a volume model was obtained perfectly matching with the predicted surfaces of the bones and skin surface (Figure 48).

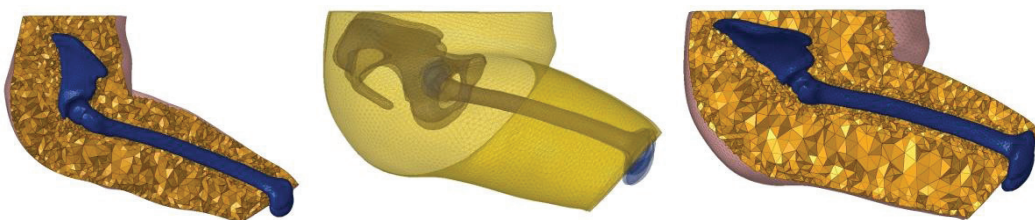
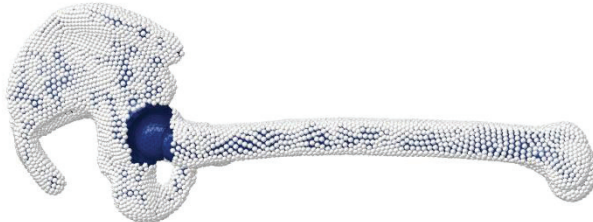


Figure 48: template mesh, target surfaces, template scaled to the surface

To avoid possible inter penetration of the bones surface at the hip joint, nodes of the femoral head and the acetabulum were excluded from the control points set of the kriging approach (nodes not in white on Figure 49). To avoid too large elements deformations at the intersection between the skin

and bone tissue at the knee, nodes on the knee plane section of the skin were also removed from the set of control points.



**Figure 49: control points on bones**

### 3.2.2 Soft tissues material properties

According to the sensitivity analysis of the chapter 2, a linear elastic law is sufficient to estimate the pressure on the seat. Consequently, a linear elastic law with a Young modulus of 30 kPa was used to model the soft tissues. A Mooney Rivlin hyperelastic law was also tested on all the subjects, with equivalent parameters. The obtained results were very similar (see Appendix 8), which confirmed the results of the sensitivity analysis. Consequently the linear elastic law was used because it reduced the computation time compared to the hyperelastic law. A linear elastic law with a Young modulus of 150 kPa was used for the skin. Bones were modeled as rigid bodies.

## 3.3 Comparison of the interface pressure predicted by the parametric FE model and experimental data

### 3.3.1 Data collection

Data was collected from 13 participants, whose stature, weight and BMI are listed in They were chosen among the subjects who participated to the collection data for building the parametric model to cover a wide variety of anthropometry.

**Table 12: Participants characteristics**

Subject	Gender	Weight (kg)	Stature (cm)	BMI (kg/m <sup>2</sup> )
1	M	108.4	1855	31,5
2	F	57.3	1635	21,4
3	F	45.6	1545	19,1

4	M	98.8	1795	30,7
5	F	87.6	1630	33,0
6	F	78.7	1630	29,6
7	F	52.5	1510	23,0
8	M	88	1680	31,2
9	F	88.8	1650	32,6
10	F	51.8	1560	21,3
11	M	104	1780	32,8
12	M	122.2	1850	35,7
13	F	97.2	1570	39,4
Mean ± (Std dev)		83.1 ± 24	1668 ± 116	29.3 ± 6

After the bones palpation (previously described), the participants were equipped with 46 reflective markers (Figure 50), the pelvis cluster remained on the sacrum. They were asked to take a sitting anatomical position (sitting on a stool with arms raised). The reflective markers positions were recorded with the Vicon Nexus system. These data were used to calculate the distance between knee and pelvis markers and the hip and lumbosacral joints.

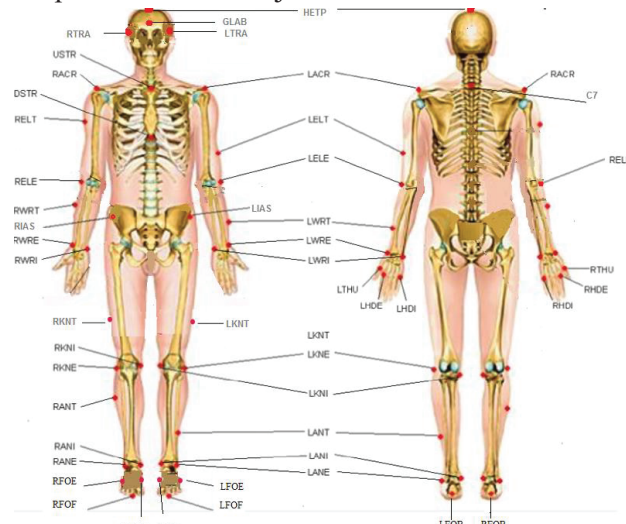


Figure 50: Vicon markers placement

Then, the participants were asked to test a seat configuration simulated by a newly built multi-adjustable experimental seat (Beurier et al, 2017). This experimental seat is composed of four main structural components (Figure 51): the supporting frame (A), seat back frame (B), seat pan frame (C) and foot support (D). There were three movable panels fixed on the seat back frame (B), providing support on the lumbar, thoracic and neck region. Each panel could rotate freely and its position was controlled by two electric actuators. A uni-axial force sensor was mounted on the axis of each actuator, allowing force measurement on each panel in the xz plane. The global contact force at the seat pan surface in the symmetric plane was measured.

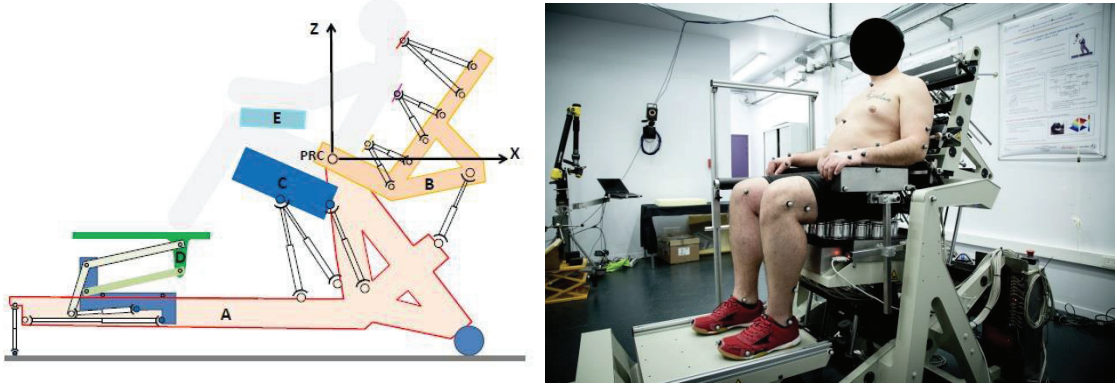


Figure 51: Experimental seat

A uniform foam used in the cushion of an aircraft seat (Z301) with a thickness of 7 cm was placed on the flat seat pan. A pressure map as the one previously used was placed on the foam. The backrest inclination was set to 20° relative to the vertical and seat pan inclination was set to 5° relative to the horizontal. The lower, middle and upper back supports were placed respectively on the L3 lumbar vertebrae, the T9 vertebrae and the occipital bone. The fore-aft position of the lower (lumbar) and upper (head) supports were self-selected by participants themselves. Once comfortably seated, markers position, pressure distribution and contact forces were recorded at the same time.

### 3.3.2 Model positioning

First, the hip joint and lumbosacral joint centers were estimated from the position of four markers attached at the pelvis (RIAS, LIAS) and knees (LFLE, RFLE). For this, first the distances between these four markers and joint centers were estimated by palpation (as previously described), then based on the markers position, the joint centers position could be calculated by finding the intersection of the three distances in the sitting position by optimization.

The pelvis and femur on the seat were then positioned using the estimated joint centers, allowing the calculation of the angle between pelvis and femur. Thanks to the parametric model developed previously, the surfaces of the bones and skin of the subject were then predicted using the 4 parameters: gender, stature, BMI and pelvis-femur angle in the sagittal plane (the two other angles were fixed for all the subjects).

The corresponding FE model was built from the surfaces as described in 2.1. It was positioned on the seat surface by rotation to have the right angle between the pelvis and the seat surface.

### 3.3.3 Foam properties

The material properties of the foam were experimentally tested. Compression tests were conducted with a sample of 5 x 5 x 7cm<sup>3</sup> using the Itron mechanical test machine (Figure 52 Foam compression test. Both loading and unloading were performed at two different speeds: 0.07 mm/s and 4.8 E-5 mm/s. Results for the two speed conditions were similar. The loading and unloading curve is shown in Figure 53.



**Figure 52 Foam compression test**

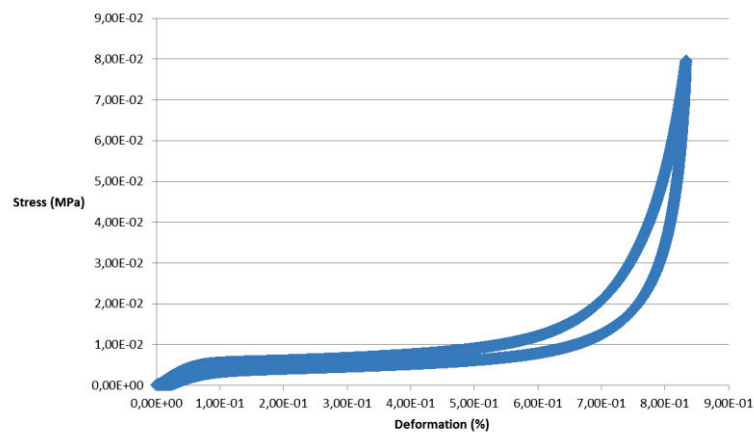


**Figure 53: Compression (Stress-deformation) curve of the foam**

The foam material behavior can be implemented in the FE software with a tabulated law, i.e. the curve are specified in the material model.

### 3.3.4 FE simulation

The following boundary conditions were defined: bones were blocked and a displacement was applied to the seat in the direction of the global force measured on the seat pan. The simulation was stopped when the total contact force on the seat pan reached the force measured by the sensor of the experimental seat.

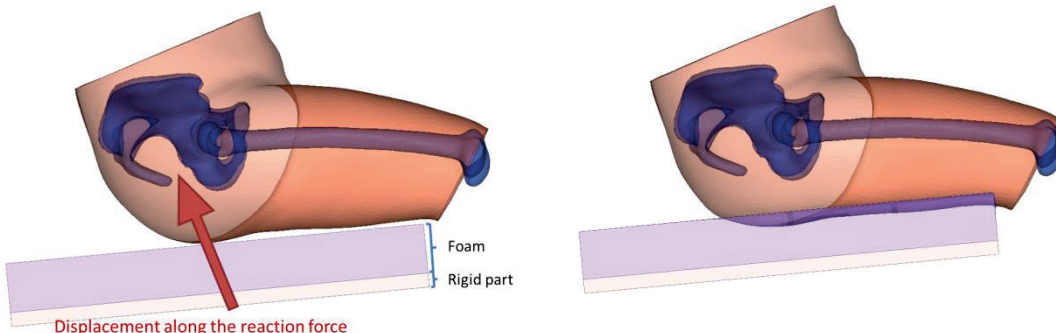


**Figure 54: Model boundary conditions (left: initial state, right: final state)**

### 3.4 Results

The measured pressure map was compared with the simulated pressure map with the corresponding model. 4 parameters were compared: mean pressure (Pmean), maximal pressure (Pmax), contact area and maximal pressure gradient. The maximal gradient was calculated on the pressure profile where all the 60 cells of a row were summed (see chapter 2). The percentage of error of these values between measurement and simulation are expressed in Table 13.

**Table 13: Percentage error between measured and simulated pressure values**

	Pmean (kPa)	Pmax (KPa)	Contact area (cm <sup>2</sup> )	Experimental values		Error percentage (%)	
				Gradient max(kPa/c m)	Pmean	Pmax	Contact area
SUB019	5,19	12,67	1524,19	74,09	37,8	4,42	27,76
SUB021	4,3	11,71	1014,52	37,48	42,21	31,34	27,95
SUB024	4,63	13,34	753,23	36,33	45,88	16,79	30,7
SUB026	5,03	8,4	1414,51	43,66	34,69	14,29	15,45
SUB027	4,59	9,41	1493,55	58,03	33,74	15,52	26,68
SUB028	4,61	8,61	1337,1	32,96	39,6	0,93	25,29
SUB029	5,05	11,87	822,58	48,8	21,7	28,81	22,56
SUB030	6,12	13,26	1058,06	54,52	40,54	33,48	25,43
SUB031	4,68	10,28	1390,32	42,02	61,74	29,38	39,87
SUB032	4,49	9,36	727,42	46,23	33,39	17,63	21,92
SUB033	5,09	9,42	1416,13	43,34	33,03	13,91	17,66
SUB034	5,33	10,69	1562,9	59,82	31,07	9,64	21,75
SUB035	4,18	9,09	1574,19	48,87	49,75	2,53	37,11
All	4,88 ± 0,49	10,39 ± 1,76	1270,32 ± 310,78	48,16 ± 11,24	38,86 ± 9,87	16,82 ± 11,06	26,16 ± 6,9
							34,01 ± 12,89

The lowest error was obtained for the maximal pressure (average error of  $16.82 \pm 11.06\%$ ). The highest error was for the mean pressure (average error of  $38.86 \pm 9.87\%$ ), which was systematically overestimated by simulation. This is linked to an underestimation of the contact area (average error of  $26.16 \pm 6.9\%$ ). When looking at the profile pressure (see Appendix 5), curves shapes were globally fitting between experimental and simulation. It was observed that the simulated pressure profile was always above the experimental curve. This phenomenon is also linked to the underestimation of the contact area which implies a greater pressure. Nevertheless, by visually comparing the pressure map (see Appendix 6), the model seemed able to simulate the subject variability.

Strong linear relationships were observed between different contact pressure values and stature or BMI both experimentally and by simulation. The two strongest correlations were found between BMI and the measured contact area (Figure 55) or the normalized mean pressure (Figure 59). Then high correlation was found between the normalized (by the person weight) maximal pressure and the BMI.

The relationships obtained between the anthropometric value and the pressure values are coherent with the literature. The found correlation coefficients between contact area and BMI are close to those

previously found in literature (Vos et al. 2006; Paul et al. 2012). The correlation found between the normalized maximal pressure and BMI ( $R^2=0.75$ ) was really closed to the one found by Moes (2007) ( $R^2=0.73$ ). Furthermore, a correlation between the contact area, maximal pressure, mean pressure, maximal gradient and BMI or stature was expected. Indeed, the higher BMI is, the more a subject has fat tissues. Therefore he/she has more tissue in contact with the seat. If the adipose tissues distribute more the pressure and reduce the maximal pressure, it induces a decrease of the maximal gradient and an increase of the mean pressure. Likewise, the taller is the subject the longer are the thigh and the greater is the contact area is

It was observed that similar relationships were found between the different parameters with the model and the measurements. The closest relationships between the experimental observations and the simulations were between the mean pressure and the BMI or between the maximal gradient and the BMI. The contact area was found closely related to stature and BMI. An offset is always observed between the simulation and measurement curves. An offset of  $138 \text{ cm}^2$  between the simulation and measurement curves of contact area function of BMI was found. The offset was of  $592 \text{ cm}^2$  for the contact area as a function of the stature. The contact area is underestimated with the simulation. If the simulation underestimates the contact area, it overestimates the mean pressure (offset of  $0.05 \text{ kPa/kg}$  for the curve of mean pressure function of the BMI). In the same way, the simulation overestimates a bit the maximal gradient (offset of  $0.37 \text{ kPa/(cm*kg)}$  for the curve of max gradient function of BMI).

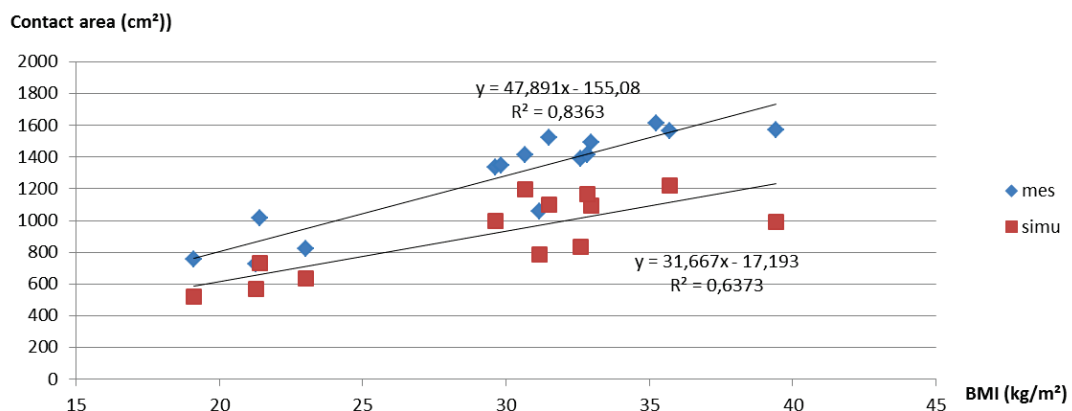


Figure 55: Contact area function of BMI for simulation (simu) and experimental measurement (mes)

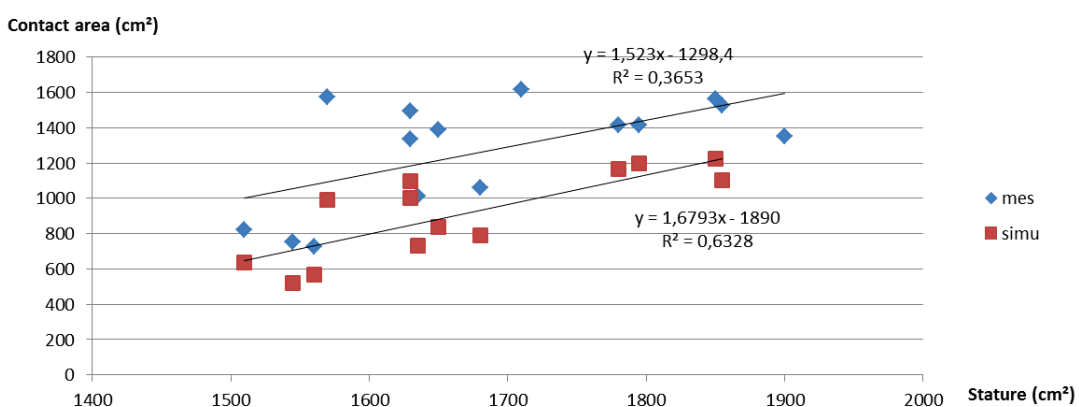


Figure 56: Contact area function of stature for simulation (simu) and experimental measurement (mes)

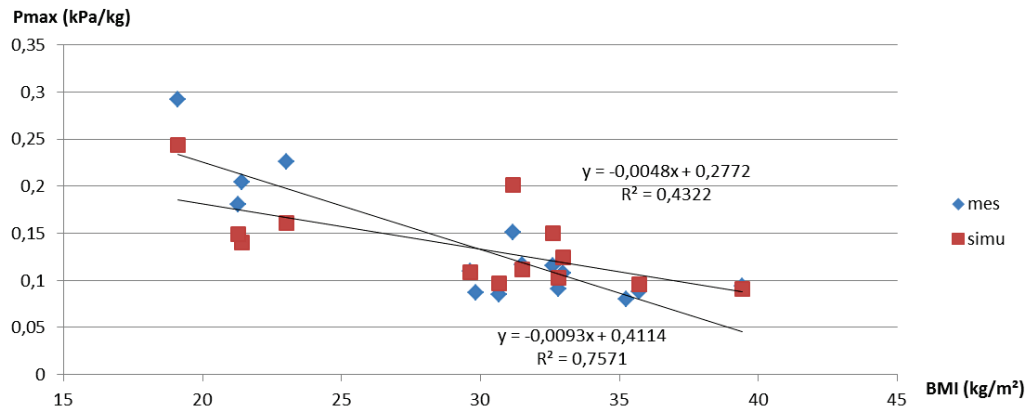


Figure 57: Maximal pressure (kPa) normalized by the subject weight (kg) function of the BMI

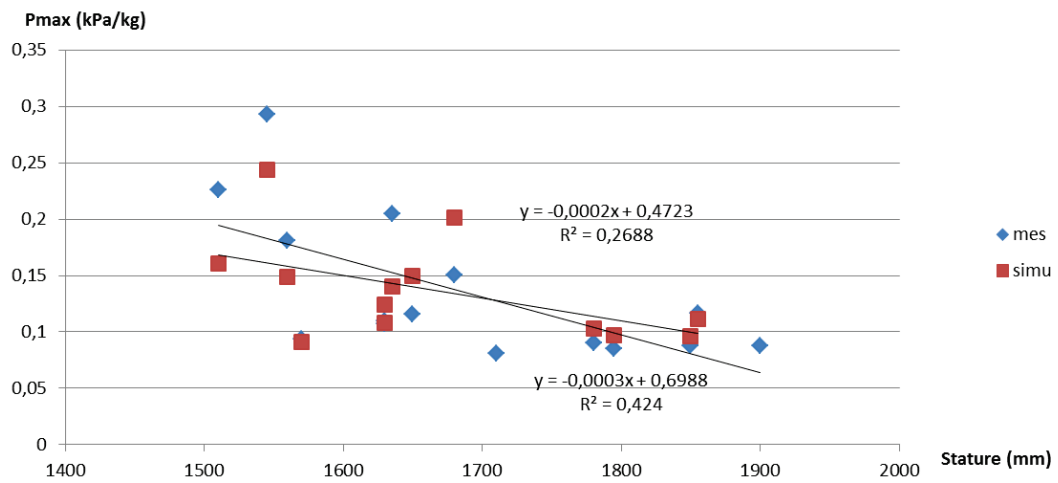


Figure 58: Maximal pressure (kPa) normalized by the subject weight (kg) function of the stature

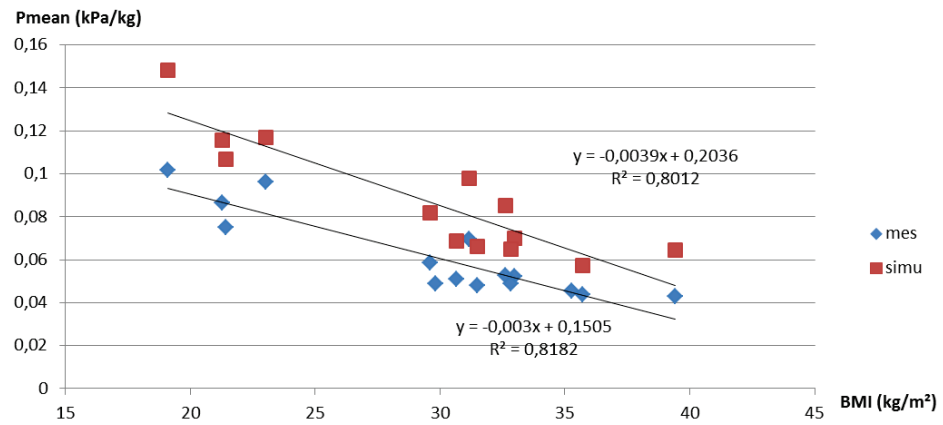


Figure 59: Mean pressure (kPa) normalized by the subject weight (kg) function of the BMI

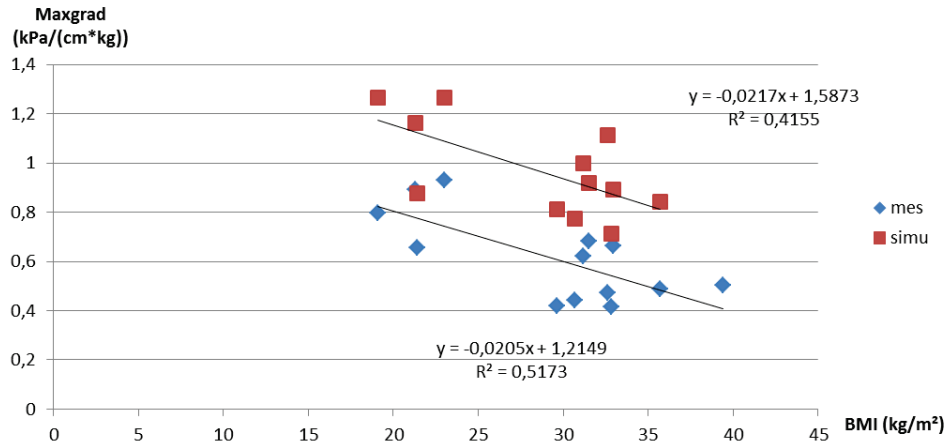


Figure 60: Maximal gradient (kPa/cm) normalized by the subject weight (kg) function of the BMI

### 3.5 Discussion

The simulations with the subject specific FE models, created using the parametric shape model developed in the present thesis, were compared with experimental data. If the absolute values showed important errors (max 62 % for the mean pressure, max 33% for the maximal pressure, max 37% for the contact area, max 58 for the maximal gradient), the results show the the model can simulate the influence of the anthropometric parameters. Relations between the anthropometry (stature and BMI) and contact pressure values (mean pressure, maximal pressure, contact area and maximal gradient) were similar with experimental and simulations results. Nevertheless, simulations provided a constant offset compared to the experimental value. Contact area was underestimated which led to an overestimation of the mean pressure. These errors are probably due to two factors. The first is probably linked to the material properties of the tissues which may be too stiff. The chosen elastic parameters may not be appropriate and should be subject-specific. To give a better estimation of the absolute pressure values, a parametric study could be performed on the material parameters with data of the 13 subjects. The second error may come from an error of model positioning on the seat. The model is positioned according to the position of the reflective markers. The soft tissue artefacts could be high especially for the subjects with a high BMI. Consequently, the estimated position can be far for the real position of the bones. This can be observed on some subjects for whom the estimated bone positions look abnormal and the difference of pressure distribution highlighted a wrong leg positioning (Figure 61).

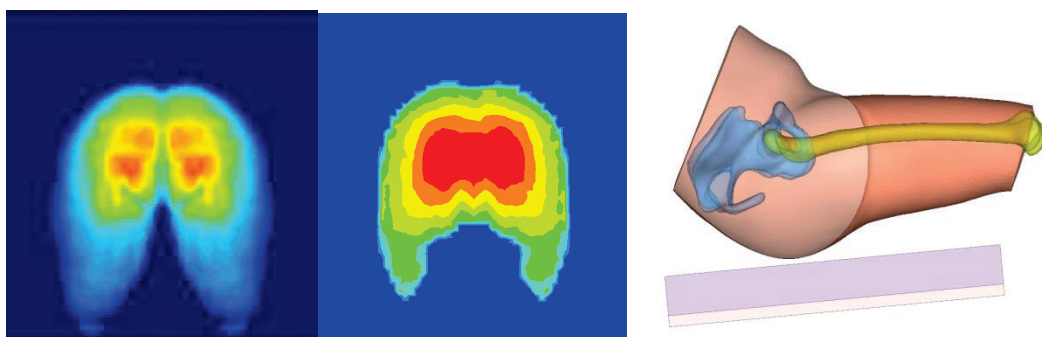


Figure 61: Measured (left), simulated (middle) pressure distribution and bones position of the subject 31

Nevertheless, the objective of this parametric model was not to simulate specific cases with one specific subject but to be able to simulate a wide range of configurations with a wide range of anthropometry.

#### 4. General conclusion

In this chapter, a parametric geometric model of the thigh-buttock complex containing both skin and bones shape has been developed. Based on this parametric model, a FE mesh template was deformed towards a target geometry. Seating simulations of this model were confronted with experimental the pressure maps of 13 subjects. The results showed the model ability to simulate the influence of anthropometric parameters. However an important error was identified, which may be due to two factors: a wrong positioning in the seat and wrong material properties. These two problematic will be investigated in the next chapters.

# Chap 4: Coupling rigid multi-body and finite element models

## 1. Introduction

In the precedent chapter, a parametric finite element (FE) model of the thigh-buttocks complex has been developed. Boundary conditions are needed to position it and apply appropriate forces. Since the goal of the current thesis is to develop a tool for simulating virtual cases, it should be possible to use this tool without any experimental data. The purpose of this chapter is to develop a process which predicts the boundary conditions to be applied to the FE model to avoid the need of experimental data. The chapter presents a method coupling a multibody (MB) model to the FE model : MB simulations provide boundary conditions (forces and bone postures) to the FE model while the FE simulations provide new posture data to the MB model until the convergence of the results. This method associating two modeling approaches has two advantages: 1/ to provide realistic boundary conditions to the FE model and 2/ to enable the prediction of a complete set of the mechanical factors related to discomfort. As explained in the first chapter, FE simulations can predict the contact pressure or soft tissue strain and stress whereas MB simulations can compute muscular activity and inter vertebral pressure. According to the literature review, these factors are the main causes of discomfort when sitting during a prolonged period. This method coupling two modeling approaches will be described in this chapter and specific cases study will be exposed.

## 2. Coupling Method

As explained in the first chapter, the model developed by Michael Daamsgard and John Rasmussen (Damsgaard et al. 2006) in the specific software Anybody Modelling System called AAUhuman was used (<http://forge.anyscript.org/gf/>).

1/ The MB model was first scaled so that its anthropometry corresponded to the FE model dimensions. 2/ Then it was placed on the seat following specific geometric rules that will be detailed later. 3/ Contact forces and muscles forces were estimated 4/ finally, a loop between the MB simulation and the FE simulation was run. All these steps will be described here.

### 2.1 MB Model personalization

First, the pelvis and femur of the MB model have to have the same geometry than the FE model. Since the femur can be considered as a segment with one principal direction, it is basically scaled by a homothety in the femur axis direction (vector between the centers of the two epicondyles and the center of the femoral head). Since the pelvis has a more complex geometry, another method is used to

scale the bone. A non-linear Radial Basis Function (RBF) transformation, method is applied using control points. The transformation function between the original and the target landmarks is defined by:

**Équation 11**

$$f(y) = \sum_{j=1}^n c_j \varphi(\|y - x_j\|) + p_q(y)$$

Where  $\varphi(r) = \sqrt{r^2 - a}$ ,  $c_j$  are the coefficients of the RBF function  $\varphi$ , computed based on the source and target landmarks and  $p$  is a polynomial of  $q$  order.

Thanks to this transformation, the geometry of the bones is scaled to correspond to the target landmarks. The muscles attachment points and the joint center related to the bones are scaled with the same transformation. In our case, the landmarks used as the control points for the transformation were the 11 pelvis landmarks: RIAS, RIPS, RIIT, RICT, RHJC, IPJ, LIAS, LIPS, LIIT, LICT, LHJC (see previous chapter).

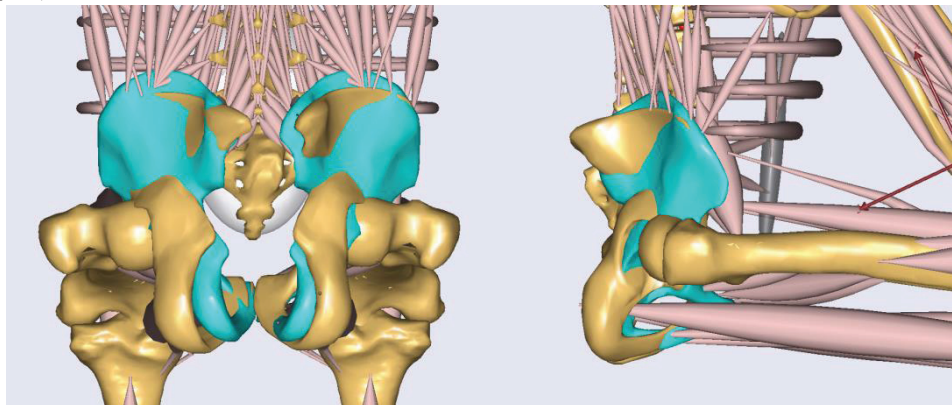


Figure 62: Morphed pelvis (in yellow) and original pelvis (in blue)

For the other parts of the body, a scaling law implemented in the Anybody software is used. Each segment, placed in his local coordinate system is scaled in the three directions with the following matrix:

$$S = \begin{bmatrix} \sqrt{\frac{k_m}{k_l}} & 0 & 0 \\ 0 & k_l & 0 \\ 0 & 0 & \sqrt{\frac{k_m}{k_l}} \end{bmatrix}$$

$k_m$  and  $k_l$  are respectively the ratio of the target mass on the initial mass and the ratio of the target length on the initial length. With this matrix, the scaling in the cross sectional direction ( $x$  and  $z$ ) differs from the scaling in the longitudinal direction ( $y$  axis) of the bones. It is based on the assumption that the cross section of the bone is linked to the mass and the length of the bones. The more the weight is important, the larger get the bone large.

Initial values correspond roughly to a 50<sup>th</sup> percentile male. The scaling can be done with joint-to-joint distance or by external distances.

Each segment's mass is calculated as a percentage of the whole weight from data provided by (Winter 2009).

Maximal muscle force is also scaled with the following law:

### Équation 12

$$F = F_{0k_m}^{2/3}$$

Where  $F_0$  is the initial muscle force.

## 2.2 MB model positioning

To position the MB model, the angles between the segments can be set directly. But it is more convenient to use marker points associated to the body segments to drive a model. The position of these markers can be provided through motion capture files for instance. The motion reconstruction is performed by solving an over-constrained reconstruction problem if the number of constraint equations is greater than the degree of freedom and an under-constrained reconstruction problem if it is lower.

In the present work, the Anybody SeatedMan model defined by (Rasmussen and Zee 2008b) was used. The spine was positioned by imposing the distance between the seat and two points of the body: the middle point between the two ischia and the T9 vertebrae (Figure 63). The feet are constrained to be in contact with the ground. Hands are also constrained to be in contact with the armrests.

The spine contained 6 joints with 3 degrees of freedom each, so the total degrees of freedom in the spine are 18. Consequently the number of constraint equations associated to the spine is too low compared to the degrees of freedom in the spine, it is an under-constrained problem. To solve this under-determinate problem, a “spinal rhythm” of the lower spine (between the pelvis and T12) is defined. This spinal rhythm is a linear combination of all the three angles between each of the following 6 joints (Pelvis-Sacrum, Sacrum-L5, L5-L4, L4-L3, L3-L2, L2-L1,) and the three angles between T12 and L1. It is based on the assumption that the passive elastic elements of the spine behaves cinematically as elastic beams (Rasmussen et al. 2009). Furthermore, an additional relationship between hip flexion and pelvis-thorax flexion is proposed with the MBSeatedMan model. A ratio of 2:1 between hip flexion and pelvis-thorax flexion is imposed (Tuby et al. 2002, Bell and Stigant 2007). If the flexion between the thorax and the thigh is  $30^\circ$ , then the hip flexion is  $20^\circ$  and the pelvis-thorax flexion is  $10^\circ$ .

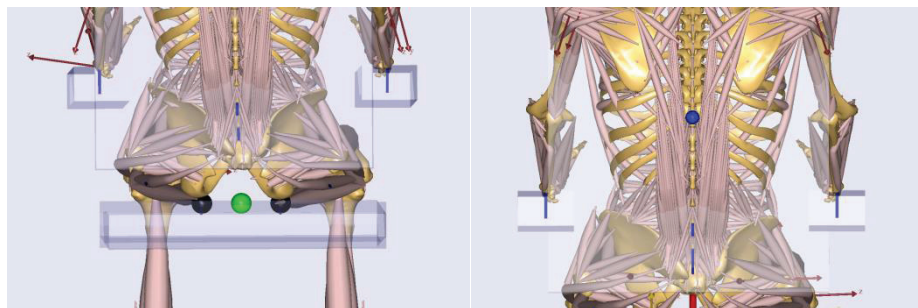


Figure 63: Landmark for pelvis position and back position (Blue point=T9 vertebrae, green point=middle point between the ischia)

These two later rules (spinal rhythm and thorax-pelvis-thighs rhythm) add positioning constraints to the model. However the model contains 44 degrees of freedom, making the number of constraints still not sufficient compare to the degree of freedom of the model. Consequently, some joint angles are fixed: pelvis-trunk joint in coronal and transverse plan, glenohumeral joint external rotation, knee flexion, elbow pronation, hip external rotation...

## 2.3 Contact and muscles forces estimation

Once the model was positioned, inverse dynamic calculations were conducted to determine the joints forces from the bones position. The muscular forces were then estimated from the joint forces and moments. Since the number of muscles is much higher than that of the degrees of freedom, there are not enough equilibrium equations to determine all individual muscle forces. This redundancy problem is solved by optimization using the min/max criteria (Rasmussen et al 2001). It minimizes the maximum of the normalized muscle forces:

**Equation 13**

$$\max \left( \frac{f_i^{(M)}}{N_i} \right)$$

$f(M)$  are the muscle forces and  $N_i$  is a measure of the muscle strength at each muscle's current working condition.

The contact forces between the seat and the body can be modeled with contact elements which provide compressive reaction and friction forces proportional to the reaction force in the element:

**Equation 14**

$$|F_f| \leq \mu R$$

Where  $F_f$  is the friction force,  $R$  is the reaction force normal to the contact and  $\mu$  is the Coulomb friction coefficient. These elements are defined as segments between multiple support points on the thighs (3 points equally distributed along each femur) and pelvis (5 points distributed around each ischium) and the seat. The reaction forces can be determined by considering them as unknown muscle forces. The normalization factors for these reaction forces are large compared to the normalized factors for the muscles (at least 10 times superior).

## 2.4 Coupling the MB and FE modeling approaches

A specific algorithm has been developed in Matlab (Mathworks, France) to associate the MB model with the FE model. The idea is to use the MB model to define the boundary conditions needed for the FE model. The MB model would be used in seating simulations to provide forces and bone postures to the FE environment. Then, the FE simulation would generate a new position of the bones due to the soft tissues and seat foam compression. Thus, it is necessary to make a loop and introduce the output bones positions from the FE simulation to the MB model (Figure 64: Loop process).

First, the MB model is positioned on the seat with the previously described contact constraints between body and seat. Then an inverse dynamic is run to estimate the joint force and moment. Pelvis and femur position are extracted to be used as the initial position for the FE model. The FE model is first positioned by simulation to correspond to this position. Then joint forces and moments estimated by Anybody are applied as FE boundary conditions to the L5/S1 joint and the knees joints, they represent the actions of the weight of the missing FE body parts (upper thorax, lower legs...). A FE simulation is run using the RADIOSS solver. At the end of the FE simulation, the new positions of the bones (knee joint, L5/S1 joint, ischia) are extracted and used to reposition the MB model. The loop is then repeated until the pelvis and femur positions converged: when the variation of the position of the pelvis or femur is less than 2 mm between two steps (i.e. a step corresponds to one loop between the FE and MB model).

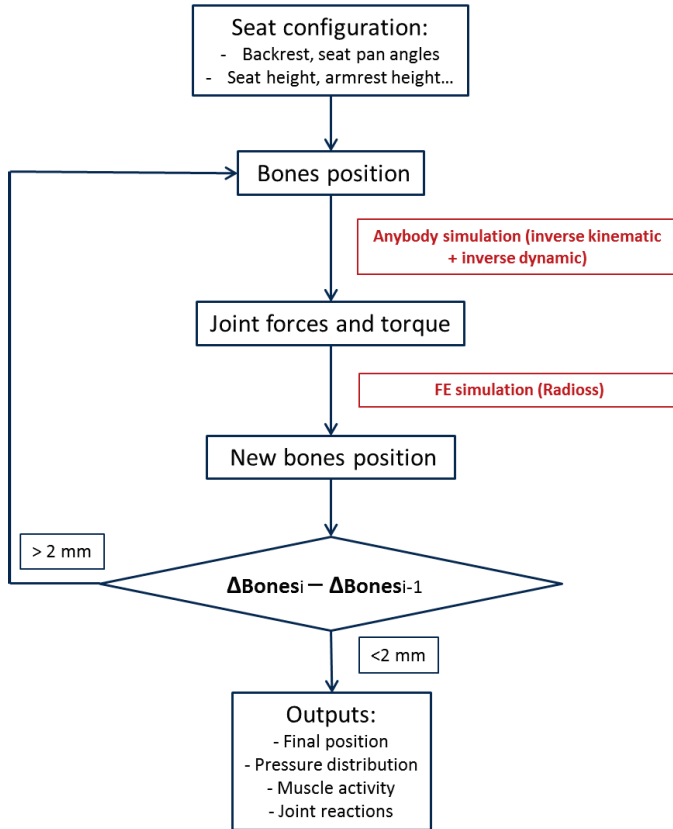


Figure 64: Loop process

### 3 Validation

The experiments described in the previous chapter were simulated with this coupling method. 6 persons from the 13 subjects were selected to have a good variety of anthropometry (Table 14).

Table 14 : Summary statistics of stature, body mass index (BMI), age and hip width of the 6 selected subjects

	Average	SD	Minimum	Maximum	Range
Stature (mm)	1666,67	132,12	1510	1850	340
BMI (kg/m <sup>2</sup> )	29,13	5,69	21,3	35,7	14,4
Age (y)	24,33	6,97	19	38	19
Hip width (mm)	346	33,25	311	393	82

The first objective was to assess the ability of the coupling method to well estimate the seat pressure distribution. Simulated and measured pressure distributions were directly compared. The second objective was to investigate the ability of the loop process to correct the bones position. It has been observed in the precedent chapter that bones position experimentally estimated with markers may not be correct. We have made the assumption that the coupling method could correct this posture, especially the knee position. The position estimated by the coupling loop differs from the experimentally one for two reasons: the initial position estimated by the geometric constraints in Anybody differs and the coupling method modifies this initial position. Consequently three different simulations have been run for each subject:

- Coupling method: Simulation without data with coupling

- No coupling simulation method: Simulation with boundary conditions based on the initial position estimated by Anybody (without coupling).
- Experimental method: Simulation with boundary conditions defined based on experimental data (without coupling, only the FE model was used)

Comparing the results of these three different cases allow investigating the effect of the coupling. Inside the coupling methods, two parameters can be studied: the effect of the initial position and the effect of the coupling loop.

### 3.1 Simulations conditions

The FE models corresponding to each subject were created using the parametric shape model previously described and the following descriptors: the gender, the stature and the BMI of the person. The MB model was also scaled thanks to the anthropometric measurements manually performed on the person. The pelvis was scaled using the RBF transformation previously described with the palpated landmarks as control points. The femur was scaled to correspond to the FE model.

The experimental seat was modeled in the Anybody Modelling system with five different parts: one backrest, one seat pan, two armrests and the ground. The seat height, seat length, seat inclination and backrest inclination were adjusted to correspond to the experiments. In all the cases, the seat pan was reclined of  $5^\circ$  and the backrest reclined of  $20^\circ$  to the vertical. The body was positioned on the seat thanks to the geometrical contact constraints described in 2.2.

A FE model of the foam was created as explained in the previous chapter.

#### 3.1.1 Coupling method

Simulations were run for each subject with the coupling process previously described. The inputs were the person anthropometry and the seat configuration (seat pan and backrest angles, seat height) (Figure 65).

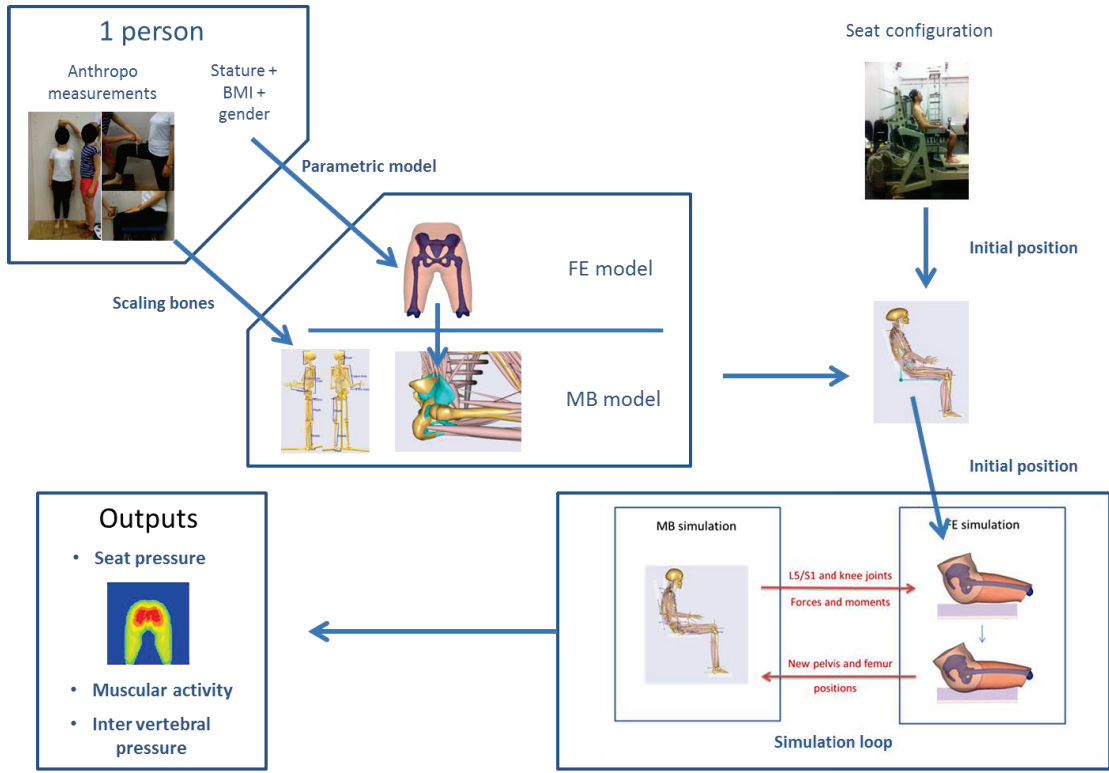


Figure 65: Process to simulate a specific case with a specific person

### 3.1.2 No coupling with initial position based on an initial Anybody simulation (simulation FE method)

To investigate the impact of the loop process, simulations of the same configurations were run without the iteration process between the FE model and the MB model. The model was positioned in the position estimated by Anybody as described before. A FE simulation was then run with the bones fixed and a displacement imposed to the seat pan. The simulation was stopped when the total contact seat force was reached (same process as in precedent chapter).

### 3.1.3 No coupling with FE boundary conditions based on experiments (experimental FE method)

This configuration corresponds to the simulations of the previous chapter except that the initial bones position differs. Here, the bones positions are defined from experimental markers positions.

The goal of this simulation case was to compare the effect of the posture predicted by simulation with Anybody or by experimental measurement (Vicon markers).

## 3.2 Coupling method convergence

All the simulations for the 6 subjects converged (according to the criterion defined previously) before 10 iterations (5 at the 5<sup>th</sup> iteration and one at the 10<sup>th</sup> iteration). Convergence was observed for the pelvis and femur position in all directions (Figure 66). For two simulations, the position of the bones oscillated (Figure 67). For these simulations, the values in between the oscillation extremum were taken. These oscillations were observed when the foot was alternatively in contact or not with the

ground in the Anybody simulation. Then the knee joint force resultant alternated between positive and negative values in the vertical axis. It leads to an oscillation of the knee.

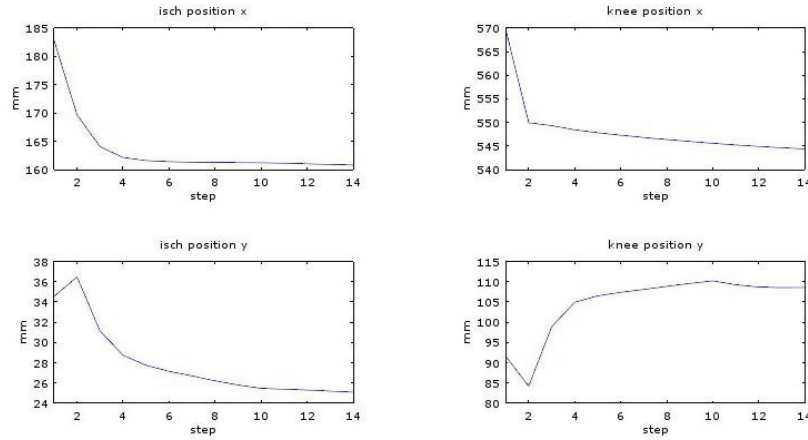


Figure 66: Ischium and knee position of a subject (sub021) along the horizontal (x) and vertical (y) axes

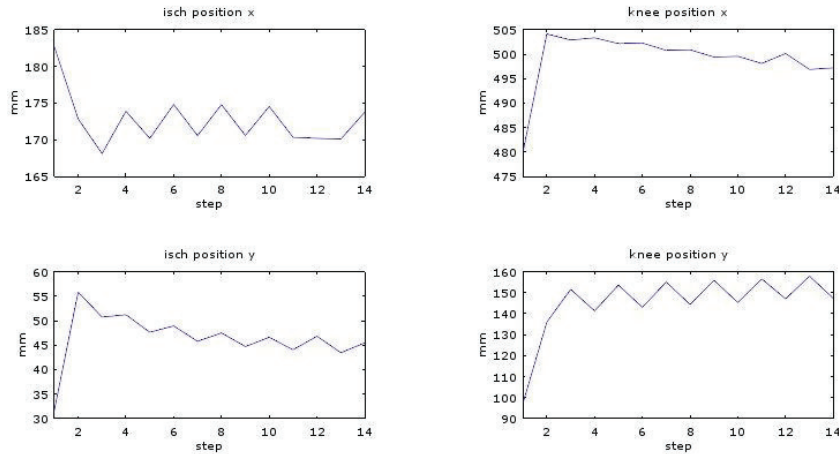
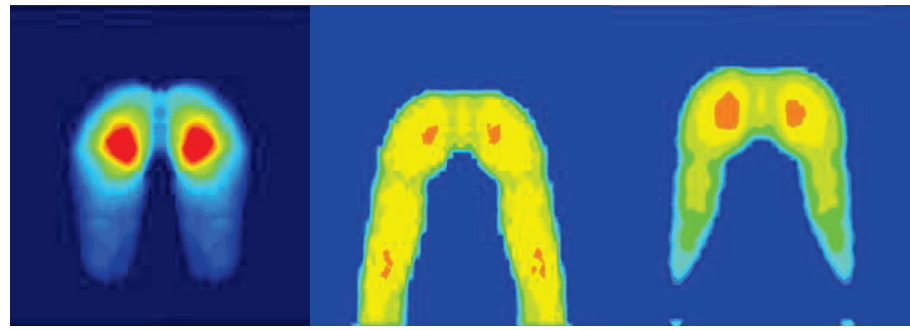


Figure 67: Ischium and knee position of a subject (sub029) along the horizontal (x) and vertical (y) axes

### 3.3 Comparison between simulation cases and experimentation

Pressure results are closer to the experiments with the coupling method than with the basic FE method with data from the experiments. This can be qualitatively observed on the following figures (Figure 68, Figure 69).



**Figure 68:** Pressure distribution of a subject (sub021) (from left to right: experimentally measured, simulated with experimental FE method , simulated with coupling method)

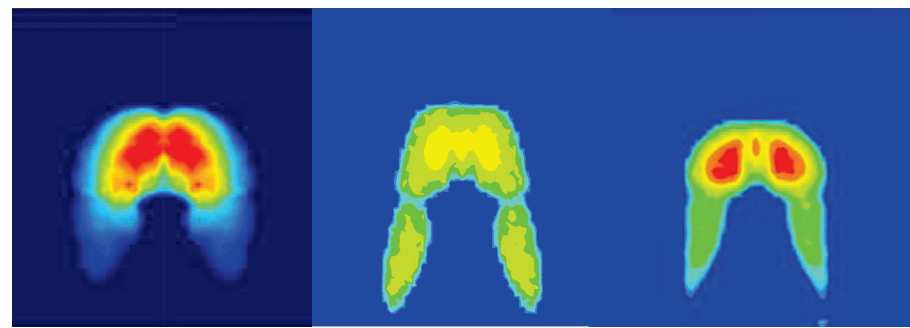


**Figure 69 :** Pressure distribution of a subject (sub029) (from left to right: measured experimentally, simulated with experimental FE method, simulated with coupling method)

Quantitatively, the mean error for the maximal pressure and mean pressure are much lower with the coupling method than with the experimental FE method. The mean of the maximal pressure percentage error over the 6 participants was  $9.3 \pm 11\%$  with the coupling method whereas it is  $20.9 \pm 9\%$  with the FE method (Table 15: ). The average of the mean pressure percentage error over the 6 participants was  $8.8 \pm 9.9\%$  with the coupling method whereas it was  $46 \pm 24\%$  with the FE method.

**Table 15: Pressure outputs with the two simulation methods compared to the experimental values**

Pmax (kPa)		% error of Pmax		Pmean (kPa)		% error of Pmean	
Expe	FE method	Coupling method		Expe	FE method	Coupling method	
		Expe	FE method			Expe	FE method
SUB021	11.71	28.3	19.4	5.19	37.8	6	
SUB026	8.4	11.9	1.2	5.03	34.6	2.9	
SUB029	11.87	28.8	11.5	5.05	21.2	2.3	
SUB031	10.28	29.3	19.3	4.68	61.2	4.1	
SUB032	9.36	17.6	7.9	4.49	33.2	9.2	
SUB034	10.69	9.6	20.7	5.33	87.4	28.5	
ALL	$10.39 \pm 1.35$	$20.9 \pm 9$	$9.3 \pm 11$	$4.96 \pm 0.32$	$46 \pm 24$	$8.8 \pm 9.9$	

An important difference was observed between the positions of the bones resulting from the two simulation methods. The difference of the angle between the pelvis and thigh (between the three points: L5S1 joint – hip joint – knee joint) in the sagittal plan can reach  $70^\circ$  between the two simulations (Table 16). A maximum difference of  $63^\circ$  in the pelvis inclination (angle between the L5S1 joint – ischium direction and the horizontal in the sagittal plane) was observed between the two simulation methods (Table 16, Figure 70). The coupling method implies an important position change

compared to the FE method, this position difference implied important differences of contact pressure (Figure 71).

**Table 16: Bones final position with two methods**

	Pelvis-thigh angle in °			Pelvis inclination in °		
	FE method	Coupling method	Difference	FE method	Coupling method	Difference
SUB021	167.739	138.364	29.375	135.88	121.1	14.78
SUB026	192.003	135.269	56.734	160.99	118.52	42.47
SUB029	196.07	154.629	41.441	168.24	129.89	38.35
SUB031	203.467	133.557	69.91	177.32	114.35	62.97
SUB032	194.598	153.707	40.891	164.5	126.84	37.66
SUB034	188.258	134.762	53.496	161.44	122.51	38.93
ALL	190.4 ± 8.9	141.7 ± 8.9	48.6 ± 13.1	161.4 ± 12.7	122.2 ± 5.1	39.2 ± 13.9

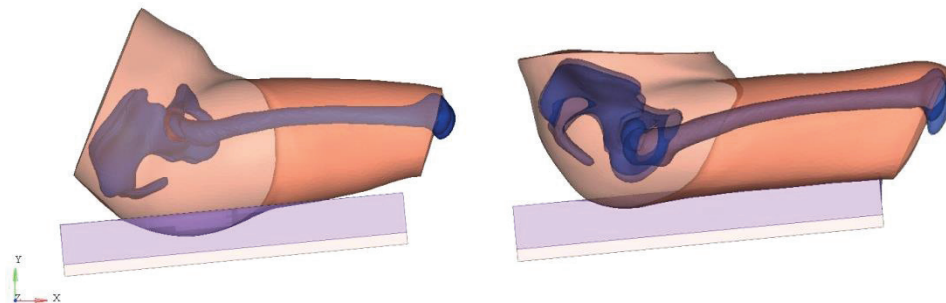


**Figure 70: Position of the model for a subject (sub31): from the experiments(left) and after coupling (right)**

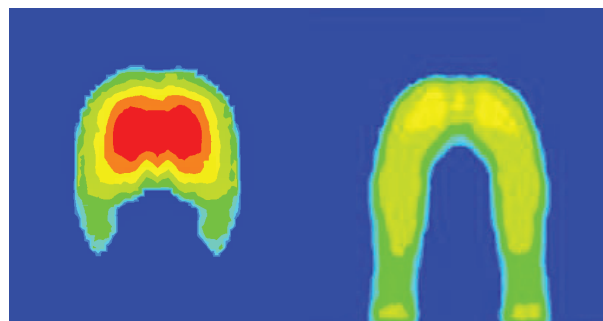


**Figure 71: Pressure map of a subject (sub31) with experimental simulation (left) and coupling simulation (right)**

A correlation ( $R^2=0.47$ ) was found between the difference of the mean pressure error between the two methods and the difference of the pelvis-thigh angle. It means that the gap of mean pressure estimation between the two methods may be linked to the difference of bones positions.

To investigate how much the coupling method changes this position and if it enhances it compared to the experiments, simulations with coupling and without coupling from the same initial position were compared. The loop modifies a bit the bones positions (Table 17, Figure 72). The angle between the thigh and pelvis can change from  $3.4^\circ$  to  $10.5^\circ$  between the two methods. The pelvis orientation from the horizontal can vary from  $6.2^\circ$  to  $13.2^\circ$  between the two methods. Qualitatively, the femur position looks more realistic after the coupling method (Figure 72).

These differences are weak compared to the differences between the coupling method and the no coupling approach using experimental positions as boundary conditions. Consequently, the previous observed differences must be more linked to the difference of initial position than to the effect of the coupling loop.

**Table 17: Bones position with coupling and without coupling**

	Pelvis-thigh angle			Pelvis orientation from horizontal		
	No coupling	Coupling	Difference	No coupling	Coupling	Difference
SUB021	141,8	138,364	3,436	109,27	121,1	11,83
SUB026	143,9	135,269	8,631	109,8	118,52	8,72
SUB029	144,1	154,629	10,529	120,61	129,89	9,28
SUB031	138,9	133,557	5,343	108,16	114,35	6,19
SUB032	148,6	153,707	5,107	117,48	126,84	9,36
SUB034	141,8	134,762	7,038	109,27	122,51	13,24
ALL	$143,2 \pm 3.3$	$141,7 \pm 9.8$	$6,7 \pm 2.6$	$112,4 \pm 5.2$	$122,2 \pm 5.6$	$9,8 \pm 2.5$

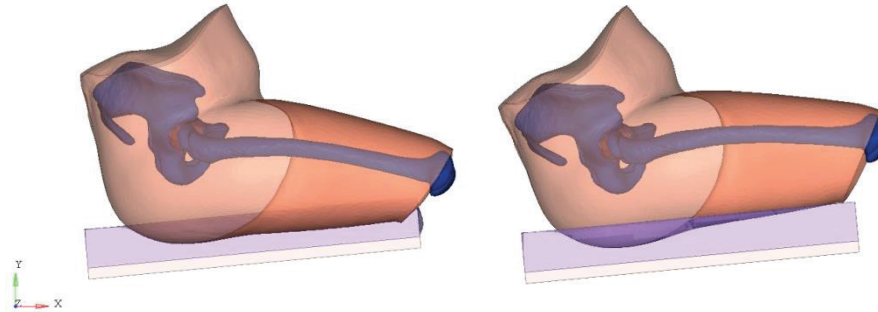


**Figure 72: Bones position of subject 34 without coupling (left) and with coupling (right)**

The coupling method modifies a bit the bones position and consequently modifies the pressure distribution. Globally the coupling method improves the pressure estimation. The mean % error for the mean pressure was  $37.9 \pm 29$  without coupling instead of  $8.8 \pm 9.9$  with coupling. The mean % error of maximal pressure was  $18.9 \pm 7$  without coupling instead of  $9.3 \pm 11$  with coupling.

**Table 18: Comparison of pressure outputs with and without coupling**

	Pmax (kPa)			% error of Pmax			Pmean (kPa)	% error of Pmean		
	Expe	No coupling	Coupling method	Expe	No coupling	Coupling method		Expe	No coupling	Coupling method
SUB021	11.71	26,6	19.4	5.19	16,11	6				
SUB026	8.4	13	1.2	5.03	29,1	2.9				
SUB029	11.87	9,9	11.5	5.05	98	2.3				
SUB031	10.28	28	19.3	4.68	30,5	4.1				
SUB032	9.36	16,7	7.9	4.49	29,4	9.2				
SUB034	10.69	19.6	20.7	5.33	24,6	28.5				
ALL	$10.39 \pm 1.35$	$18,9 \pm 7$	$9.3 \pm 11$	$4.96 \pm 0.32$	$37,9 \pm 29$	$8.8 \pm 9.9$				

The correction of bones position by the coupling method which leads to a better pressure estimation can be observed qualitatively for some subjects (Figure 73, Figure 67). It can be observed that the loop process enhanced the wrong thighs positions initially estimated by Anybody.

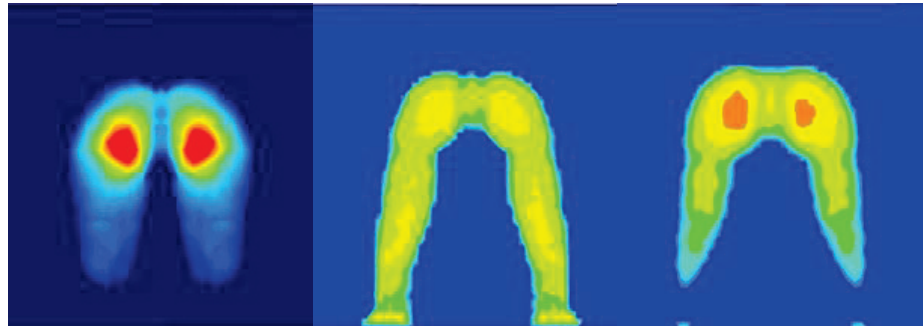


**Figure 73: Pressure distribution of a subject (sub021) (from left to right experimentally measured, simulated without coupling , simulated with coupling)**

## 4. Discussion / Conclusion

A method coupling two modeling approaches, MB and FE modeling, was developed to simulate a person sitting on a seat. This method has two advantages: first, giving the boundary conditions to a the FE model and secondly estimates all the mechanical factors leading to discomfort (pressure distribution with the FE model and disc pressure and muscular activity with the MB model (see Appendix 8)).

Results of this simulation process were confronted to experimentally measured pressure and to the previously simulated pressure with a basic FE approach using experimental data. It has been observed that the pressure simulated with this coupling approach was closer to the experimental results than with the FE method. It has been shown that this difference may be linked to the change of bones positions. Important differences of bones positions were noticed between this coupling approach and the method using the markers to position the bones (until 70° of difference). The position in the coupling approach depends on the initial position defined by the contact constraints between the body and the seat but also on the coupling loop which modifies the bones positions at each iteration. We observed that the coupling method globally improves the pressure estimation by correcting mainly the thighs position. Nevertheless the main change of position is linked to the initial position estimated by Anybody MB simulation. To conclude, when looking at the error of pressure estimation, it appeared that the bones positions estimated from the experiments (by the motion capture analysis of the markers on the bone landmarks) was wrong and the bones positions estimated by simulation with this coupling process may be more correct. This assumption is made only on the pressure comparison because the real bones positions couldn't be measured during the experiments.

If this simulation process seems to correctly estimate bones positions, a certain number of uncertainties exist. First the initial position was estimated thanks to an inverse kinematic which depends on coupling law for joint angles like the spine rhythm for the vertebrae angles, and the thorax-pelvis-thighs rhythm for the pelvis position. These coupling laws haven't been validated but have a strong influence on the position. Secondly, the boundary conditions applied to the FE model (joint forces and torques) depends on the inverse dynamics and the forces estimation. The muscular forces estimation depends on the optimization criterion. The choice of this criterion and its influence on the

results has not been investigated. Furthermore, the joint forces estimation depends also from the seat contact forces estimations which depends on their formulation. The influence of the contact points, their quantity and their disposition have not be investigated. Consequently, a sensitivity analysis of the results to all these simulation parameters should be conducted in the future.

# **Chapter 5: Comparison of simulated tissue deformations with experimental MRI data**

## **1. Introduction**

In the precedent chapters, models have been developed in the purpose of predicting the contact pressure at the seat interface. However as it has been explained in the first chapter, the external contact pressure is not correlated to the sub dermal tissue loading (Oomens et al. 2003). The internal tissue deformations are the proper source of discomfort because of the nerves and vessels compression (Reed et al. 1994). We know that above a certain stress value, blood flow is limited (Chow & Odell 1978). Several studies have also linked the deformations to the cell necrosis in the muscles (Breuls et al. 2003; Gefen et al. 2008). To fully understand the impact of the seat on the body and what leads to discomfort, it is important to study the internal soft tissue deformations. FE models have the advantage of simulating these deformations which are difficult to measure experimentally. However the model ability to calculate these deformations has to be quantified by comparing simulations results and experimental observations. If a lot of models have been developed to study the soft tissue deformations, especially for pressure ulcer investigation (Todd & Thacker 1994; Linder-Ganz & Gefen 2004; Linder-Ganz et al. 2007a; Makhsous et al. 2007; Wagnac et al. 2008; Tang et al. 2010; Oomens et al. 2013; Mohanty & Mahapatra 2014; Luboz et al. 2014), very few have described a validation process. Only 3 studies gave an error percentage between simulated and measured internal soft tissue deformations. However, all these studies have limitations. The first one (Todd & Thacker 1994) studied deformations in only one plane and in a lying posture which implies a tissue loading different from sitting. The second one (Makhsous et al. 2007) applied a load very different from sitting, since it was a pressure applied with an inflated cushion around the thigh circumference. Finally, the first study which compared simulated and measured soft tissue deformations under sitting conditions is the one from Al-Dirini et al. (2016). However, in this study, the loading is unknown (subjects were sitting in an MRI device, the load under their buttocks was not measured) and only one configuration was studied.

The goal of this chapter was to investigate the impact of sitting on soft tissues deformations and validate the ability of a specific FE model to simulate these deformations. Since it is known that loading conditions have an impact on the tissue strain (shear forces have to be considered as much as normal forces (Ming Zhang & Roberts 1993)), several loading conditions have been tested. If the seat contact pressure generally presents two maximal peaks, there can be several local stress maxima in the tissue (Silber & Then 2009). Consequently, deformations will be studied in several locations and in three dimensions and not only in a plane as in most of the previous studies (see Chapter 1). Furthermore, contrary to most of the previous models developed to study internal tissue strains, the model was developed in three dimensions and distinguished fat and muscles layers to better investigate the strains sustained by each layers.

This chapter describes first the collection of MR images, secondly the development of a detailed FE model based on these images and finally the comparison of the simulated deformations to the observed deformations.

## 2. Data collection on MRI

MR images of the buttocks-thigh area were required to:

- Get the geometry to build the FE model
- Get images of the tissue compression in different sitting configurations

An open-MRI located in Manchester (GB) was used to realize the experimentation (Manchester European Scanning Center). The configuration (vertical double donuts) and dimensions (56 cm width and 1.94 m height) of the MRI device allows to adopt sitting postures (Figure 74). This MRI build by Paramed Company (Naperville, Illinois, US) has a magnetic field of 0.5 Tesla.



Figure 74: Open MRI

A volunteer, a male of 1.64m and 68 kg was solicited for the experiment. The following configurations were realized with this volunteer in the MRI.

### 2.1 Unloaded configuration

The first objective of the MRI experimentation was to get the geometry of the tissue in an initial state to develop the FE model. The goal was to get images of the thighs and pelvis in a position corresponding to sitting, *i.e* an angle of 115° between the leg and the trunk, but without any support under the thighs. A dedicated device (Figure 75) was built to help the person having this position in the MRI. The person was supported under the arms and in front of the knee. The backrest was strongly reclined (50° from vertical) to carry most of the weight of the person. The knee support was adjusted to the person to have an angle between the trunk and the legs of 105°. The angle was checked under the thigh with a dedicated wedge.

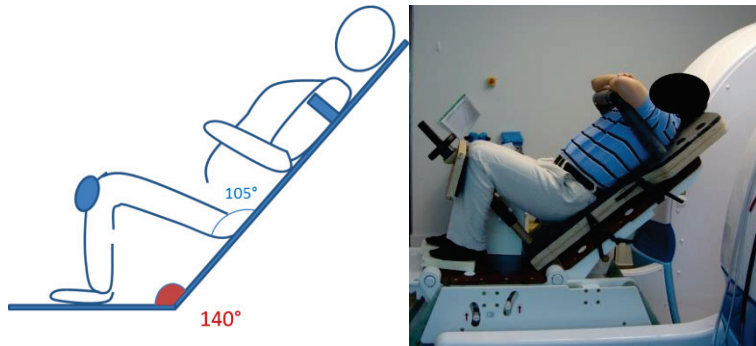


Figure 75: Device for the initial configuration

## 2.2 Reference (rigid) configuration

A reference sitting configuration was needed as a reference state of tissue compression. A seat pan with an inclination of 7° was added. The backrest was reclined of 22° from the vertical (Figure 76). These angle corresponds to values found in a previous experimental study were the preferred seat pan angle was asked to participants (Wang 2017). These angles are in the range of the common aircraft seat configuration which can be found in the Boeing 787 or Airbus 350 (Hiemstra-van Mastrigt 2015).

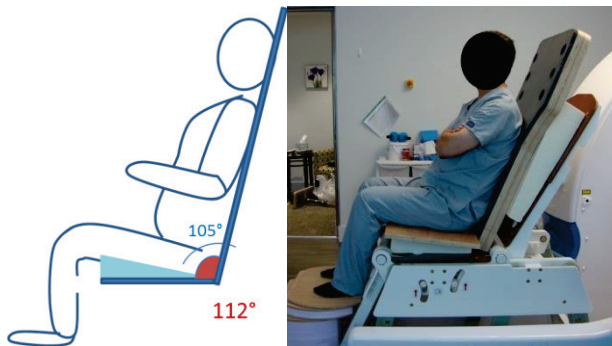


Figure 76: Reference configuration

It was asked to the person to have the whole back in contact with the backrest. The seat height was adjusted to have the whole thigh in contact with the seat. The person was asked to stay still with the arms crossed.

## 2.3 Foam configuration

A loading configuration corresponding to sitting on a real aircraft seat was needed to observe the consequences on the sub dermal soft tissues. The foam presents in the cushions of aircraft seats Z301 and previously used in the experiments (Chapter 3) was positioned on the seat pan. This foam was 5 cm thick and covered the whole seat pan (Figure 77). The seat pan and backrest angles are kept the same as the previous configuration.

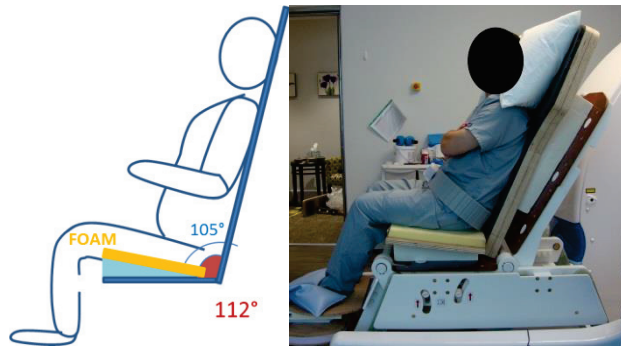


Figure 77: Foam configuration

## 2.4 Shear configuration

To investigate the impact of shear forces on the subdermal tissues, a configuration which increases the shear under the thighs has been realized. By reclining forward the seat pan, the shear forces are increased. The seat pan was positioned to the horizontal to maximize the shear forces (Figure 78).

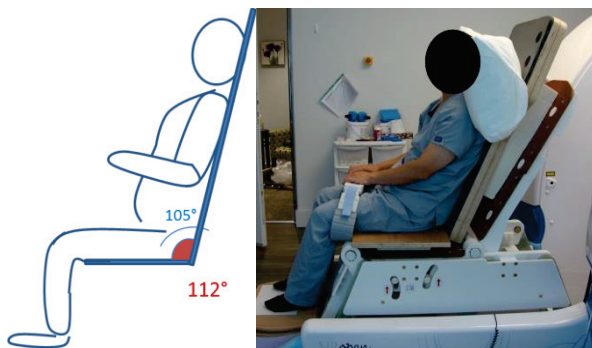


Figure 78: Shear configuration

For all these configurations, the thighs and pelvis were imaged with a 3D Gradient Field Echo sequence. The acquisition window was  $30 \times 30 \times 15 \text{ cm}^3$ , consequently several acquisitions were required for each configuration to cover the whole wanted area. The person had to stay still during all the acquisitions performed for one configuration.

### 3. Finite element model development

#### 3.1 Geometry

To build the FE model corresponding to this person, geometries of the anatomical parts were needed. Bones (pelvis and femur), muscles and fat were each segmented as performed previously (see chapter 2) with the 3d slicer software ([www.slicer.org](http://www.slicer.org)).

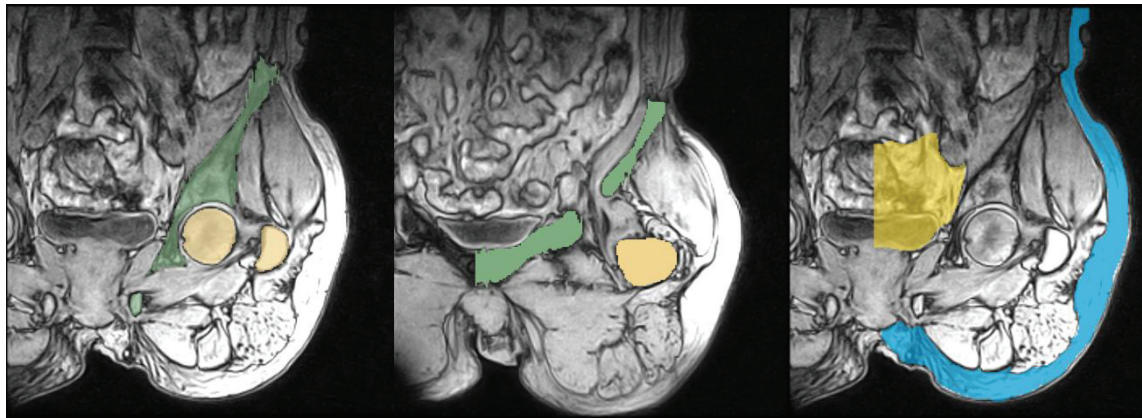


Figure 79: Pelvis (green), femur (white), fat (blue) and organs (yellow) segmentation

The obtained surfaces were meshed using the Hypermesh software. Bones were meshed with shell triangles of 5 mm length. Muscles and organs were meshed with 3D tetrahedron of 5 mm length from the segmented surfaces. Muscles were meshed in one block from the volume between the bones and the fat layer. Consequently the FE model contained a continuous mesh. All the 3D meshes were tetrahedron of 5 mm length.

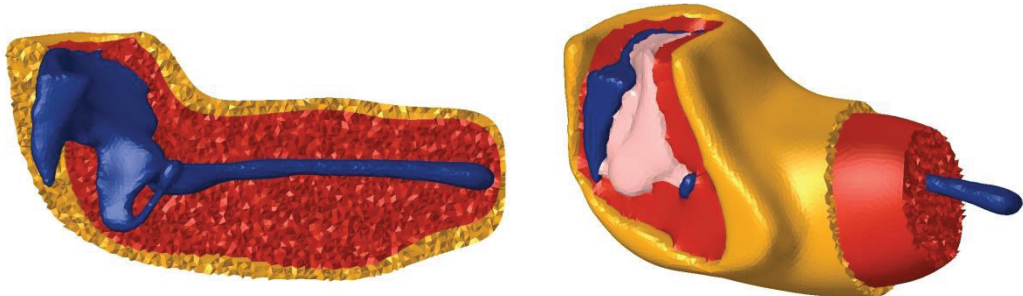


Figure 80: Mesh with bones (in blue), muscles (in red), fat (in yellow) and organs (in pink)

As before, by symmetry hypothesis, only one leg and half of the pelvis were meshed. It reduces the model size and so the computation time.

A homogeneous model with all the soft tissues (fat and muscles) undifferentiated was also built to correspond to the parametric FE model previously developed in chapter 3. For that, the two layers were assembled in one component (Figure 81).

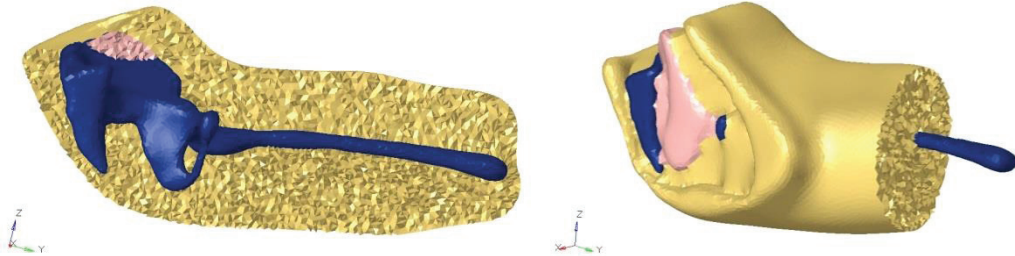


Figure 81: Homogeneous model with bones (in blue) and soft tissues (in yellow)

### 3.2 Material

Bones were modeled as rigid and soft tissues were modeled as an isotropic hyper elastic material. For the detailed model, the Ogden material law at the first order was used to model the hyper elastic behavior (5) as in the study of Al-Dirini et al. (2016).

**Equation 15**

$$W(\lambda_1, \lambda_2, \lambda_3) = \sum_{p=1}^N \frac{\mu_p}{\alpha_p} (\lambda_1^{\alpha_p} + \lambda_2^{\alpha_p} + \lambda_3^{\alpha_p} - 3)$$

Material parameters values were set as in the literature,  $\mu = 1.17 \text{ kPa}$   $\alpha = 16.2$  for fat and skin and  $\mu = 1.91 \text{ kPa}$  and  $\alpha = 4.6$  for muscles.

For the homogeneous model, same hyper elastic Mooney Rivlin law with material parameters as in the precedent chapters was used.

## 4. Simulation of experiments

The different experiment cases were simulated with both FE model.

### 4.1 Model positioning

To simulate the experiment cases, the model has to be positioned exactly as the person during the experiment. Consequently the pelvis-femur and the pelvis-seat pan angles of the simulations had to be

adjusted to correspond to the experimental angles. The pelvis and femur have been segmented on the MRI images (Figure 82).



Figure 82: Bones segmentation

The angle between the femur and the pelvis in the sagittal plane was defined as the projection on the sagittal plane of the angle between the vector defined by the femur axis and the vector defined by the two following points: the center of the femoral head and the anterior superior iliac spine (RIAS) landmark (Figure 83).

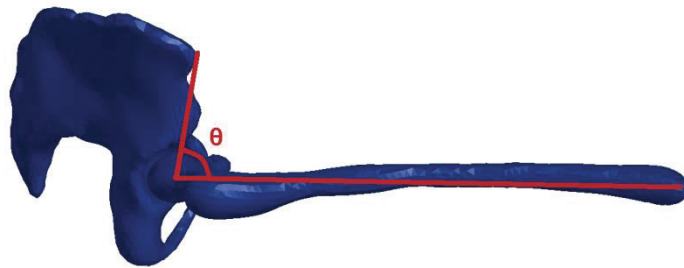


Figure 83: Pelvis-femur angle

This angle was  $101.5^\circ$  on the initial unloading configuration (which has been used for the model development) whereas it was  $79.6^\circ$  for the reference configuration. This difference was due to the position change of the person during the experiment. If the angle between trunk and legs was fixed at  $105^\circ$ , the exact position of the bones was not controlled during the experiment. To correct this angle, a simulation was run where a rotation of  $21.9^\circ$  in the sagittal plane was applied to the femur. At the end the relative position of the femur to the pelvis corresponded to the one of the person in the reference configuration (Figure 84).

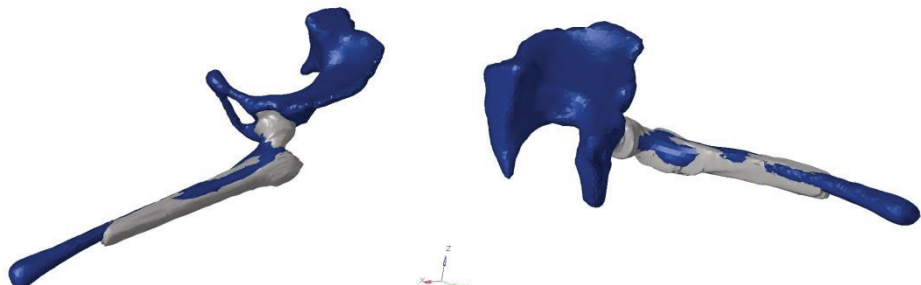
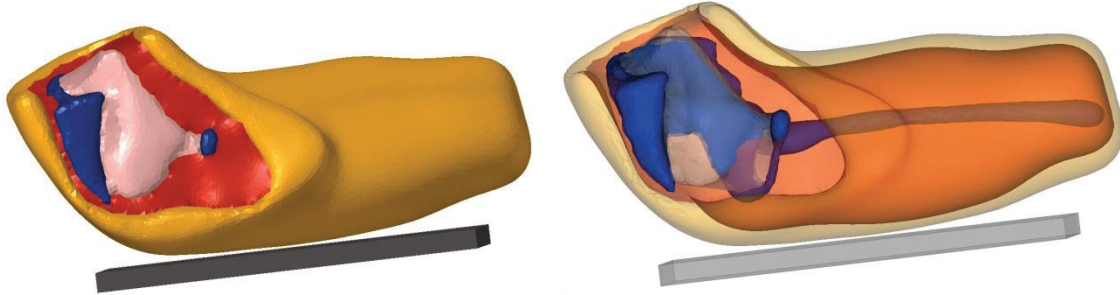


Figure 84: Mesh position (in blue) compared to MRI position (in grey) in reference configuration

Then, the pelvis had to be oriented to have the right angle compared to the seat pan. The transformation between the two pelvis positions (initial position and reference position) have been calculated by an iterative closest point algorithm between the original pelvis mesh and the segmented pelvis on the reference position. The seat pan was then segmented in the reference position and added to the model.

Consequently the seat pan was move down of 27 mm to not penetrate the tissue (Figure 85).



**Figure 85: Model position**

This process was realized for each of the experiment configurations.

## 4.2 Loading conditions

### 4.2.1 Experiment reproduction

To simulate the experimental sitting on the MRI, a loading should be applied on the model. The MRI constraints, especially the strong magnetic field, prevented the use of force sensor. Consequently we had to reproduce later the experiment in our own lab to measure the force. The experimental seat described in chapter 3 was used to reproduce the experiment of the MRI. Seat pan and backrest were set to be plane as the device used in the MRI and their inclination respectively set to 7° and 112° from the horizontal (Figure 86). The person was asked to seat on this configuration while the global force on the seat pan was recorded. The trial was repeated 6 times.



**Figure 86: Reproduction of the experiment on the experimental seat in the lab**

**Table 19: Variations of seat contact forces on the 6 trials**

	Min (N)	Max (N)	Mean (N)	Range (N)	Range (% of mean)
Fx	97.2	80.3	$87.3 \pm 7.2$	16.9	19.3
Fz	471.2	505.7	$481.9 \pm 12.4$	34.5	7.1

The maximum of inter-trial variability was of 7.1 % for the normal force and 19.3% for the shear force. The global inter-trial variability was low enough to make the assumption that the mean value of all the trial is close to the value of the experiment on the MRI.

#### 4.2.2 Simulation boundary conditions

To reproduce the experiment by simulation, the bones of the model were constrained in all directions and a displacement was applied on the seat pan in the direction of the measured contact forces (Figure 86). The displacement was stopped when the contact force reach the target value, *i.e.* the experimental contact force previously measured.

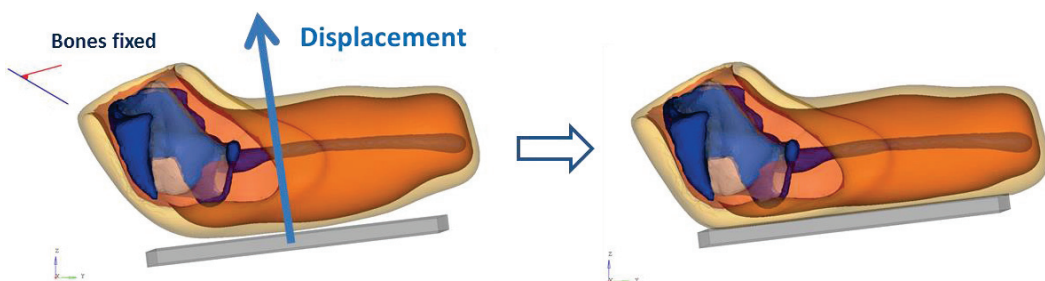


**Figure 87: Simulation boundary conditions**

For the foam configuration, the foam was modeled with a tabulated hyper elastic foam material. The strain-stress curve was measured experimentally (see Chapter 3) and set as a tabulated material property in the model.

## 5. Responses definition

### 5.1 Landmarks displacement

The defined simulations outputs were the displacement of the two tissue layers: the muscle and the fat. A plane was defined: perpendicular to the seat pan and with the normal in the pelvis symmetry plane. Origin of this plane was set at the ischium. The displacements of the tissue layers were defined as the difference of the thickness of the fat and muscles tissues, in this plane, in the non-loaded configuration and a seated configuration (Figure 88).

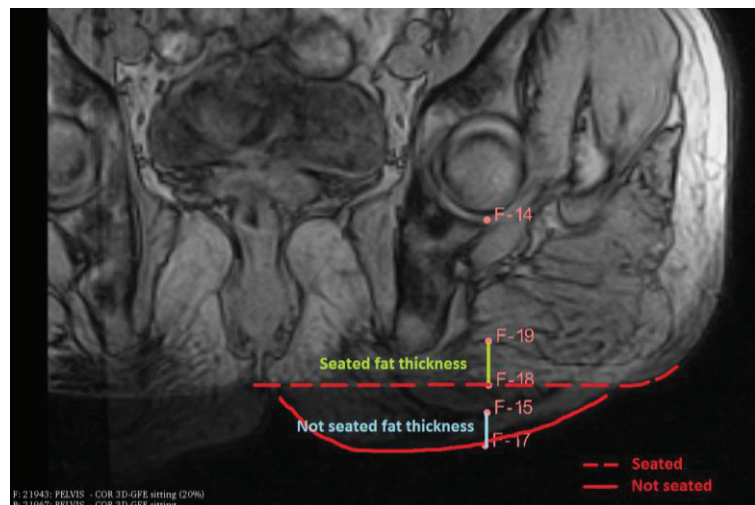
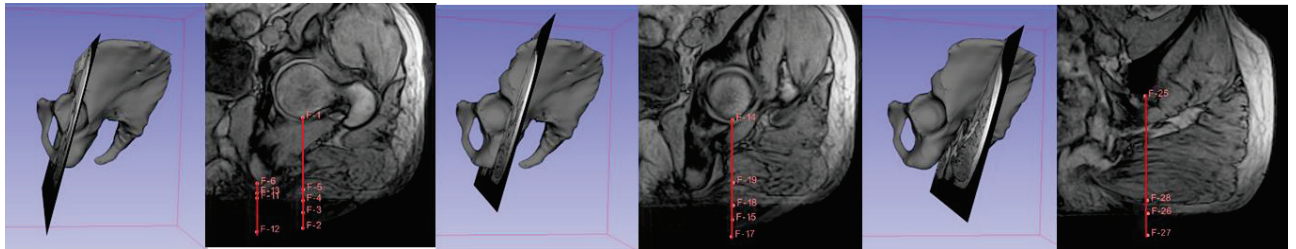


Figure 88: Tissue layers for displacement measurement

More specifically, on this first plane, two thicknesses were considered, one under the ischium and one under the femoral head. Two other planes have been defined from the first one (Figure 89). They are parallel from it but with an offset backward of respectively 1.6 cm and 5.5 cm. The thickness was measured under the acetabulum on the second plan and under the ilium on the third plan (Figure 89). These several thicknesses were defined to characterize different layers of soft tissues in different anatomical area.



**Figure 89: The three plane of displacement measurement**

As for the FE simulations, the position of the corresponding mesh node for each measurement point was exported the simulated displacement. The displacement of each node, 8 in total, were the outputs of the simulation.

## 5.2 Hausdorff distance

The tissue deformation was also in three dimensions. For that, the distances between the initial and deformed segmented or simulated surfaces of the different tissue layers were computed with the Hausdorff algorithm. This integrated function in Meshlab finds the closest point of a second mesh for each vertex of a first mesh. Then distance between these two points is computed.

## 6 Results

### 6.1 Tissue deformation

The tissue deformations were compared between the rigid and foam configuration. The shear configuration was realized to study the impact on shear forces on the tissue deformations and the model ability to simulate it. However, the image resolution didn't allow measuring the shear deformation on the tissues. To measure the shear field, it would have been necessary to detect landmarks inside the fat or muscle layers.

In this configuration the vertical tissue deformation was exactly the same as in the reference configuration. The two experiments can't be distinguished. Consequently, this configuration was not analyzed.

Globally, deformations of soft tissue (fat and muscles) are reduced with the foam configuration. The reduction of strain can reach 42,4 % between the two configuration. However, the global deformation of soft tissue is not so importantly affected by the foam. At the back of the ischium (plan 2 and 3), the deformation of the global envelope is quasi the same between the two configurations, but in these plans the deformation of the two layers differs between the two configurations. The fat

deformation is reduced and the muscle deformation is increased. On the plan of the ischium, the global envelope deformation is more affected by the foam.

To conclude the foam reduces the global deformation under the ischium and change the internal proportion of deformation elsewhere.

**Table 20: Soft tissue deformations in the rigid and foam configurations**

	Rigid		Foam	
	Displacement (mm)	Strain (%)	Displacement (mm)	Strain (%)
<b>Plan 1 (femur)</b>				
skin	28.4	27.4	21.3	20.6
muscle	29.4	29.4	22.2	24.9
fat	-1	-6.9	-0.9	-6.3
<b>Plan 1 (ischium)</b>				
skin	25.3	61.1	22.2	54
muscle	1.9	14.7	5.4	42
fat	23.4	82.1	16.8	59
<b>Plan 2</b>				
skin	26.5	66.3	26.6	66.5
muscle	7.8	49.1	12.2	76.7
fat	18.7	77.5	14.4	59.8
<b>Plan 3</b>				
skin	20.4	22.5	20.3	22.4
muscle	4.7	7.2	15.2	23.2
fat	15.7	62.8	5.1	20.4

It was observed negative deformations of the fat layer under the femoral head. This can be explained by a displacement of the fat tissue under the ischium to the lateral side of the thigh.

When looking more globally on the difference of deformations, the bigger difference between the two configurations was located away from the ischium (Figure 90). The foam leads to more tissue displacement (until 12 mm of differences) to the external sides of the buttocks.

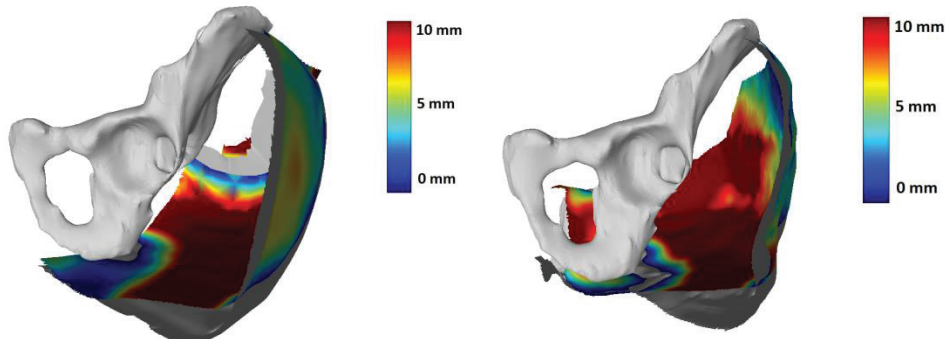


**Figure 90: Distance between the rigid (in grey) and the foam for the skin surface (left) and the muscles surface (right)**

## 6.2 Simulation comparison

### 6.2.1 Detailed model

In most of the observation planes, the error between measurement and simulation for the outer envelope (skin) displacement was below 25% (

Table 21) for both configurations. This error can be locally more important (until 63.2%) for the foam configuration.

Important disparities were observed for the muscle tissue displacements. Depending, on the location, the error varied from 3.9 % to 1112%. The highest error was located under the ischium for both configurations.

It was observed that errors were less important for the outer envelope estimation with the rigid configuration than with the foam configuration. On the contrary, errors were more important for the muscle layer estimation with the rigid configuration.

Globally, the error was more important for the foam configuration.

**Table 21: Layers displacement measured (meas) and simulated (sim) for the reference (rigid) and foam configurations**

	Rigid			Foam		
	Meas (mm)	Sim (mm)	Error (%)	Meas (mm)	Sim (mm)	Error (%)
<b>Plan 1 (femur)</b>						
skin	28.4	31.9	12.5	21.3	33.3	56.7
muscle	29.4	28.3	3.9	22.2	32.2	45.1
<b>Plan 1 (ischium)</b>						
skin	25.3	28.5	12.6	22.2	27.7	24.9
muscle	1.9	22.5	1112	5.4	20.7	286
<b>Plan 2</b>						
skin	26.5	30.1	13.7	26.6	25.9	2.2
muscle	7.8	18.1	132	12.2	14.7	20.1
<b>Plan 3</b>						
skin	20.4	27.0	32.8	20.3	33.1	63.2
muscle	4.7	22.1	367	15.2	27.6	81.5

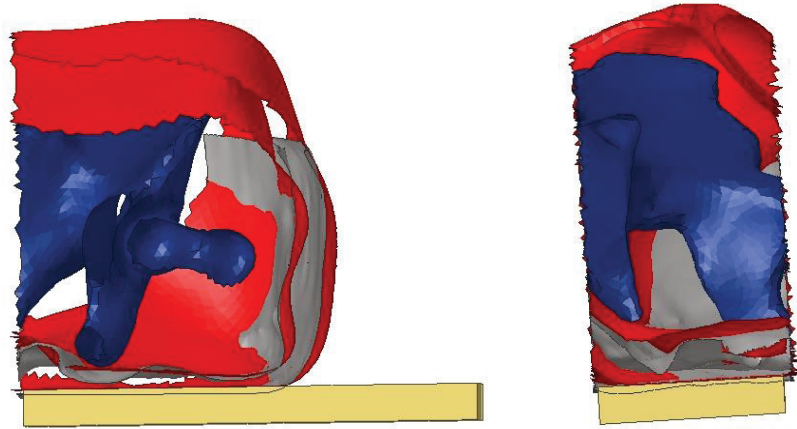


**Figure 91:** Comparison of simulated (red) and segmented on MRI (grey) fat layer for the reference configuration

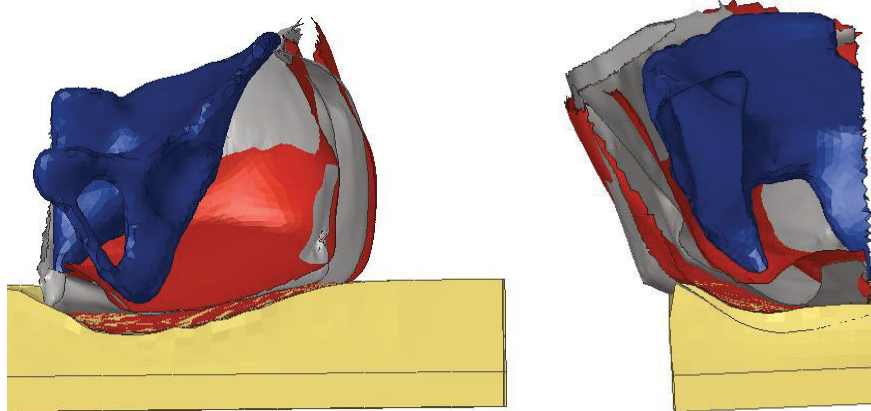


**Figure 92:** Comparison of simulated (red) and segmented on MRI (grey) fat layer for the foam configuration

It is observed that the simulated deformations were more uniform than the observed deformation (Figure 93, Figure 94).

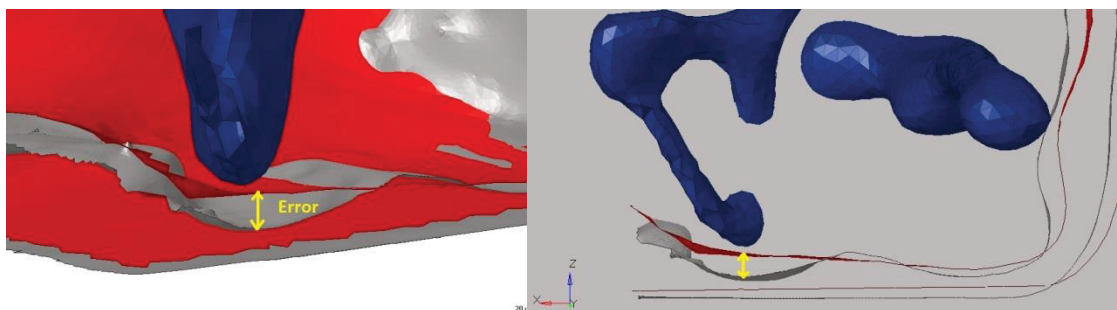


**Figure 93:** Error between the simulated (red) and segmented (grey) fat layer for rigid configuration

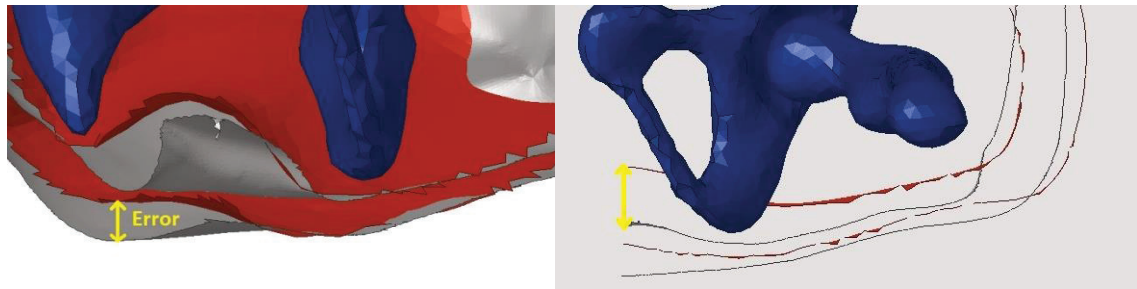


Figure 94: Error between the simulated (red) and segmented (grey) fat layer for foam configuration

The maximal errors were located under the sacrum and not under the ischium.

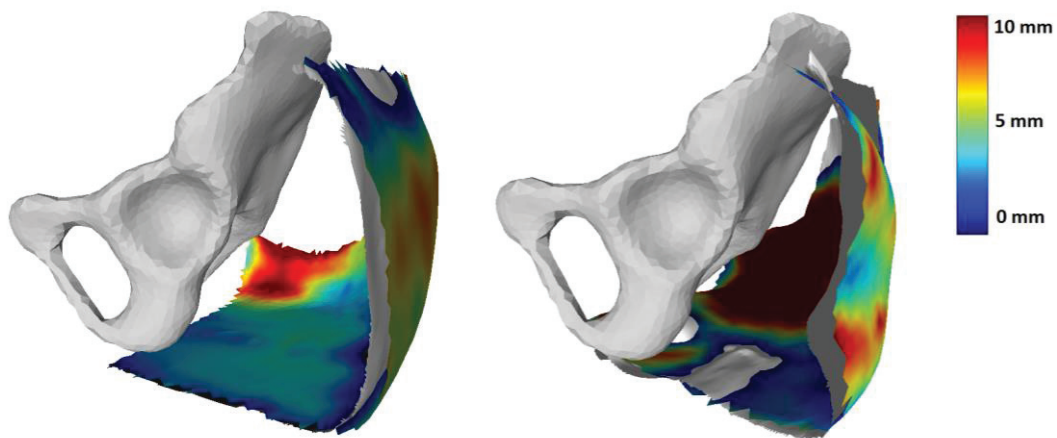


Figure 95: Distance between the measured and simulated skin surface for rigid (left) and foam (right)

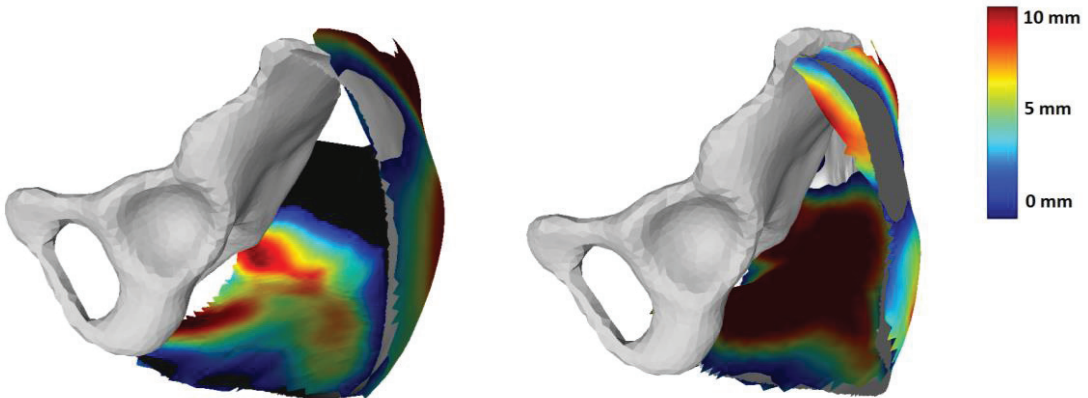


Figure 96: Distance between the measured and simulated internal fat layer for rigid (left) and foam (right)

The average Hausdorff distances was lower for both skin and fat for the rigid configuration than for the foam configuration (Table 22). The maximal error didn't exceed 15.4%. These errors were computed only on the segmented surface which was limited on the area between the back and the front part of the pelvis.

Table 22: Hausdorff distance (in mm) between measured and simulated surfaces

Rigid	Foam
-------	------

	Fat	Skin	Fat	Skin
Min	0.002	0.009	0.007	0.003
Max	13.2	13.9	13.6	15.4
Mean	4.7	4.5	5.7	5.3

### 6.2.2 Homogeneous model

The error of deformation for the homogeneous model was very low for the rigid configuration, between 0 and 3.8% (Table 23). For the foam configuration, the errors were a bit more important but still under 20%. These errors are much less important than with the detailed model.

**Table 23: Layers displacement measured (meas) and simulated (sim) for the reference (rigid) and foam configurations for the homogeneous model**

	Rigid			Foam		
	Meas (mm)	Sim (mm)	Error (%)	Meas (mm)	Sim (mm)	Error (%)
<b>Plan 1 (femur)</b>						
skin	28.4	28.2	0.8	21.3	25.1	18
<b>Plan 1 (ischium)</b>						
skin	25.3	24.5	3.8	22.2	21.8	1.3
<b>Plan 2</b>						
skin	26.5	26.5	0	26.6	21.5	19
<b>Plan 3</b>						
skin	20.4	20.2	0.1	20.3	22.1	8.7

For both configurations, much of the error was located under the sacrum. The error under the ischium was very low (Figure 97,Figure 98,Figure 99).

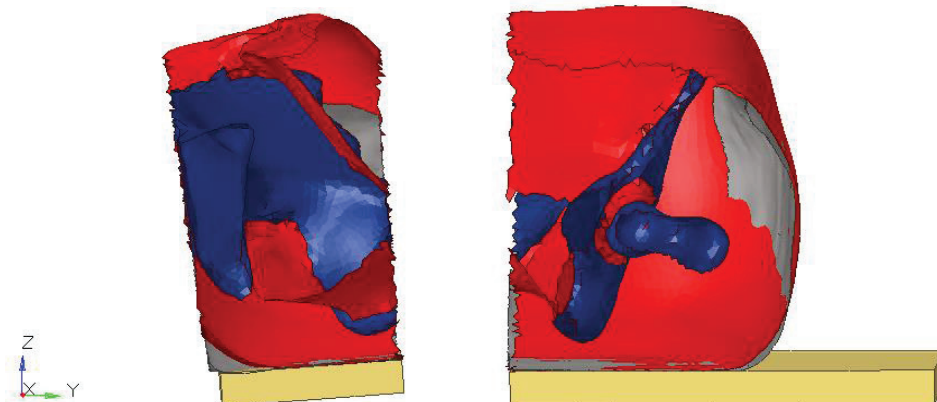


**Figure 97: Comparison of simulated (red) and segmented on MRI (grey) fat layer for the reference configuration for homogeneous model**

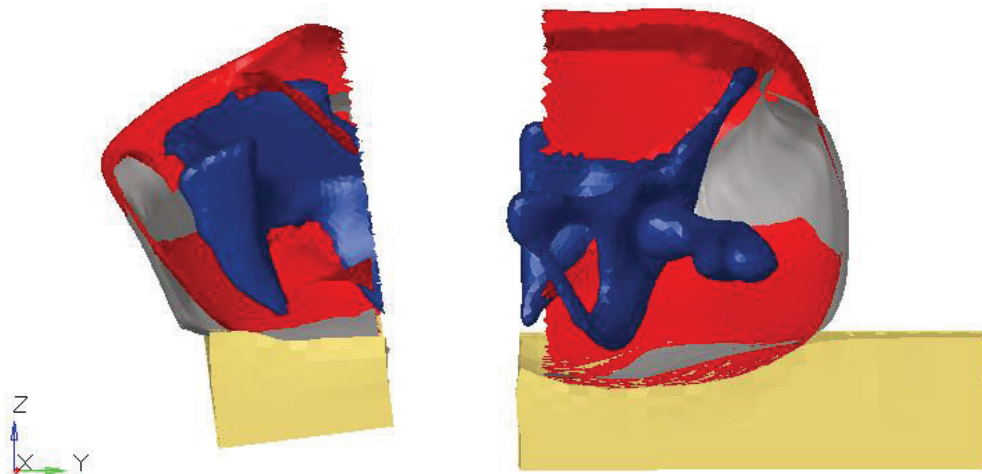


**Figure 98:** Comparison of simulated (red) and segmented on MRI (grey) fat layer for the foam configuration for homogeneous model

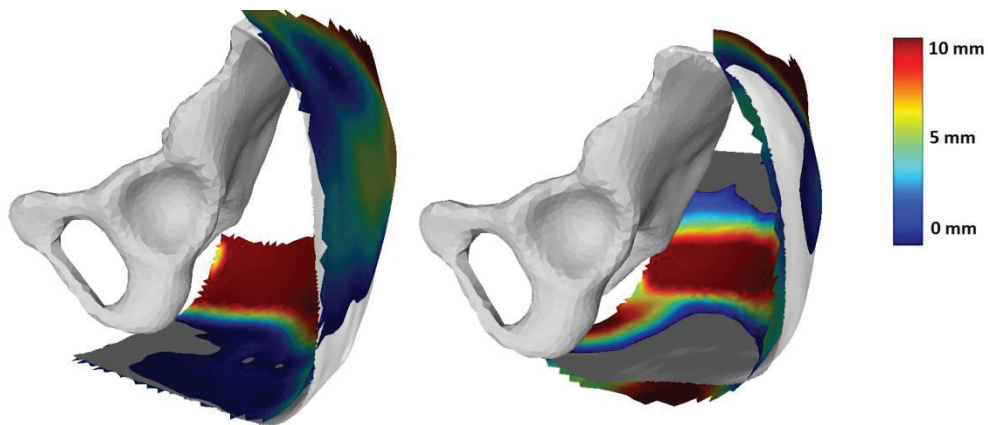


**Figure 99:** Distance between the measured and simulated skin surface for rigid (left) and foam (right) for homogeneous model

The average Hausdorff distance between the segmented and simulated skin surface over the segmented area was lower for the rigid configuration (4.3 mm) than for the foam configuration (5.6 mm) (Table 24). These errors were in the same magnitude as for the detailed model. If the error was less important under the ischium, this error was more important under the sacrum than with the detailed model.

**Table 24: Hausdorff distance (in mm) between measured and simulated surfaces for homogeneous model**

	Rigid	Foam
Min	0.001	0.000
Max	14.3	15.1
Mean	4.3	5.6

## 5. Discussion/Conclusion

The observations of soft tissue deformations showed that high level of strain appeared when sitting on a rigid surface. The deformations are higher in the fat (maximum of 82.1%) than in the muscles (maximum of 49.1%). This is contrary to the finding of Al-Dirini et al. (2015) who found that

the average strain on 6 subject under the ischium was 38.1% for the muscle and 11.8% for the fat. However the strain in the muscle was conform to the values found by (Linder-Ganz et al. 2007b) in a study with 6 person sitting on a rigid plan (strain between 36 and 55%). These stress levels undergo the threshold for cell necrosis. According to Gefen et al. (2008) or Gawlitza et al. (2007), cells are tolerable to only 50% of stress for one hour.

The level of strain was reduced a little bit under the ischium when the person was sitting on the foam. In particularly the foam reduced the strain in the fat. However the tissue placed on the lateral sides of the buttocks undergo larger deformations. The effect of foam is to displace the strain from the ischium to the lateral tissue of the thigh.

The model showed a good ability to simulate the global soft tissue deformations in two configurations. The homogeneous model showed a very good estimation of soft tissue deformation: errors below 20%. The mean distance between the simulated and segmented surface was 4.3mm and 5.6 mm for respectively the rigid and foam configuration. These error value are lower than the error calculated by (Makhsous et al. 2007), who found a gap between the simulated and measured position of 30 landmarks on the tissue of 6.2 mm. It means that the material properties picked from the literature for the global soft tissues could be considered as valid to simulate soft tissue deformation in this kind of configuration, at least for this kind of morphology. The detailed model shows a slightly higher error, especially for the internal deformations. The error between the simulated and observed muscle layer shows irregularities. At some very locals' area, this error can be important. This may be due to the anisotropy of the tissue which has not been taken into account in the model. However the model estimated well (errors below 13%) the global soft tissue deformations for the rigid configuration. The mean error between the simulated and measured fat and skin surface was between 4.5 mm and 5.7 mm. These results are in the same magnitude as those from Al-Dirini et al. (2016) who found a mean error of 4.7mm with the soft tissue simulated with a similar model. These results mean that the material parameters for fat and muscles from literature could also be considered as valid in this kind of configuration.

The main limitation of this study was the fact that the contact forces were not measured inside the MRI but on a replicated configuration in the lab. If the global seat pan contact force doesn't vary a lot for a same configuration (maximum of 6% for the normal force and 17% for the shear force), the error between the measured force in the lab and the actual force on the MRI may have some impact on the simulation.

Finally, only one subject was studied. The morphology and the muscles/fat proportion in the body have a strong impact on the tissue deformations (Al-Dirini et al. 2015). The influence of these anatomical parameters should be investigated.

Future work could focus on modeling the heterogeneity of the different layers and study the impact of morphology by doing the same methodology with several people with different BMI and percentage of fat. The foam characteristics impact on the tissue deformations could also be studied. Finally, a work could focus on the impact of shear forces by finding an efficient way to measure the shear deformation on the MRI.

# Conclusion

## 6. Main results

This thesis is aimed at developing a digital tool to assess the seating discomfort induced by an aircraft seat. The proposed tool consists of 1) a parametric FE model of the buttock-thigh complex developed in the present work, 2) an existing seated musculoskeletal model of whole body from Anybody software, and 3) a method which can exchange the data between FE and MSK models.

To simulate the biomechanical response of a person sitting in a seat, the user of the proposed tool first needs to define the personalized model based on his/her anthropometric dimensions. The geometry of the skin and bones of the buttocks-thigh complex of a specific subject is predicted from the predictors being stature, BMI, gender and hip joint angles. A FE model containing rigid bones (femur and pelvis) and soft tissue is created from this predicted geometry. The existing whole body MSK model Anybody is scaled to correspond to the sitter's anthropometry. The MSK model is positioned into the seat by inverse kinematics by specifying contact geometrical constraints. Joint positions estimated by the Anybody solver are used as an initial guess to position the FE buttock-thigh model into the seat. The resultant forces and moments at the cutting sections (at the pelvis and the knees) and contact forces on the seat estimated by the Anybody inverse dynamics solver are used as boundary conditions for the FE model. A FE simulation is performed by the RADIOSS solver. The new bones position estimated by the FE simulation is exported to the MSK model, leading to an adjustment of the MSK model position and new boundary conditions for the FE model. This iterative process is repeated until the position of the pelvis and two femurs is stable.

This simulation tool can provide a certain number of biomechanical responses by both models. First the seat/sitter contact pressure can be estimated. The user can then follow the existing recommendations concerning the pressure distribution in terms of the maximal pressure, the mean pressure or the gradients defined by Mergl et al. (2005) or Reed et al. (1994). For example, the pressure should be distributed along the seat, but with the peak pressure being under the ischia and low pressure on the frontal area of the thigh. Maximal values of tolerable pressure can also be found on the literature, but no consensus exists on it. The tool also calculates the shear forces, the internal strain, the internal stress, the muscular activity in the whole body as well as the intervertebral disc load. As for the maximum tolerable pressure, there are no criteria today for all these factors, the seat designer could refer to simulated biomechanical responses for comparing different seat design options. For instance, lower shear force at seat contact surface is generally recommended (Goossens et al. 2000). A better seat design should maintain a posture which requires lower muscle activities and lower inter-disc pressure (Franz 2010).

Thanks to the parametric model developed in this work, a family of models with different anthropometric dimensions representing a target sitter population can be easily simulated. The proposed tool will help seat design engineers in answering the question "how to fit a seat to all".

This tool has been validated at different levels. First the prediction of the external shape was evaluated by a leave-one-out process. An average error of  $26.6 \pm 9.3$  mm on the shape prediction over 36 subjects was found. Secondly, the seat contact pressure estimated by the FE model build from the shape prediction was compared with pressure of 12 subjects measured on an experimental seat. The effects of anthropometric parameters on the simulated pressure seemed to correspond to the experimental observations. However, by looking at the individual pressure estimation, important errors were found (for example: max error of 62 % for the mean pressure, of 33% for the maximal pressure, of 37% for the contact area). One of the error sources may be related to the uncertainty in position estimation of the pelvis and femurs. The contact pressure distribution was then simulated with the MSK-FE models coupling process for 6 subjects and compared to experimental data. The error was lower (for example: max error of 28.5% for the mean pressure) with the coupling process than without. It appeared that the coupling process was able to correct the model position initially estimated by MSK model. By correcting the posture, it better estimates the seat interface pressure which is strongly linked to the position of the bones. Another source of the errors may be due to the material parameters. The parameters used come from the literature. The simulated internal soft tissue deformations were compared to the deformation measured on MRI only for one subject. The global simulated soft tissue deformation corresponds to the measured one (max error of 19% for tissue displacement). Nonetheless, this is valid for only one specific subject and error may be more important with another person, because of the inter-individual material properties variations.

## 7. Limitations and perspectives

The proposed tool has several limitations that need to be pointed out. The first concerns the different sub models used for defining personalized FE and MSK models. At first, the parametric model of the buttock thigh complex was built with the data from only 36 subjects. A larger number of subjects would give a better shape prediction accuracy, in particular for extreme values. The internal bone PCA model was based on the data of different subjects from those for skin surface. Concerning the MSK model, an existing model developed by Anybody was scaled. However, the scaling law used and proposed by the Anybody software have not been evaluated and validated.

The second main limitation of the tool is the uncertainties of the model position in a seat. The model position highly depends on the initial position estimated by Anybody. This position is estimated by means of geometrical constraints and internal coupling laws between different spine joint angles and between femur-pelvis and pelvis-spine angles. The geometrical constraints were defined to correspond to the experiment but the impact on the estimated position was not investigated. The internal coupling laws were defined by the Anybody model developers. No validation of these coupling laws can be found in the literature.

One of the perspectives could be consequently to evaluate the positioning of the MSK model into the seat estimated by Anybody. We have seen that the posture had an important impact on the pressure prediction. It would be necessary to study the real position adopted by the person using imagery in order to better position the model in future. The existing internal joint angle coupling law could be replaced or improved.

The third uncertainty is the material properties used to model the soft tissue. The model showed good estimation of deformation in two configurations for one subject. However it does not mean that the used parameters coming from literature would be valid for other subjects in other configuration. The material properties can vary between people depending on sex, age or BMI. The model does not take into account these possible material property variations.

Future work could focus on the validation of the soft tissue deformation estimated by the model with a large panel of subjects with different anthropometries. The influence of fat proportion could be added in the model and compared with MRI data. The observed influence of age, sex or BMI on the soft tissue deformations could also be taken into account in the model material properties.

Furthermore, the developed tool is not stand alone because it does not contain the biomechanical discomfort criteria. The tool provides mechanical values which need to be interpreted with existing discomfort criteria defined in the literature. A coefficient could be assigned to each mechanical factor to define a discomfort or fatigue function as suggested by Grujicic et al. (2010).

The existing criteria could be completed and new criteria could be defined; for example, soft tissue compression based discomfort criteria could be developed, taking into consideration the shear force. The impact of shear forces on soft tissue could be investigated thanks to MRI images. Subjective discomfort assessment should be done with participants to investigate the effect of shear forces on the perceived discomfort.

Finally, research should be performed to find the mechanisms leading to fatigue. The assumption was made that fatigue appeared when an uncomfortable position was maintained over a long period of time. Nevertheless, it would seem that a short-term comfortable position could become uncomfortable in the long term. It would, therefore, be interesting to study the evolution of the criteria with time. The influence of time could also be taken into account in the model. One of the options would be to experimentally study the evolution of the soft tissue material properties with time. This would give a model which evolves with respect to the simulation time. The long term sitting effect on soft tissues could then be investigated.

## Bibliography

- Al Nazer R, Rantalainen T, Heinonen A, Sievänen H, Mikkola A. 2008. Flexible multibody simulation approach in the analysis of tibial strain during walking. *J Biomech.* 41:1036–1043.
- Al-Dirini RMA, Reed MP, Hu J, Thewlis D. 2016. Development and Validation of a High Anatomical Fidelity FE Model for the Buttock and Thigh of a Seated Individual. *Ann Biomed Eng.* 44:2805–2816.
- Al-Dirini RMA, Reed MP, Thewlis D. 2015a. Deformation of the gluteal soft tissues during sitting. *Clin Biomech.* 30:662–668.
- Al-Dirini RMA, Reed MP, Thewlis D. 2015b. Deformation of the gluteal soft tissues during sitting. *Clin Biomech.* 30:662–668.
- Aliah binti Abdul Majid N, Notomi M, Rasmussen J. 2011. Musculoskeletal computational analysis of the influence of car-seat design/adjustment on fatigue-induced driving. In: 2011 4th Int Conf Model Simul Appl Optim ICMSAO. [place unknown]; p. 1–6.
- Allen B, Curless B, Popović Z. 2003a. The Space of Human Body Shapes: Reconstruction and Parameterization from Range Scans. In: ACM SIGGRAPH 2003 Pap [Internet]. New York, NY, USA: ACM; [cited 2017 Dec 15]; p. 587–594. Available from: <http://doi.acm.org/10.1145/1201775.882311>
- Allen B, Curless B, Popović Z. 2003b. The Space of Human Body Shapes: Reconstruction and Parameterization from Range Scans. In: ACM SIGGRAPH 2003 Pap [Internet]. New York, NY, USA: ACM; [cited 2017 Apr 18]; p. 587–594. Available from: <http://doi.acm.org/10.1145/1201775.882311>
- AltairKorea. 22:31:07 UTC. HyperStudy 10 Training Manual [Internet]. [cited 2018 Jan 3]. Available from: <https://fr.slideshare.net/AltairKorea/hyperstudy-10-training-manual>
- Andersson BJ, Ortengren R. 1974. Lumbar disc pressure and myoelectric back muscle activity during sitting. II. Studies on an office chair. *Scand J Rehabil Med.* 6:115–121.
- Andersson GB, Ortengren R, Nachemson A. 1977. Intradiskal pressure, intra-abdominal pressure and myoelectric back muscle activity related to posture and loading. *Clin Orthop.*:156–164.
- Bader DL, Hawken MB. 1990. Ischial Pressure Distribution Under the Seated Person. In: Bader DL, editor. Press Sores - Clin Pract Sci Approach [Internet]. [place unknown]: Macmillan Education UK; [cited 2016 Dec 20]; p. 223–233. Available from: [http://link.springer.com/chapter/10.1007/978-1-349-10128-3\\_17](http://link.springer.com/chapter/10.1007/978-1-349-10128-3_17)
- Baek S-Y, Lee K. 2012. Parametric human body shape modeling framework for human-centered product design. *Comput-Aided Des.* 44:56–67.
- Bar. 1998. Pressure: Why measure it and how. Present 14th Int Seat Symp.
- Bell JA, Stigant M. 2007. Development of a fibre optic goniometer system to measure lumbar and hip movement to detect activities and their lumbar postures. *J Med Eng Technol.* 31:361–366.
- Bendix T. 1987. Adjustment of the seated workplace--with special reference to heights and inclinations of seat and table. *Dan Med Bull.* 34:125–139.
- Bendix T. 1994. Low back pain and seating. *Hard Facts Soft Mach Ergon Seat.*:147–156.

Bendix T, POULSEN V, KLAUSEN K, JENSEN CV. 1996. What does a backrest actually do to the lumbar spine? *Ergonomics*. 39:533–542.

Bennett, Kauver, Lee, Trainor. 1979. Shear vs. pressure as causative factors in skin blood flow occlusion. :309–314.

Blok M, Vink P, Kamp I. 2007. Comfortable flying: Comfort in aircraft interiors seen through the eyes of the passengers. *Tijdschr Voor Ergon*. 32:4–11.

Bogduk N, Macintosh JE, Pearcy MJ. 1992. A Universal Model of the Lumbar Back Muscles in the Upright Position. *Spine*. 17:897.

Bosboom EMH, Hesselink MKC, Oomens CWJ, Bouter CVC, Drost MR, Baaijens FPT. 2001. Passive transverse mechanical properties of skeletal muscle under in vivo compression. *J Biomech*. 34:1365–1368.

Breuls RGM, Bouter CVC, Oomens CWJ, Bader DL, Baaijens FPT. 2003. Compression Induced Cell Damage in Engineered Muscle Tissue: An In Vitro Model to Study Pressure Ulcer Aetiology. *Ann Biomed Eng*. 31:1357–1364.

Brosh T, Arcan M. 2000. Modeling the body/chair interaction – an integrative experimental-numerical approach. *Clin Biomech*. 15:217–219.

Bryan R, Surya Mohan P, Hopkins A, Galloway F, Taylor M, Nair PB. 2010. Statistical modelling of the whole human femur incorporating geometric and material properties. *Med Eng Phys*. 32:57–65.

Bush TR, Mills FT, Thakurta K, Hubbard RP, Vorro J. 1995. The Use of Electromyography for Seat Assessment and Comfort Evaluation [Internet]. Warrendale, PA: SAE International; [cited 2015 Mar 9]. Available from: <http://papers.sae.org/950143/>

Carcone SM, Keir PJ. 2007. Effects of backrest design on biomechanics and comfort during seated work. *Appl Ergon*. 38:755–764.

Chaffin DB. 1987. Occupational biomechanics—a basis for workplace design to prevent musculoskeletal injuries. *Ergonomics*. 30:321–329.

Chen, J., J. Hong, E. Zhang, J. Liang. 2007. Body Pressure Distribution of Automobile Driving Human Machine Contact Interface.”. *Chin J Mech Eng*. 20:66–70.

Cheng Z, Smith JA, Pellettieri JA, Fleming SM. 2007a. Considerations and Experiences in Developing an FE Buttock Model for Seating Comfort Analysis [Internet]. Warrendale, PA: SAE International; [cited 2015 Apr 24]. Available from: <http://papers.sae.org/2007-01-2458/>

Cheng Z, Smith JA, Pellettieri JA, Fleming SM. 2007b. Considerations and Experiences in Developing an FE Buttock Model for Seating Comfort Analysis [Internet]. Warrendale, PA: SAE International; [cited 2015 Apr 24]. Available from: <http://papers.sae.org/2007-01-2458/>

Choi HY, Kim KM, Han J, Sah S, Kim S-H, Hwang S-H, Lee KN, Pyun J-K, Montmayeur N, Marca C, et al. 2007. Human Body Modeling for Riding Comfort Simulation. In: Duffy VG, editor. *Digit Hum Model* [Internet]. [place unknown]: Springer Berlin Heidelberg; [cited 2015 Apr 24]; p. 813–823. Available from: [http://link.springer.com/chapter/10.1007/978-3-540-73321-8\\_92](http://link.springer.com/chapter/10.1007/978-3-540-73321-8_92)

Chow WW, Odell EI. 1978. Deformations and Stresses in Soft Body Tissues of a Sitting Person. *J Biomech Eng*. 100:79–87.

Christophy M, Senan NAF, Lotz JC, O'Reilly OM. 2012. A Musculoskeletal model for the lumbar spine. *Biomech Model Mechanobiol*. 11:19–34.

Ciacca FRDAS, Sznelwar LI. 2012. An approach to aircraft seat comfort using interface pressure mapping. *Work J Prev Assess Rehabil*. 41:240–245.

Claus A, Hides J, Moseley GL, Hodges P. 2008. Sitting versus standing: Does the intradiscal pressure cause disc degeneration or low back pain? *J Electromyogr Kinesiol*. 18:550–558.

Conine TA, Hershler C, Daechsel D, Peel C, Pearson A. 1994. Pressure ulcer prophylaxis in elderly patients using polyurethane foam or Jay wheelchair cushions. *Int J Rehabil Res Int Z Für Rehabil Rev Int Rech Réadapt*. 17:123–137.

Damsgaard M, Rasmussen J, Christensen ST, Surma E, de Zee M. 2006. Analysis of musculoskeletal systems in the AnyBody Modeling System. *Simul Model Pract Theory*. 14:1100–1111.

De Carvalho DE, Callaghan JP. 2011a. Passive stiffness changes in the lumbar spine and effect of gender during prolonged simulated driving. *Int J Ind Ergon*. 41:617–624.

De Carvalho DE, Callaghan JP. 2011b. Passive stiffness changes in the lumbar spine and effect of gender during prolonged simulated driving. *Int J Ind Ergon*. 41:617–624.

De Looze MP, Kuijt-Evers LFM, Van Dieën J. 2003. Sitting comfort and discomfort and the relationships with objective measures. *Ergonomics*. 46:985–997.

Delp SL, Loan JP, Hoy MG, Zajac FE, Topp EL, Rosen JM. 1990. An interactive graphics-based model of the lower extremity to study orthopaedic surgical procedures. *IEEE Trans Biomed Eng*. 37:757–767.

van Dieën JH. 1997. Are recruitment patterns of the trunk musculature compatible with a synergy based on the maximization of endurance? *J Biomech*. 30:1095–1100.

Doriot N, Cheze L. 2003. A three dimensional dynamic model of the lower limb during the stance phase of gait. *Recent Res Dev Biomech*.:247–267.

Ferrari E, Chevallier T, Chapelier A, Baudouy M. 1999. Travel as a risk factor for venous thromboembolic disease\*: A case-control study. *Chest*. 115:440–444.

Fluit R, Andersen MS, Kolk S, Verdonschot N, Koopman HFJM. 2014. Prediction of ground reaction forces and moments during various activities of daily living. *J Biomech*. 47:2321–2329.

Franz MM. 2010. Comfort, experience, physiology and car seat innovation: Theory, Design and Evaluation [Internet]. [cited 2018 Jan 5]. Available from: <http://resolver.tudelft.nl/uuid:665f677e-9974-4498-8e2d-f20e31a4647b>

Gawlitza D, Oomens CWJ, Bader DL, Baaijens FPT, Bouter CVC. 2007. Temporal differences in the influence of ischemic factors and deformation on the metabolism of engineered skeletal muscle. *J Appl Physiol*. 103:464–473.

Gefen A, Haberman E. 2007. Viscoelastic properties of ovine adipose tissue covering the gluteus muscles. *J Biomech Eng*. 129:924–930.

Gefen A, van Nierop B, Bader DL, Oomens CW. 2008. Strain-time cell-death threshold for skeletal muscle in a tissue-engineered model system for deep tissue injury. *J Biomech*. 41:2003–2012.

Goossens. 1998. Measuring factors of discomfort in office chairs. *Glob Ergon*. 2:371–374.

Goossens. 2009. Fundamentals of pressure, shear and friction and their effects on the human body at supported postures. *Bioeng Res Chronic Wounds*.:1–30.

Goossens RHM, Pas MA, Teeuw R, Snijders CJ. 2000. Decubitus Risk: Is Shear More Important than Pressure? *Proc Hum Factors Ergon Soc Annu Meet*. 44:700–703.

Goossens RHM, Zegers R, van Dijke GAH, Snijders CJ. 1994a. Influence of shear on skin oxygen tension. *Clin Physiol*. 14:111–118.

Goossens RHM, Zegers R, van Dijke GAH, Snijders CJ. 1994b. Influence of shear on skin oxygen tension. *Clin Physiol*. 14:111–118.

Graf M, Guggenbühl U, Krueger H. 1993. Investigations on the effects of seat shape and slope on posture, comfort and back muscle activity. *Int J Ind Ergon*. 12:91–103.

Grujicic M, Pandurangan B, Arakere G, Bell WC, He T, Xie X. 2009a. Seat-cushion and soft-tissue material modeling and a finite element investigation of the seating comfort for passenger-vehicle occupants. *Mater Des*. 30:4273–4285.

Grujicic M, Pandurangan B, Arakere G, Bell WC, He T, Xie X. 2009b. Seat-cushion and soft-tissue material modeling and a finite element investigation of the seating comfort for passenger-vehicle occupants. *Mater Des*. 30:4273–4285.

Grujicic M, Pandurangan B, Xie X, Gramopadhye AK, Wagner D, Ozen M. 2010a. Musculoskeletal computational analysis of the influence of car-seat design/adjustments on long-distance driving fatigue. *Int J Ind Ergon*. 40:345–355.

- Grujicic M, Pandurangan B, Xie X, Gramopadhye AK, Wagner D, Ozen M. 2010b. Musculoskeletal computational analysis of the influence of car-seat design/adjustments on long-distance driving fatigue. *Int J Ind Ergon.* 40:345–355.
- Guo L-X, Dong R-C, Zhang M. 2016. Effect of lumbar support on seating comfort predicted by a whole human body-seat model. *Int J Ind Ergon.* 53:319–327.
- Gyi DE, Porter JM. 1999. Interface pressure and the prediction of car seat discomfort. *Appl Ergon.* 30:99–107.
- H Gray. 1918. Anatomy of the human body. Lea & Febiger. [place unknown].
- Hamner SR, Seth A, Delp SL. 2010. Muscle contributions to propulsion and support during running. *J Biomech.* 43:2709–2716.
- Harrison DD, Harrison SO, Croft AC, Harrison DE, Troyanovich SJ. 1999. Sitting biomechanics Part I: Review of the Literature. *J Manipulative Physiol Ther.* 22:594–609.
- Hartung. 2006. Objektivierung des statischen Sitzkomforts auf Fahrzeugsitzen durch die Kontaktkräfte zwischen Mensch und Sitz, Dissertation am Lehrstuhl für Ergonomie, Technische Universität München.
- Hartung J, Mergl C, Henneke C, Madrid-Dusik R, Bubb H. 2004. Measuring Soft Tissue Compliance of the Human Thigh [Internet]. Warrendale, PA: SAE International; [cited 2015 Mar 10]. Available from: <http://papers.sae.org/2004-01-2158/>
- Hasler N, Stoll C, Sunkel M, Rosenhahn B, Seidel H-P. 2009. A Statistical Model of Human Pose and Body Shape. *Comput Graph Forum.* 28:337–346.
- Helander, M.G., Zhang. 1997. Field studies of comfort and discomfort in sitting. *Ergon* 40.
- Hiemstra-van Mastrigt S. 2015. Comfortable passenger seats: Recommendations for design and research [Internet]. [cited 2017 Dec 12]. Available from: <http://resolver.tudelft.nl/uuid:eedd25e6-c625-45e9-9d32-f818aa89c19d>
- Hirao A, Kitazaki S, Yamazaki N. 2006. Development of a New Driving Posture Focused on Biomechanical Loads [Internet]. Warrendale, PA: SAE International; [cited 2015 Jun 19]. Available from: <http://papers.sae.org/2006-01-1302/>
- Holmes MWR, Carvalho DED, Karakolis T, Callaghan JP. 2015. Evaluating Abdominal and Lower-Back Muscle Activity While Performing Core Exercises on a Stability Ball and a Dynamic Office Chair. *Hum Factors J Hum Factors Ergon Soc.* 57:1149–1161.
- Hosea. 1986. Myoelectric Analysis of the Paraspinal Musculature in Relati... : Spine. LWW [Internet]. [cited 2015 Mar 16]. Available from: [http://journals.lww.com/spinejournal/Fulltext/1986/11000/Myoelectric\\_Analysis\\_of\\_the\\_Paraspinal\\_Musculature.13.aspx](http://journals.lww.com/spinejournal/Fulltext/1986/11000/Myoelectric_Analysis_of_the_Paraspinal_Musculature.13.aspx)
- Hoy MG, Zajac FE, Gordon ME. 1990. A musculoskeletal model of the human lower extremity: The effect of muscle, tendon, and moment arm on the moment-angle relationship of musculotendon actuators at the hip, knee, and ankle. *J Biomech.* 23:157–169.
- Huang M, Lee T, Gibson I, Hajizadeh K. 2012. Effect of Sitting Posture on Spine Joint Angles and Forces. In: Proc 6th Int Conf Rehabil Eng Assist Technol [Internet]. Kaki Bukit TechPark II,, Singapore: Singapore Therapeutic, Assistive & Rehabilitative Technologies (START) Centre; p. 42:1–42:4. Available from: <http://dl.acm.org/citation.cfm?id=2501134.2501184>
- Huang S, Zhang Z, Xu Z, He Y. 2015. Modeling of human model for static pressure distribution prediction. *Int J Ind Ergon.* 50:186–195.
- Huynh KT, Gibson I, Jagdish BN, Lu WF. 2015. Development and validation of a discretised multi-body spine model in LifeMOD for biodynamic behaviour simulation. *Comput Methods Biomed Engin.* 18:175–184.
- Jackson C, Emck AJ, Hunston MJ, Jarvis PC. 2009. Pressure Measurements and Comfort of Foam Safety Cushions for Confined Seating. *Aviat Space Environ Med.* 80:565–569.
- Jan S van S. 2007. Color Atlas of Skeletal Landmark Definitions E-Book: Guidelines for Reproducible Manual and Virtual Palpations. [place unknown]: Elsevier Health Sciences.

Jeukendrup Asker, Gleeson Michael. 2009. Sport Nutrition-2nd Edition - Asker Jeukendrup, Michael Gleeson. Hum-Kinet [Internet]. [cited 2017 Sep 28]. Available from: <http://www.humankinetics.com/products/all-products/sport-nutrition---2nd-edition>

Kamijo, Tsujimura, Obara, Katsumata. 1982. Evaluation of seating comfort. SAE Conf.

Kelley DE, Slasky BS, Janosky J. 1991. Skeletal muscle density: effects of obesity and non-insulin-dependent diabetes mellitus. *Am J Clin Nutr.* 54:509–515.

Kim KH, Young KS, Bernal Y, Boppana A, Vu LQ, Benson EA, Jarvis S, Rajulu SL. 2016. A Parametric Model of Shoulder Articulation for Virtual Assessment of Space Suit Fit [Internet]. In: 30 Nov. - 1 Dec. 2016, Switzerland; [cited 2016 Dec 12]. Available from: <https://ntrs.nasa.gov/search.jsp?R=20160007862>

Klein Horsman MD, Koopman HFJM, van der Helm FCT, Prosé LP, Veeger HEJ. 2007. Morphological muscle and joint parameters for musculoskeletal modelling of the lower extremity. *Clin Biomech.* 22:239–247.

Kolich. 2004. Predicting automobile seat comfort using a neural network. *Int J Ind Ergon* 33.:285–293.

Komura T, Shinagawa Y, Kunii TL. 2000. Creating and retargetting motion by the musculoskeletal human body model. *Vis Comput.* 16:254–270.

Kosiak M. 1961. Etiology of decubitus ulcers. *Arch Phys Med Rehabil.* 42:19–29.

Krouskop TA, Reddy NP, Spencer WA, Secor JW. 1978. Mechanisms of decubitus ulcer formation — An hypothesis. *Med Hypotheses.* 4:37–39.

Kuroda S, Akimoto M. 2005. Finite element analysis of undermining of pressure ulcer with a simple cylinder model. *J Nippon Med Sch Nippon Ika Daigaku Zasshi.* 72:174–178.

Kwang TS, Gibson I, Jagdish BN. 2009. Detailed Spine Modeling with LifeMOD™. In: Proc 3rd Int Conv Rehabil Eng Assist Technol [Internet]. New York, NY, USA: ACM; p. 25:1–25:5. Available from: <http://doi.acm.org/10.1145/1592700.1592729>

Kyung G, Nussbaum MA. 2008a. Driver sitting comfort and discomfort (part II): Relationships with and prediction from interface pressure. *Int J Ind Ergon.* 38:526–538.

Kyung G, Nussbaum MA. 2008b. Driver sitting comfort and discomfort (part II): Relationships with and prediction from interface pressure. *Int J Ind Ergon.* 38:526–538.

Larrabee WF. 1986. A finite element model of skin deformation. I. Biomechanics of skin and soft tissue: a review. *The Laryngoscope.* 96:399–405.

Lee, K. S., Ferraiuolo, P., Temming, J. 1993. Measuring Seat Comfort. *SAE Tech Pap Ser* 930105.:25–30.

Lee KS, Waikar AM, Wu L. 1988. Physical stress evaluation of microscope work using objective and subjective methods. *Int J Ind Ergon.* 2:203–209.

Levy A, Kopplin K, Gefen A. 2014. An air-cell-based cushion for pressure ulcer protection remarkably reduces tissue stresses in the seated buttocks with respect to foams: Finite element studies. *J Tissue Viability.* 23:13–23.

Li S, Zhang Z, Wang J. 2013. A New Custom-Contoured Cushion System Based on Finite Element Modeling Prediction. *J Mech Med Biol.* 13.

Li W, Zhang M, Lv G, Han Q, Gao Y, Wang Y, Tan Q, Zhang M, Zhang Y, Li Z. 2015. Biomechanical response of the musculoskeletal system to whole body vibration using a seated driver model. *Int J Ind Ergon.* 45:91–97.

Li Z, Hu J, Reed MP, Rupp JD, Hoff CN, Zhang J, Cheng B. 2011. Development, Validation, and Application of a Parametric Pediatric Head Finite Element Model for Impact Simulations. *Ann Biomed Eng.* 39:2984–2997.

Lin F, Moran B, Bankard J, Hendrix R, Makhsoos M. 2004. FEM model for evaluating buttock tissue response under sitting load. *Conf Proc Annu Int Conf IEEE Eng Med Biol Soc IEEE Eng Med Biol Soc Annu Conf.* 7:5088–91.

Linder-Ganz E, Gefen A. 2004. Mechanical compression-induced pressure sores in rat hindlimb: muscle stiffness, histology, and computational models. *J Appl Physiol.* 96:2034–2049.

- Linder-Ganz E, Shabshin N, Itzchak Y, Gefen A. 2007a. Assessment of mechanical conditions in sub-dermal tissues during sitting: A combined experimental-MRI and finite element approach. *J Biomech.* 40:1443–1454.
- Linder-Ganz E, Shabshin N, Itzchak Y, Gefen A. 2007b. Assessment of mechanical conditions in sub-dermal tissues during sitting: A combined experimental-MRI and finite element approach. *J Biomech.* 40:1443–1454.
- Lis AM, Black KM, Korn H, Nordin M. 2006. Association between sitting and occupational LBP. *Eur Spine J.* 16:283–298.
- Liu Z, Wang J. 2011. Influences of Sitting Posture and Interface Activity on Human Physical and Psychological Reaction. In: 2011 5th Int Conf Bioinforma Biomed Eng. [place unknown]; p. 1–4.
- Luboz V, Petrizelli M, Bucki M, Diot B, Vuillerme N, Payan Y. 2014. Biomechanical modeling to prevent ischial pressure ulcers. *J Biomech.* 47:2231–2236.
- Lueder. 2004. Ergonomics of seated movement a review of the scientific literature. *Ergon Rev Humanics Ergosystems.*
- Macintosh JE, Bogduk N, Pearcy MJ. 1993. The effects of flexion on the geometry and actions of the lumbar erector spinae. *Spine.* 18:884–893.
- Makhsous M, Lim D, Hendrix R, Bankard J, Rymer WZ, Lin F. 2007. Finite Element Analysis for Evaluation of Pressure Ulcer on the Buttock: Development and Validation. *IEEE Trans Neural Syst Rehabil Eng.* 15:517–525.
- Martin JD, Simpson TW. 2005. Use of Kriging Models to Approximate Deterministic Computer Models. *AIAA J.* 43:853–863.
- Mastrigt SH, Groenesteijn L, Vink P, Kuijt-Evers LFM. 2017. Predicting passenger seat comfort and discomfort on the basis of human, context and seat characteristics: a literature review. *Ergonomics.* 60:889–911.
- McGill SM, Norman RW. 1986. Partitioning of the L4-L5 dynamic moment into disc, ligamentous, and muscular components during lifting. *Spine.* 11:666–678.
- Mergl. 2005. Predicting Long Term Riding Comfort in Cars by Contact Forces Between Human and Seat [Internet]. [cited 2016 Feb 5]. Available from: <http://papers.sae.org/2005-01-2690/>
- Mergl C, Anton T, Madrid-Dusik R, Hartung J, Librandi A, Bubb H. 2004. Development of a 3D Finite Element Model of Thigh and Pelvis [Internet]. Warrendale, PA: SAE International; [cited 2015 Apr 24]. Available from: <http://papers.sae.org/2004-01-2132/>
- Mergl C, Klendauer M, Mangen C, Bubb H. 2005. Predicting Long Term Riding Comfort in Cars by Contact Forces Between Human and Seat [Internet]. Warrendale, PA: SAE International; [cited 2015 Mar 4]. Available from: <http://papers.sae.org/2005-01-2690/>
- Michida N, Okiyama H, Nishikawa K, Nouzawa T. 2001. A Study of Drivers' Fatigue Mechanisms During Long Hour Driving [Internet]. Warrendale, PA: SAE International; [cited 2015 May 22]. Available from: <http://papers.sae.org/2001-01-0381/>
- Ming Zhang, Roberts VC. 1993. The effect of shear forces externally applied to skin surface on underlying tissues. *J Biomed Eng.* 15:451–456.
- Mircheski I, Kandikjan T, Sidorenko S. 2014. Comfort Analysis of Vehicle Driver's Seat Through Simulation of the Sitting Process. *Teh Vjesn-Tech Gaz.* 21:291–298.
- Moes N. 2005. Analysis of sitting discomfort, a review. *Contemp Ergon.* 200–204.
- Moes, N. C. C. M., Horvath. 2002. Finite elements model of the human body: Geometry and non-linear material properties. *Proc TMCE.*:22–26.
- Moes NCCM. 2007. Variation in sitting pressure distribution and location of the points of maximum pressure with rotation of the pelvis, gender and body characteristics. *Ergonomics.* 50:536–561.
- Mohanty PP, Mahapatra SS. 2014. A finite element approach for analyzing the effect of cushion type and thickness on pressure ulcer. *Int J Ind Ergon.* 44:499–509.
- Mooney M. 1940. A Theory of Large Elastic Deformation. *J Appl Phys.* 11:582–592.

- Nachemson A, Elfström G. 1970. Intravital dynamic pressure measurements in lumbar discs. A study of common movements, maneuvers and exercises. *Scand J Rehabil Med Suppl.* 1:1–40.
- Nerot A, Skalli W, Wang X. 2016. A principal component analysis of the relationship between the external body shape and internal skeleton for the upper body. *J Biomech.* 49:3415–3422.
- Nissan M, Gilad I. 1986. Dimensions of human lumbar vertebrae in the sagittal plane. *J Biomech.* 19:753–758.
- Ogden RW, Saccomandi G, Sgura I. 2004. Fitting hyperelastic models to experimental data. *Comput Mech.* 34:484–502.
- Olesen CG, Zee M de, Rasmussen J. 2010a. Missing links in pressure ulcer research—An interdisciplinary overview. *J Appl Physiol.* 108:1458–1464.
- Olesen CG, Zee M de, Rasmussen J. 2010b. Missing links in pressure ulcer research—An interdisciplinary overview. *J Appl Physiol.* 108:1458–1464.
- Oomens CWJ, Bressers OFJT, Bosboom EMH, Bouten CVC, Bader DL. 2003. Can Loaded Interface Characteristics Influence Strain Distributions in Muscle Adjacent to Bony Prominences? *Comput Methods Biomed Engin.* 6:171–180.
- Oomens CWJ, Zenhorst W, Broek M, Hemmes B, Poeze M, Brink PRG, Bader DL. 2013a. A numerical study to analyse the risk for pressure ulcer development on a spine board. *Clin Biomech.* 28:736–742.
- Oomens CWJ, Zenhorst W, Broek M, Hemmes B, Poeze M, Brink PRG, Bader DL. 2013b. A numerical study to analyse the risk for pressure ulcer development on a spine board. *Clin Biomech.* 28:736–742.
- Oudenhuijzen A, Tan K, Morsch F. 2003. The Relationship Between Seat Pressure and Comfort [Internet]. Warrendale, PA: SAE International; [cited 2015 Mar 19]. Available from: <http://papers.sae.org/2003-01-2213/>
- Palevski A, Glaich I, Portnoy S, Linder-Ganz E, Gefen A. 2006. Stress relaxation of porcine gluteus muscle subjected to sudden transverse deformation as related to pressure sore modeling. *J Biomech Eng.* 128:782–787.
- Pankoke S, Siefert A. 2007a. Virtual Simulation of Static and Dynamic Seating Comfort in the Development Process of Automobiles and Automotive Seats: Application of Finite-Element-Occupant-Model CASIMIR [Internet]. Warrendale, PA: SAE International; [cited 2015 Apr 24]. Available from: <http://papers.sae.org/2007-01-2459/>
- Pankoke S, Siefert A. 2007b. Virtual Simulation of Static and Dynamic Seating Comfort in the Development Process of Automobiles and Automotive Seats: Application of Finite-Element-Occupant-Model CASIMIR [Internet]. Warrendale, PA: SAE International; [cited 2015 Apr 24]. Available from: <http://papers.sae.org/2007-01-2459/>
- Park, S E, Mp R. 2017. A parametric model of child body shape in seated postures. *Traffic Inj Prev.* 18:533–536.
- Paul G, Daniell N, Fraysse F. 2012. Patterns of correlation between vehicle occupant seat pressure and anthropometry. *Work.* 41:2226–2231.
- Peng J, Panda J, Van Sint Jan S, Wang X. 2015. Methods for determining hip and lumbosacral joint centers in a seated position from external anatomical landmarks. *J Biomech.* 48:396–400.
- Peterson MJ, Adkins HV. 1982. Measurement and Redistribution of Excessive Pressures During Wheelchair Sitting. *Phys Ther.* 62:990–994.
- Pintar FA, Yoganandan N, Myers T, Elhagediab A, Sances Jr. A. 1992. Biomechanical properties of human lumbar spine ligaments. *J Biomech.* 25:1351–1356.
- Porter JM, Gyi DE, Tait HA. 2003. Interface pressure data and the prediction of driver discomfort in road trials. *Appl Ergon.* 34:207–214.
- Principal Component Analysis | I.T. Jolliffe | Springer. [place unknown]; [cited 2017 Mar 29]. Available from: <http://www.springer.com/us/book/9780387954424>
- Rasmussen J, Tørholm S, de Zee M. 2009a. Computational analysis of the influence of seat pan inclination and friction on muscle activity and spinal joint forces. *Int J Ind Ergon.* 39:52–57.

Rasmussen J, Tørholm S, de Zee M. 2009b. Computational analysis of the influence of seat pan inclination and friction on muscle activity and spinal joint forces. *Int J Ind Ergon.* 39:52–57.

Rasmussen J, Zee M de. 2008a. Design Optimization of Airline Seats [Internet]. Warrendale, PA: SAE International; [cited 2015 Mar 4]. Available from: <http://papers.sae.org/2008-01-1863/>

Rasmussen J, Zee M de. 2008b. Design Optimization of Airline Seats [Internet]. Warrendale, PA: SAE International; [cited 2015 Mar 4]. Available from: <http://papers.sae.org/2008-01-1863/>

Rasmussen J, Zee M de, Tørholm S. 2007a. Muscle Relaxation and Shear Force Reduction May Be Conflicting: A Computational Model of Seating [Internet]. Warrendale, PA: SAE International; [cited 2015 Mar 4]. Available from: <http://papers.sae.org/2007-01-2456/>

Rasmussen J, Zee M de, Tørholm S. 2007b. Muscle Relaxation and Shear Force Reduction May Be Conflicting: A Computational Model of Seating [Internet]. Warrendale, PA: SAE International; [cited 2015 Mar 4]. Available from: <http://papers.sae.org/2007-01-2456/>

Reed MP, Parkinson MB. 2008. Modeling Variability in Torso Shape for Chair and Seat Design. :561–569.

Reed MP, Schneider LW, Ricci LL. 1994. SURVEY OF AUTO SEAT DESIGN RECOMMENDATIONS FOR IMPROVED COMFORT [Internet]. [cited 2015 Mar 4]. Available from: <http://trid.trb.org/view.aspx?id=410745>

Reed MP, Sochor MM, Rupp JD, Klinich KD, Manary MA. 2009. Anthropometric specification of child crash dummy pelvis through statistical analysis of skeletal geometry. *J Biomech.* 42:1143–1145.

Reed, Raschke, Tirumali, Parkinson. 2014. Developing and Implementing Parametric Human Body Shape Models in Ergonomics Software. *Int Digit Hum Model Conf* 3rd Tokyo Jpn.

Reichel. 1958. Shear force as a factor in decubitus ulcers in paraplegics. :762–763.

Richards L.C. 1980. On the psychology of passenger comfort. Oborne DJ Levis JA Eds *Hum Factors Transp Res.*

Rivlin RS. 1948. Large Elastic Deformations of Isotropic Materials. In: Barenblatt GI, Joseph DD, editors. *Collect Pap RS Rivlin* [Internet]. [place unknown]: Springer New York; [cited 2016 Dec 21]; p. 90–108. Available from: [http://link.springer.com/chapter/10.1007/978-1-4612-2416-7\\_8](http://link.springer.com/chapter/10.1007/978-1-4612-2416-7_8)

Salvia P, Jan SVS, Crouan A, Vanderkerken L, Moiseev F, Sholukha V, Mahieu C, Snoeck O, Rooze M. 2009. Precision of shoulder anatomical landmark calibration by two approaches: A CAST-like protocol and a new anatomical palpator method. *Gait Posture.* 29:587–591.

Scales. 1982. Pressure sore prevention. *Care.*:9–17.

Sember J. 1994. The biomechanical relationship of seat design to the human anatomy. *Hard Facts Soft Mach Egon Seat.*:221–230.

Silber, Then. 2009. Numerical Analysis of the Interactions between Human Body Soft Tissue and Body Supports.

Søndergaard KHE, Olesen CG, Søndergaard EK, de Zee M, Madeleine P. 2010. The variability and complexity of sitting postural control are associated with discomfort. *J Biomech.* 43:1997–2001.

Stevenson A, editor. 2010. *Oxford Dictionary of English* [Internet]. [place unknown]: Oxford University Press; [cited 2018 Jan 3]. Available from: <http://www.oxfordreference.com/view/10.1093/acref/9780199571123.001.0001/acref-9780199571123>

Stokes IAF, Gardner-Morse M. 1995. Lumbar spine maximum efforts and muscle recruitment patterns predicted by a model with multijoint muscles and joints with stiffness. *J Biomech.* 28:173–186.

SWEARINGEN JJ, WHEELWRIGHT CD, GARNER JD. 1962. AN ANALYSIS OF SITTING AREAS AND PRESSURES OF MAN. [place unknown].

Tang CY, Chan W, Tsui CP. 2010. Finite Element Analysis of Contact Pressures between Seat Cushion and Human Buttock-Thigh Tissue. *Engineering.* 02:720–726.

Tang CY, Tsui CP. 2006. Method of modeling muscular tissue with active finite elements [Internet]. [cited 2016 Mar 29]. Available from: <http://ira.lib.polyu.edu.hk/handle/10397/137>

Tewari VK, Prasad N. 2000. Optimum seat pan and back-rest parameters for a comfortable tractor seat. *Ergonomics*. 43:167–186.

Thakurta K, Koester D, Bush N, Bachle S. 1995. Evaluating Short and Long Term Seating Comfort [Internet]. Warrendale, PA: SAE Technical Paper; [cited 2017 Sep 14]. Available from: <http://papers.sae.org/950144/>

Todd, Thacker. 1994. Three-dimensional computer model of the human buttocks, *in vivo*. *J Rehabil Res Dev.*:111–111.

Trochu F. 1993. A contouring program based on dual kriging interpolation. *Eng Comput.* 9:160–177.

Udo H, Fujimura M, Yoshinaga F. 1999. The Effect of a Tilting Seat on Back, Lower Back and Legs during Sitting Work. *Ind Health.* 37:369–381.

Vergara M, Page A. 2000. System to measure the use of the back rest in sitting-posture office tasks. *Appl Ergon.* 31:247–254.

Verver MM, van Hoof J, Oomens CWJ, Wismans JSHM, Baaijens FPT. 2004a. A Finite Element Model of the Human Buttocks for Prediction of Seat Pressure Distributions. *Comput Methods Biomed Engin.* 7:193–203.

Verver MM, van Hoof J, Oomens CWJ, Wismans JSHM, Baaijens FPT. 2004b. A Finite Element Model of the Human Buttocks for Prediction of Seat Pressure Distributions. *Comput Methods Biomed Engin.* 7:193–203.

Vink P, Hallbeck S. 2012a. Editorial: Comfort and discomfort studies demonstrate the need for a new model. *Appl Ergon.* 43:271–276.

Vink P, Hallbeck S. 2012b. Editorial: Comfort and discomfort studies demonstrate the need for a new model. *Appl Ergon.* 43:271–276.

Volpe Y, Governi L, Furferi R. 2015. A Computational Model for Early Assessment of Padded Furniture Comfort Performance. *Hum Factors Ergon Manuf Serv Ind.* 25:90–105.

Vos GA, Congleton JJ, Steven Moore J, Amendola AA, Ringer L. 2006. Postural versus chair design impacts upon interface pressure. *Appl Ergon.* 37:619–628.

Wagnac EL, Aubin C-E, Dansereau J. 2008a. A New Method to Generate a Patient-Specific Finite Element Model of the Human Buttocks. *IEEE Trans Biomed Eng.* 55:774–783.

Wagnac EL, Aubin C-E, Dansereau J. 2008b. A New Method to Generate a Patient-Specific Finite Element Model of the Human Buttocks. *IEEE Trans Biomed Eng.* 55:774–783.

Wang CCL. 2005. Parameterization and parametric design of mannequins. *Comput-Aided Des.* 37:83–98.

Wenyu W, Chenqi X, Lindong L. 2013. Characteristic parameters of cushion in high-speed train (CRH) contribute to seat pressure distribution analysis. In: Zhao H, Liu K, Yu X, editors. *Adv Des Manuf Technol Iii Pts 1-4*. Vol. 397–400. Stafa-Zurich: Trans Tech Publications Ltd; p. 593–598.

Wilke H-J, Neef P, Hinz B, Seidel H, Claes L. 2001. Intradiscal pressure together with anthropometric data – a data set for the validation of models. *Clin Biomech.* 16, Supplement 1:S111–S126.

Winter DA. 2009. *Biomechanics and Motor Control of Human Movement*. [place unknown]: John Wiley & Sons.

Xiaoming D, Jindong R, Chunlei S, Lemeng L. 2013. Simulation of the Interaction between Driver and Seat. *Chin J Mech Eng.* 26:1234–1242.

Yamazaki, S., Kouchi, M., Mochimaru, M. 2013. Markerless landmark localization on body shape scans by non-rigid model fitting. *Proc 2nd Digit Hum Model.*

Yun, Donges, Freivalds. 1992. Using force sensitive resistors to evaluate the driver seating comfort. *Adv Ind Ergon Saf.*

de Zee M, Hansen L, Wong C, Rasmussen J, Simonsen EB. 2007. A generic detailed rigid-body lumbar spine model. *J Biomech.* 40:1219–1227.

Zhang, Helander, M. G., C. G. 1996. Identifying factors of comfort and discomfort in sitting. *Hum Factors J Hum Factors Ergon Soc.*:377–389.

Zhang M, Zheng YP, Mak AFT. 1997. Estimating the effective Young's modulus of soft tissues from indentation tests—nonlinear finite element analysis of effects of friction and large deformation. *Med Eng Phys.* 19:512–517.

Zheng YP, Mak AFT. 1999. Extraction of Quasi-Linear Viscoelastic Parameters for Lower Limb Soft Tissues From Manual Indentation Experiment. *J Biomech Eng.* 121:330–339.

# Appendices

## 1. Cabin environment discomfort factors

Feeling of discomfort and fatigue can come from very various sources when a person travels by plane. First of all, the psychological state of the person plays an important role. As explains Bor (2007), factors leading to stress during a flight are numerous: anxieties about safety, fear of missing the flight, or even separation from loved ones. In a study on 291 trip reports of passengers, all kind of source of discomfort were reported (Blok M et al. 2007) and it appears that the majority comes from the psychological state (due to Delay, Impolite crew, Lack of info...) (Figure 100).

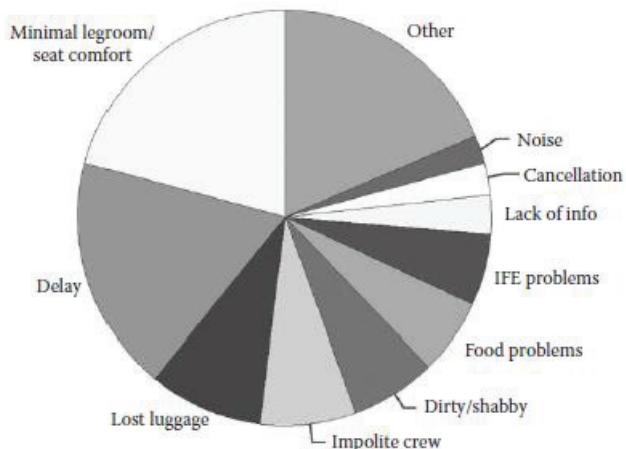
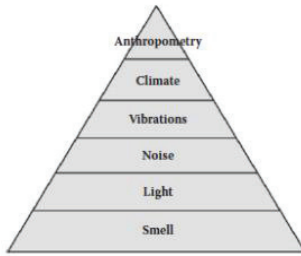


Figure 100: Discomfort sources from trip report (Block, Vink, Kamp 2007)

This study also shows that noise can be a cause of discomfort. Several studies highlight the importance of the cabin environment in the discomfort appearance. Richards (1977) performed one of the first studies on comfort with 861 passengers and found that some environment factors like noise or up/down motion of the plane showed high gamma coefficient (respectively 0.41 and 0.46) with discomfort. Bubb R (2008) defined a pyramid of discomfort factor influence (Figure 101). According to him, the smell overruled all the others factors, that means that if the smell is bad, the other factors won't play a role in discomfort. Other environment factors like light or noise come after and the last one, the only one involving the seat is the anthropometry.



**Figure 101:Bubb (2008) discomfort pyramid**

The specificities of an aircraft cabin imply some effects on the body. Each aspect specific to the cabin environment and its effect on the body often found in the literature will be described further.

## 1.1 Cabin Pressure

Modern airplanes cruise at an altitude between 30 000 and 40 000 ft (9150 and 12 200 m) but the cabin pressure varies from sea level (760 mmHg) to 8 000 ft (2 500 m) (567 mmHg).

This variation of pressure leads to a decrease of the oxygen saturation level from 95% to 90 % ( $\pm 3\%$ ) after 30 min and possible further decrease under 80%. Under a level of 85%, there can be impairments of the mental functions and an appreciable handicap can appear under 70 % of oxygen saturation (Peacock 1998). This saturation could be dangerous only for people with ischemic heart disease.

Furthermore, the incidence of low pressure on deep vein thrombosis has been studied (Bendz et al. 2000; Boccalon et al. 2005; Toff et al. 2006; Schobersberger et al. 2007) and it appears that this health issue due to blood coagulation is more linked to the seated position than the cabin pressure.

## 1.2 Motion and vibrations

Specific motion of the plane can also have an effect on the body. Unusual vibrations, motion and centrifugal forces in particular with turbulent flight conditions can lead to dyspeptic symptoms. In a questionnaire survey of 923 passengers on 38 commercial airline flights (Turner et al. 2000), 0.5 % of passengers reported vomiting, 8.4% reported nausea and 16.2% reported illness. The motion sickness depends on the predisposition of the person and on the air turbulence which causes vertical motion on the vestibular organ.

### 1.3 Cabin air quality

According to a study done by Pierce et al. (1999), inadequate air quality may cause symptoms of fatigue, dizziness and respiratory and ocular discomfort. Cabin air quality can be determined by measuring the CO<sub>2</sub> concentration. Lee et al. (1999) measured concentrations in business class greater than 1 000 ppm (parts per million), which is the maximum concentration recommended, and reach sometimes 2 900 ppm (during take-off and landing). Most commercial provide 2.8 L/s/p (Litre/second/person) whereas McFarland (1953) found that 9 L/s/p is the adequate volume of fresh air for passenger comfort and 7 L/s/p is the minimum to maintain CO<sub>2</sub> concentration below 1 000 ppm.

The relative cabin humidity drops from 47% to 11% during 30 min of ascent and can reach 2-3% at the end of the flight (Eng et al. 1982). This very dry air is source of discomfort for 60 % of cabin crew people during a survey on long-haul flight. This humidity rate is much lower than the comfortable level of 40-70% at sea level. Nevertheless, increasing humidity mean reducing outside flow and Strøm-Tejsen et al. (2007) have shown that increasing humidity to 28% by reducing air flow to 1.4 l/s has adverse effects on dizziness or headache symptoms.

### 1.4 Noise

A study done by Mellert et al. (2008) shows that noise has a great impact on discomfort and fatigue because passengers feel more aware of pain under noisy conditions. Even if the level of sound is not in itself a source of discomfort or health risk (below 85 dB during a flight), it affects the perception of comfort and increases the effects of the other sources of comfort. For instance, awareness of swollen feet increases of 43 percent in noisy conditions. Passengers feel also more the neck pain and the air quality, degradation of air quality is felt for 15 % of passengers with noise while no change in the effective air quality.

### 1.5 Temperature

A pleasant climate is often not noticed but a high or low temperature attracts attention and lead to discomfort for passenger. In the study made by Vink (2011) on 10 032 passengers, less than 5 % complained about temperature. Several theories on the ideal temperature exist, (Strøm-Tejsen et al. 2007) advises a temperature of 21 °C in the beginning of the flight, 22-23 °C after 3h and 21° after 6h. Liping (2013) proposed the following for comfortable temperature:

$$T = 21.5^{\circ}\text{C} + 0.11 \text{ ET} \quad 1)$$

ET: departure city temperature

The thermal comfort depends on the person and the sex, women are more sensitive to low temperature (Marggraf-Micheel et al. 2010). Nevertheless, only extreme temperatures, more than 31°, increase the sick building syndrome (headache, irritated eyes....) leading to discomfort and fatigue.

Each of this environment factors have individually a weak effect on discomfort but when all of them are added, it contribute to create an unusual environment for the body. The human body may then be suffering from these specific conditions which lead to more fatigue with the duration of the flight. For instance Hinninghofen & Enck (2006) explain that "Aircraft vibration is usually well tolerated, but together with aircraft motion, noise and low humidity, it may cause some degree of discomfort and contribute to travel fatigue". It means that determine the relation between each of this factor and the discomfort feeling can be a difficult task. The second difficulty in analyzing relation between these factors and discomfort is about the very personalized response of the body to these parameters. For example, it has been described that the pressure cabin has an impact only for people with health problem predisposition. We can suppose that the discomfort feeling is even more dependent of the person and its global health state. All these environmental factors haven't been take into consideration in the rest of thesis.

## 2. Regressions between distances from landmarks to hip joint (HJC) and lumbosacral joint (LSJC) and pelvis dimensions (pelvis width PW, pelvis depth PD, pelvis height PH, (see Figure 102)

Following regressions have been found in (Peng et al. 2015) :

$$\text{Distance}(HJC - RIAS) = 18.7 + 0.132 * PW + 0.493 * PH$$

$$\underline{\text{Distance}(HJC - LIAS) = 51.7 + 0.5491 * PW + 0.441 * PH}$$

$$\underline{\text{Distance}(HJC - RIPS) = 38.4 + 0.580 * PD_1}$$

$$\underline{\text{Distance}(HJC - IPJ) = 36.2 + 0.119 * PW + 0.164 * PD_1 + 0.128 * PH}$$

$$\underline{\text{Distance}(LSJC - RIAS) = 17.8 + 0.424 * PW + 0.175 * PD}$$

$$\underline{\text{Distance}(LSJC - PJC) = 41.2 + 0.264 * PW + 0.501 * PH}$$

$$\underline{\text{Distance}(LSJC - IPS) = 67.8}$$

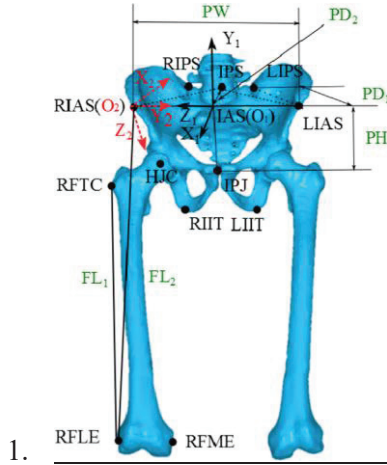


**Figure 102: Pelvis and femur anatomical landmarks and bones dimensions (Peng et al. 2015)**

Each of the three joint centers (Right Hip Joint Center, Left Hip Joint Center, Lumbosacral Joint Center) was located by using four target ALs ( $T_i$ ). The joint center (C) was considered as the point which gives the shortest distance to the spheres centered at the target ALs with corresponding distances  $d_i$  as radius:

$$\text{minimize } f(C) = \sum_{i=1}^n (\sqrt{C - T_i} - d_i)^2$$

Finally, a regular symmetrized mesh corresponding to the subject scan was obtained with bony landmarked placed in the same local reference system (pelvis reference system described previously).

### 3. Regressions between PCs and predictors

$$PC1 = 690.482 + 102.96 * \theta_1 - 314.727 * \theta_2 + 12.9478 * \theta_3 + 321.738 * BMI - 345.415 * Sexe + 17.5597 \\ * Stature$$

$$PC2 = -27070.4 + 187.84 * \theta_1 + 277.55 * \theta_2 + 9.229 * \theta_3 + 357.836 * BMI - 181.734 * Sexe + 8.33642 \\ * Stature$$

$$PC3 = 26669.6 + 459.177 * \theta_1 + 60.732 * \theta_2 + 10.017 * \theta_3 - 298.634 * BMI - 400.073 * Sexe - 32.2863 \\ * Stature$$

$$PC4 = -9718.86 - 609.028 * \theta_1 + 50.1718 * \theta_2 + 7.6843 * \theta_3 + 30.7555 * BMI - 89.8438 * Sexe + 2.161 \\ * Stature$$

$$PC5 = 87.5863 - 288.215 * \theta_1 + 0.23332 * \theta_2 - 1.18763 * \theta_3 + 238.029 * BMI - 166.65 * Sexe + 18.4957 \\ * Stature$$

### 4. Local predictors

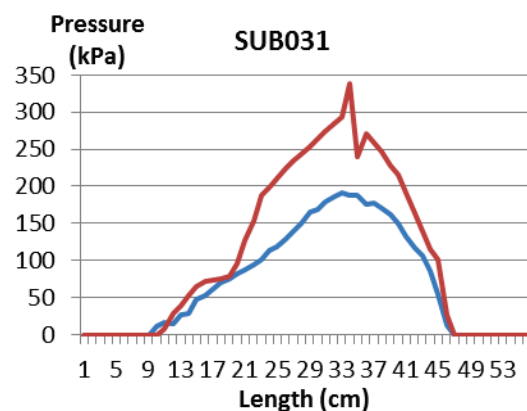
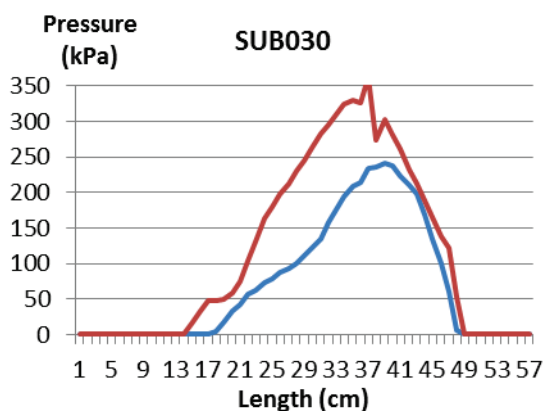
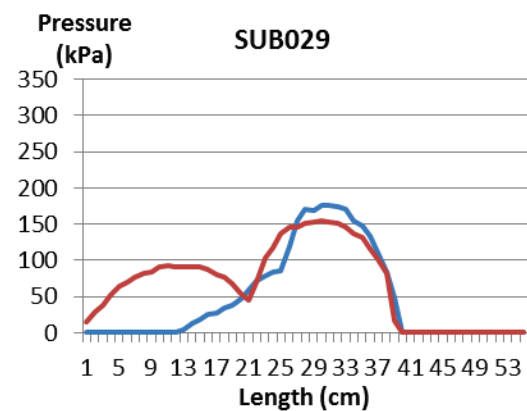
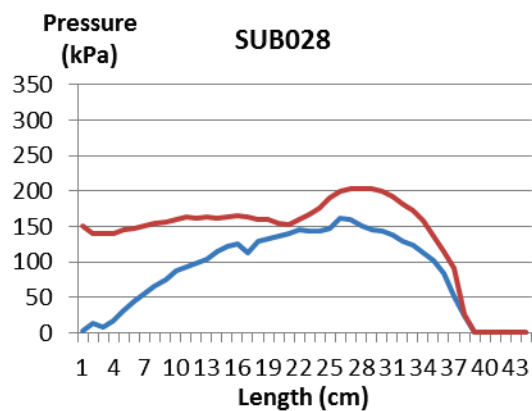
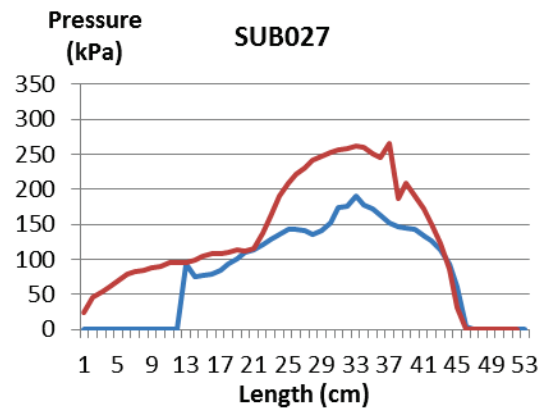
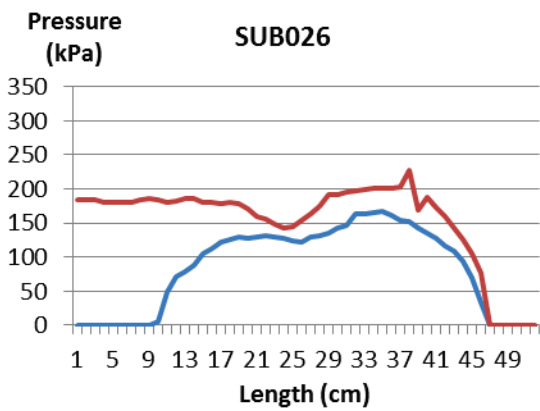
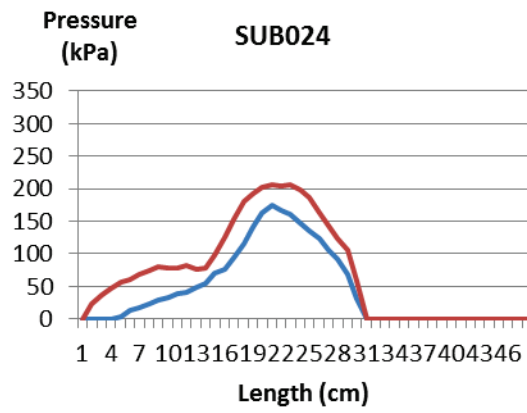
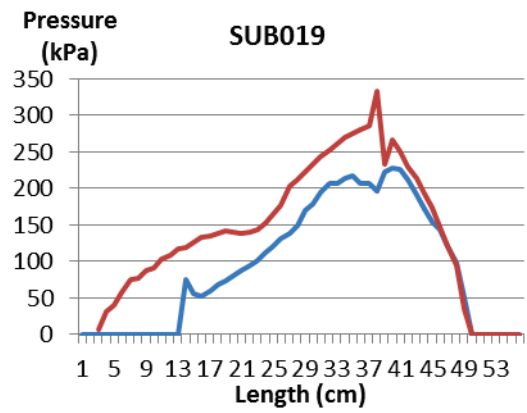
The same process has also been done with buttock-thigh related predictors as the waist circumference and the thigh length instead of global stature and BMI parameters. Several

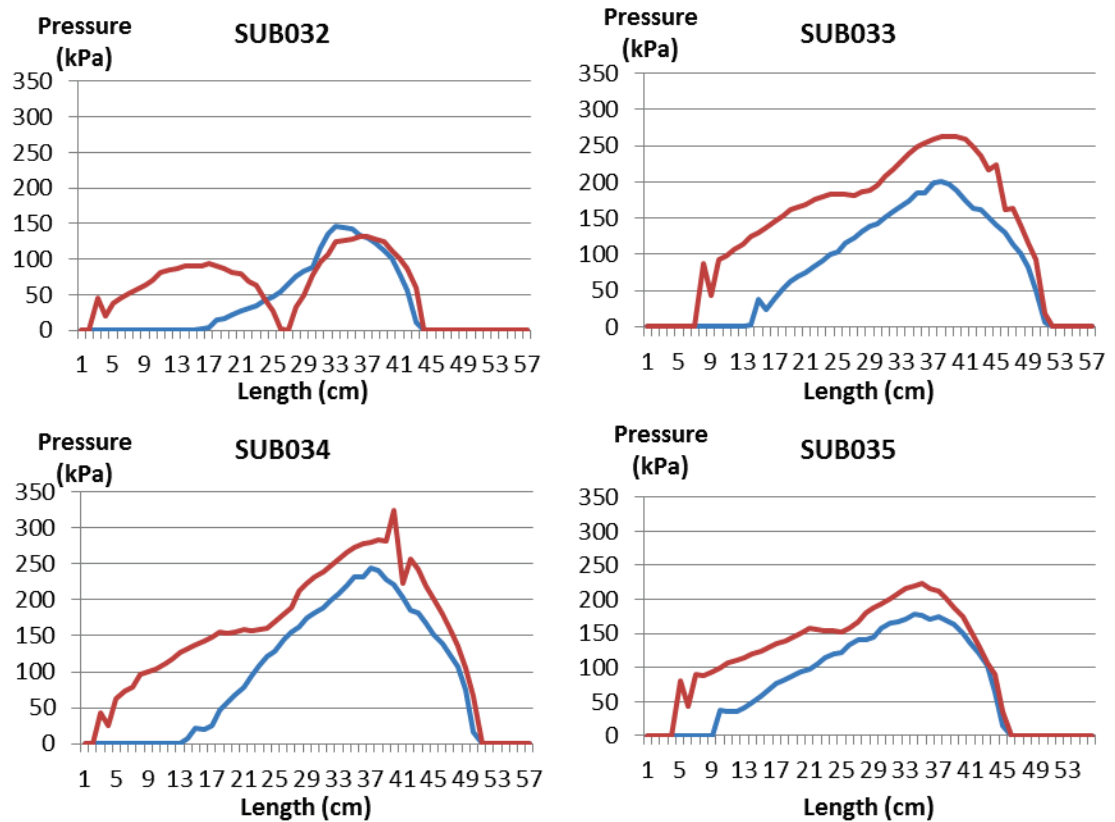
combinations have been tested (Table 25). Regressions have been calculated between the PC scores and these local anthropometric parameters. Then the leave-one-out process was applied. The averages of the mean distances between the predicted and measured external shape and bones landmarks over the 36 subjects for the different combinations are expressed in the Table 25. The external shape error was closed to the one found with global parameters. Only one combination (Thigh section, waist section, hip width, thigh length, gender) gave a smaller error ( $26,39 \pm 10,67$  mm instead of  $26,60 \pm 9,30$ ) for the shape prediction. The bones landmarks errors were more important.

**Table 25: Error of shape and landmarks prediction with parametric models build with different predictors**

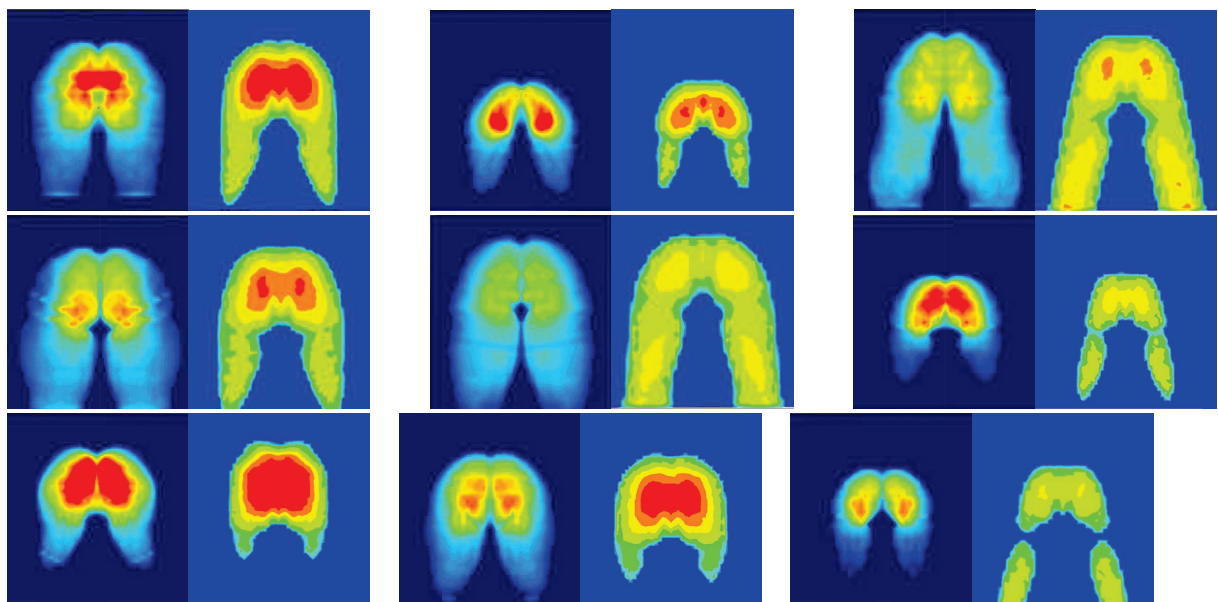
Parameters	Average of the mean error shape prediction(in mm) over the 36 subjects	Average of the mean error ALs (in mm) over the 36 subjects
Thigh section, waist section, hip width, thigh length, gender	$26,39 \pm 10,67$	$24,06 \pm 13,07$
Thigh section, waist section, thigh length, gender	$27,61 \pm 11,31$	$23,9 \pm 13,01$
Thigh section, hip width, thigh length, gender	$27,87 \pm 12,09$	$24,26 \pm 13,75$
Waist section, thigh length, gender	$26,85 \pm 10,72$	$24,09 \pm 10,22$
Stature, BMI, gender	$26,60 \pm 9,30$	$21,70 \pm 6,20$

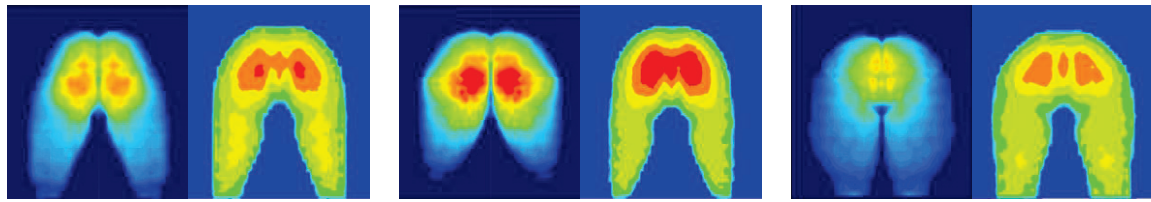
## 5. Profile pressure measured (blue) and simulated (red)





6. Comparison of measured (left) and simulated (right) pressure map





## 7. Comparison between elastic linear and hyperelastic law

Simulations have been proceeding with a Mooney Rivlin hyperelastic incompressible law for the soft tissues. Parameters used are the one described in chapter 2: C1 = 1.65 Kpa and C2 = 3.35 kPa.

**Table 26: Comparison of the mean pressure (Pmean) in kPa, the maximal pressure (Pmax) in kPa, the contact area (Area) in cm<sup>2</sup> between the linear elastic and the hyperelastic model**

	Pmean		Pmax		Contact area	
	Elastic	Hyperelastic	Elastic	Hyperelastic	Elastic	Hyperelastic
SUB019	7,15	7,09	12,11	13,63	1101	1104
SUB021	6,11	5,89	8,04	11,55	731	700
SUB024	6,75	6,61	11,1	10,55	522	528
SUB026	6,78	6,71	9,6	9,49	1196	1201
SUB027	6,14	6,4	10,87	10,3	1095	1052
SUB028	6,44	6,17	8,53	8,61	999	1009
SUB029	6,15	5,63	8,45	8,52	637	645
SUB030	8,6	8,49	17,7	17,66	789	794
SUB031	7,57	7,18	13,3	13,17	836	840
SUB032	5,99	5,4	7,71	7,9	568	576
SUB033	6,77	6,6	10,73	10,31	1166	1104
SUB034	6,99	6,55	11,72	11,52	1223	1227
SUB035	6,26	6,2	8,86	9,99	990	993

Table 26 presents the outputs values for both elastic linear and hyperelastic model. The results are very closed. The difference never exceeds 5%. This can be observed on the pressure map (Figure 103)

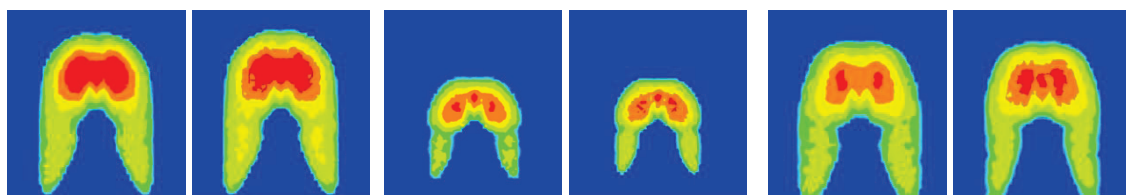


**Figure 103: Comparison of pressure map between linear model (left) and hyperelastic model (right)**

Consequently, with equivalent parameters, the two models gave same results whatever the model anthropometry.

## Comparison between bones scaled by kriging or by PCA model

The two methods for scaling bones from anatomical landmarks were compared on three subjects. These three subjects have been chosen to cover a wide variety of anthropometry (BMI of 19,1 31,5 and 39,4 kg.m<sup>-2</sup> and stature of 1,55m, 1,57m and 1,85m). When looking at the results of the pressure distribution for the different methods, it appeared that the PCA method gives better results.

The results are summarized in Table 27

**Table 27: Comparison of results (absolute values) of the two methods for bones scaling with experimental (Expe)**

	Pmean (kPa)			Pmax (kPa)			Grad_max (kPa/cm)		
	PCA	Kriging	Expe	PCA	Kriging	Expe	PCA	Kriging	Expe
SUB019	7,15	8,11	5,19	12,11	16,26	12,67	47,69	42,75	74,09
SUB024	6,75	6,71	4,63	11,1	9,09	13,34	29,24	27,54	36,33
SUB035	6,26	6,83	4,18	8,86	11,2	9,09	13,18	19,32	48,87

It can be observed that main difference between the two methods concerns the maximal pressure. The difference vary from 8,25% for the subject 29, to 18% for the subject 24 and reach 20,9% for the subject 35. In all the cases, the PCA method gives results closer to the experiment. This can be verified by comparing the simulated pressure map with the pressure map recorded (for example on Figure 104).

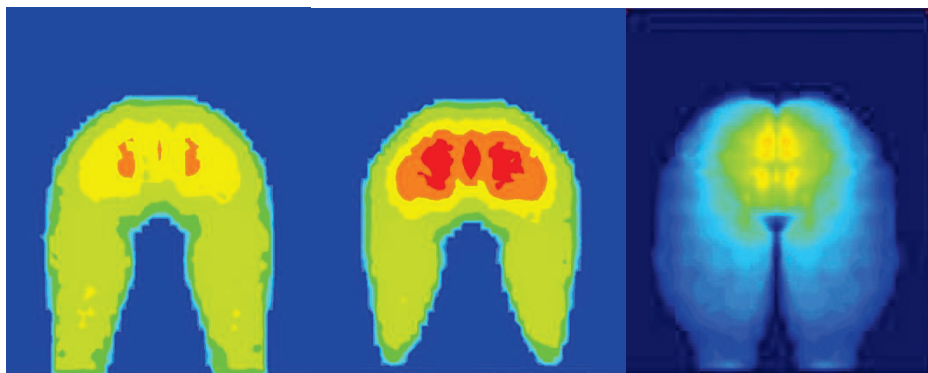


**Figure 104: Pressure map of one subject with PCA model (left) and kriging model (middle) and experiment (right)**

## 9. Muscular activity and disc load estimation

The coupling method has the advantage, compared to the other methods, to also compute the muscular activity and the joint reactions forces in addition to the tissue compression. These values were estimated for the 6 persons of this study. However, no EMG has been recorded during the experiment, and the joint forces are very difficult to measure, consequently no validation could be

done. Relations between the person position and the muscular activity or back joint reactions forces can be nevertheless observed.

## 8. Muscular activity

The maximal muscle activity (in % of maximum voluntary contraction) can vary a lot between the different persons. Important correlations were found between the maximal muscle activity and the pelvis-thigh angle ( $R^2 = 0.8138$ ) (Figure 105) or the pelvis inclination ( $R^2 = 0.7646$ ) (Figure 106) or the BMI ( $R^2 = 0.7165$ ) (Figure 107). The more the pelvis is reclined and the less the muscle activity is high. The more the BMI is important, the more the muscle activity will be high.

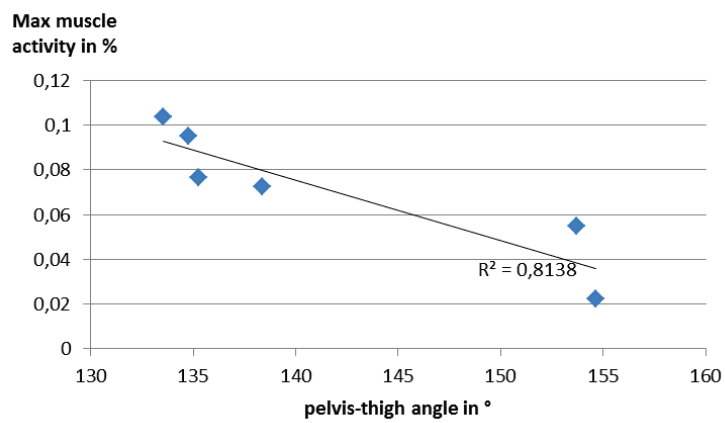


Figure 105: Maximum muscle activity function of pelvis-thigh angle

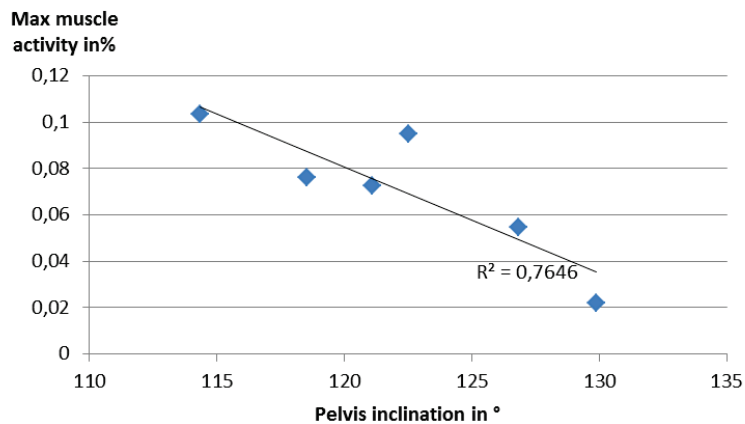


Figure 106: Maximum muscle activity function of pelvis inclination

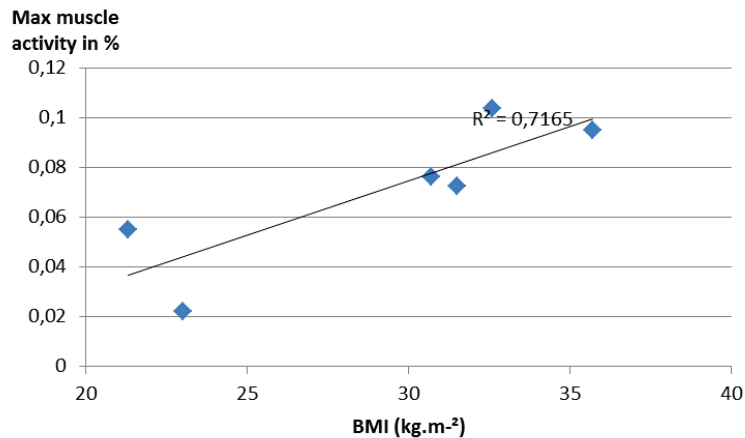


Figure 107: Maximum muscle activity function of BMI

## 9. Disk load

Important correlation ( $R^2=0.6337$ ) was found between the L5/S1 joint reaction force and the weight of the person (Figure 108). These results were expected, because the joint have to carry the weight of the person.

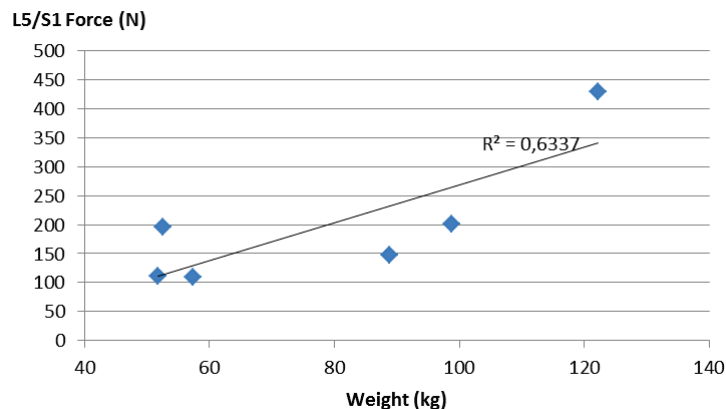
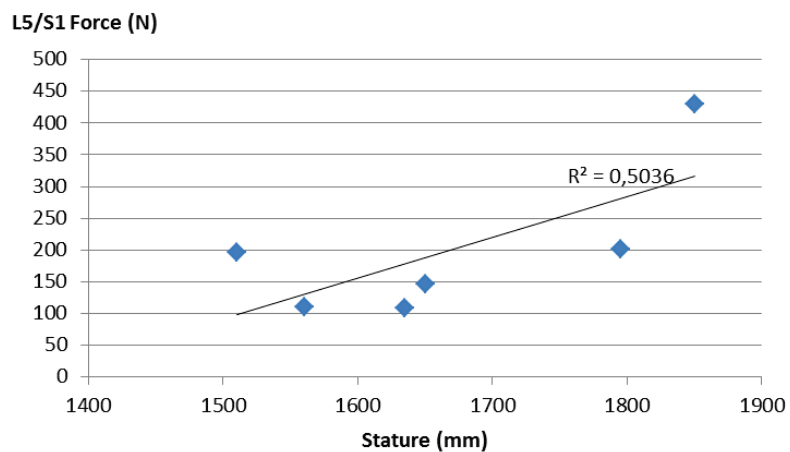


Figure 108: L5/S1 force function of weight

A bit lower correlation ( $R^2=0.5036$ ) was found between the L5/S1 joint reaction force and the stature (Figure 109).



**Figure 109: L5/S1 force function of stature**

# French Abstract

## 1. Intro

### 1.1 Contexte

Dans nos sociétés industrialisées où le secteur tertiaire prend une place de plus en plus importante, la population passe la plupart de son temps en position assise. Les nord-américains passent par exemple plus de 10 heures par jour en position assise en moyenne (Holmes et al. 2015), que ça soit dans une chaise, une voiture, dans un avion, pour le travail ou les activités de loisirs ou pour des causes de handicap et d'immobilité. Cette position assise peut entraîner sur le long terme des troubles musculo squelettiques (Vink & Hallbeck 2012), cela peut augmenter le risque de douleurs lombaires (Lis et al. 2006) et peut même mener à la formation d'escarres pour les personnes immobilisées dans un lit ou une chaise roulante (Olesen et al. 2010).

La diminution de l'inconfort du passager d'avion est une préoccupation majeure pour les compagnies aériennes car c'est un moyen d'attirer les passagers dans un secteur très concurrentiel. De grands progrès ont été réalisés ces dernières décennies, une étude réalisée en 2007 (Block, Vink, et Kamp, 2007) a montré que les nouveaux avions (A330 et Boeing 737 nouvelle génération) étaient décrits comme plus confortables par les passagers que les anciens (A300, A 310, Boeing 737-300 et 737-400). Cependant, des améliorations peuvent être faites notamment au niveau de la classe économique. Une étude récente réalisée par Air France a relevé que les passagers de la classe business donnaient une note moyenne de confort de 7/10 alors que ceux de première classe donnaient une note moyenne de 5/10. La question de l'évaluation de l'inconfort d'un siège dans sa phase de conception est donc une priorité aujourd'hui pour les constructeurs de siège comme Zodiac Seats France (ZSFR).

### 1.2 Confort/inconfort

Le confort et l'inconfort doivent être considérés comme deux entités séparées (Zhang et al. 1996; Helander et al. 1997), même si ceux-ci étaient considérés dans le passé comme deux niveaux sur une échelle continue (Richards L.C 1980). Selon Zhang et al. (1996), l'absence d'inconfort n'implique pas forcément la présence de confort ; de plus, l'inconfort est généralement relié à des facteurs biomécaniques alors que le confort est plutôt associé à un sentiment de bien-être et le ressenti sur les aspects esthétiques et la conformité avec les goûts personnels. Les personnes évaluent une situation comme confortable quand ils ressentent quelque chose d'inattendu comme un accueil plus que chaleureux, un environnement luxueux, un sentiment de grande sécurité, une très bonne qualité de

repas. Les définitions suivantes peuvent être formulées : « le sentiment de confort est vu comme un état de bien être ou de relaxation ressenti par une personne en interaction avec son environnement » alors que « le sentiment d'inconfort est vu comme un état de gêne d'un être humain en réaction à son environnement physique ». Dans cette thèse le confort sera exclu de l'étude étant donné qu'il est relié à des considérations esthétiques et de design. Le travail se concentrera sur l'inconfort généré par les interactions entre le corps et son environnement.

La fatigue est définie dans le dictionnaire Larousse comme un « Etat physiologique consécutif à un effort prolongé, à un travail physique ou intellectuel intense et se traduisant par une difficulté à continuer cet effort ou ce travail ». La fatigue peut être physique ou mentale et provient d'une situation sollicitant le corps pendant une certaine période. La fatigue est donc une situation apparaissant sur la durée. Nous faisons l'hypothèse que la fatigue est fortement liée à l'inconfort. Nous considérons qu'une situation impliquant de l'inconfort à un moment donné impliquera de la fatigue sur le long terme.

### 1.3 Objectifs

Cette étude se concentre sur l'interaction biomécanique entre le passager et le siège. Ce travail a été réalisé en collaboration avec Zodiac Seats France, un des plus gros fabricants de siège d'avion mondial. Cette entreprise est intéressée dans l'amélioration de l'ergonomie du siège afin de réduire l'inconfort qu'il peut induire. Le principal objectif de cette thèse est de développer un outil numérique permettant d'estimer l'inconfort lié au siège lors de sa phase de conception. Cet outil, basé sur des modèles biomécaniques du corps humain permet d'estimer l'impact du siège sur le passager en prédisant différents facteurs d'inconfort.

Pour réaliser cet objectif, les sous-objectifs suivants ont été réalisés :

- Réalisation d'un état de l'art des facteurs d'inconfort en position assise et des modèles développés pour l'évaluation de l'inconfort (Chapitre 1)
- Développement d'un modèle éléments finis (EF) du complexe bassin-cuisse pour la simulation de l'assise (Chapitre 2)
- Développement d'un modèle paramétrique permettant de représenter tout type de morphologie et validation de celui-ci par comparaison avec des données expérimentales de plusieurs sujets (Chapitre 3)
- Développement d'une méthode couplant la modélisation élément finis et multi corps (Chapitre 4)
- Etude des déformations internes : comparaison entre l'expérimental et des données IRM (Chapitre 5)

## 2. Chapitre 1 : Etat de l'art des facteurs d'inconfort et des modèles dédiés à l'évaluation de l'inconfort

Afin de développer un outil évaluant l'ergonomie d'un siège, il est nécessaire de connaître les facteurs impliqués dans les mécanismes menant à l'inconfort. Une revue de littérature sur les facteurs biomécaniques existants a été réalisée. Un état de l'art des modèles développés pour l'étude de l'impact du siège sur la personne a également été réalisé afin de déterminer les besoins existants.

## 2.1 Facteurs biomécanique menant à l'inconfort

D'après une revue de la littérature, plusieurs facteurs biomécaniques d'inconfort entrent en jeu lors de la position assise.

Tout d'abord la compression des tissus mous au niveau des fessiers entraîne une diminution du flux sanguin induisant ainsi un manque d'oxygénation des tissus (Olesen et al. 2010). Ces contraintes dans les tissus entraînant de l'inconfort sont causées par les forces de contact à la fois normales et tangentialles à l'interface entre le siège et le passager. Des critères de pression maximale (Ciaccia & Szniewar 2012), de répartition de pression (Hartung et al. 2004; Mergl et al. 2004) ont été proposés afin de diminuer l'inconfort. Aucun critère n'a été proposé concernant les forces tangentielles du fait de la difficulté de mesurer ces forces mais Zhang et al. (1996) et Goossens (2009) expliquent que celles-ci devaient être considérées de la même manière que les forces normales et devaient être ainsi minimisées.

Ensuite, de nombreuses études s'accordent à dire que l'activité musculaire maintenue sur une longue période était source d'inconfort (Andersson et al. 1977; Hosea 1986; Bush et al. 1995; Rasmussen et al. 2007; Grujicic et al. 2010; De Carvalho & Callaghan 2011) et que celle-ci devait donc être minimisée.

Enfin, la compression des disques intervertébraux lors d'une position statique entraîne un manque d'irrigation des nucleus et peut induire de l'inconfort. Des mesures expérimentales faites par Franz (2010) montrent qu'une répartition de pression idéale au niveau de l'interface avec l'assise implique une compression des disques minimale.

Tous ces facteurs mécaniques permettent d'estimer de manière objective l'inconfort. Ceux-ci peuvent être calculés par des modèles numériques afin d'estimer l'inconfort d'un siège sans avoir à réaliser d'expérimentation. Les modèles en éléments finis historiquement développés pour la sécurité automobile sont aujourd'hui de plus en plus utilisés pour des études de confort. Ceux-ci permettent de simuler les compressions internes et externes des tissus et donc de vérifier la conformité du siège aux critères de pressions et de forces de cisaillement. Les modèles musculo-squelettiques premièrement développés pour l'étude du mouvement commencent également à être utilisés pour des études d'inconfort car ils permettent de calculer les couples articulaires ainsi que les forces musculaires pour une position donnée.

## 2.2 Etat de l'art des modèles

Une revue de littérature a permis de répertorier 27 études ayant développé un modèle EF pour l'étude de l'impact du siège sur l'homme. La plupart des modèles répertoriés (15 sur 27) ont été développés dans le but d'améliorer le confort du siège, que ce soit dans le domaine automobile, aéronautique ou ferroviaire. Un grand nombre de ces études (12 sur 27) ont également été menées dans un but clinique pour étudier le phénomène d'apparition des escarres. Parmi tous ces modèles il existe une très grande variété de niveau de détail et de composition de ceux-ci. Ainsi, 10 modèles sont simplement des modèles plans représentant une tranche anatomique de quelques cm d'épaisseur. Ces modèles sont principalement dédiés à l'étude des déformations des tissus mous sous les ischions pour l'apparition d'escarres. Parmi les autres modèles développés en trois dimensions, 6 représentent le corps entier et 8 sont limités aux cuisses et fessiers. Parmi l'ensemble des modèles répertoriés, 14 contiennent tous les tissus mous rassemblés dans une seule couche, 4 dissocient la peau des autres

tissus et 11 différencient les tissus adipeux des muscles. Une très grande variété de propriétés matériaux est également utilisée pour modéliser les tissus mous. Les tissus mous sont modélisés dans certains cas par une loi simplement linéaire élastique et dans d'autres cas par une loi hyper élastique du 1<sup>er</sup> ordre ou du 2<sup>nd</sup> ordre. De plus parmi les modèles utilisant le même type de loi, différents paramètre matériaux sont utilisés pour caractériser les tissus, ces paramètres provenant souvent d'études expérimentales antérieures. Ensuite, la plupart des modèles représentent une seule morphologie (dans la plupart des cas le 50<sup>ème</sup> percentile), seulement 4 études développent 2 modèles ou plus permettant de représenter d'autres types d'anthropométrie en mettant à l'échelle un modèle de base. Enfin, très peu d'études décrivent un processus de validation. Sur les 13 études s'intéressant à la prédiction de pression de contact, seulement 6 études ont comparé la pression simulée à une pression mesurée. Parmi les 14 études se focalisant sur la prédiction des déformations, seulement 4 études ont comparé les déformations simulées et observées expérimentalement par IRM ou rayons X.

Très peu de modèles musculo-squelettiques ont été utilisés dans des recherches sur l'inconfort. Un modèle en deux dimensions réalisé par Hirao et al. (2006) contenant 13 segments rigides et 63 muscles a été utilisé afin d'étudier l'activité musculaire au niveau des lombaires pour deux positions d'assise. Kwang et al. (2009) a développé un modèle détaillé de la colonne vertébrale afin de simuler le comportement musculo-squelettique lors d'une interface personne-chaise roulante afin d'offrir des solutions d'amélioration du design. Ce modèle a été amélioré par Huynh et al. (2015) qui a affiné les segments vertébraux en ajoutant des ligaments et certains muscles lombaires et abdominaux. Ce modèle a été utilisé par Huang et al. (2012) dans l'étude de l'effet de la posture sur le corps.

Le modèle développé par Michael Damsgaard et John Rasmussen (Damsgaard et al. 2006) « SeatedHuman » a été utilisé dans plusieurs études sur l'inconfort d'assise. Ce modèle contenant plus de 500 muscles a été réalisé à partir de données anthropométriques provenant de plusieurs sources selon la partie anatomique (Nissan & Gilad (1986) pour la colonne, Klein Horsman et al. (2007) pour la jambe). Ce modèle a été développé dans son propre langage et est disponible dans un logiciel : « Anybody Modeling System » permettant la simulation de ce modèle. Les chercheurs ayant développé ce modèle ont étudié l'effet des inclinaisons du siège sur l'activité musculaire, les forces de cisaillement et les réactions articulaires (Rasmussen et al. (2007), (2008), (2009), (2011)). Grujicic et al. (2009) a étudié l'influence de quatre paramètres (inclinaison du dossier, coefficient de friction, position du siège et présence du support lombaire) sur la fatigue du conducteur avec ce modèle. Enfin, Li et al. (2015) a réalisé une étude dynamique sur l'effet de l'inclinaison et de la fréquence vibratoire sur l'activité musculaire.

Le modèle « Anybody » développé par Damsgaard et Rasmussen est celui ayant été le plus utilisé dans le domaine de l'étude de l'inconfort, de plus c'est le modèle le plus adapté à nos besoins, il sera donc utilisé dans cette étude.

Une grande variété de modèles EF a été répertoriée dans cet état de l'art. Cette variété de composition et de propriétés matériaux implique un besoin de réaliser une étude de sensibilité afin d'étudier l'influence de ces paramètres sur les sorties du modèle. De plus cet état de l'art a révélé que la plupart des modèles ne prenaient pas en compte les variations anthropométriques. Il y a donc un besoin de développer un modèle personnalisable capable de représenter tout type d'anthropométrie. Enfin, cette revue de littérature a révélé que très peu d'études ont validé leur modèle en le confrontant à des données expérimentales, et plus particulièrement celles s'intéressant aux déformations internes. Il y a donc un besoin de valider le modèle EF en le confrontant à des données expérimentales d'imagerie.

Enfin, les deux types de modèles fournissant chacun une partie des facteurs expliquant l'apparition de l'inconfort, il est nécessaire de les associer afin de couvrir l'ensemble des facteurs impliquant de l'inconfort lors de l'assise.

### 3. Chapitre 2 : Développement du modèle FE et analyse de sensibilité

Afin de réaliser une étude de sensibilité sur les paramètres de modélisation précédemment cité, un modèle EF a été réalisé à partir d'images IRM. Une étude de sensibilité a ensuite été réalisée en faisant varier les paramètres du modèle.

#### 3.1 Modèle développement

Un protocole expérimental a été réalisé afin d'obtenir des images IRM du bassin et des cuisses d'un homme moyen (22 ans, 1m74, 65 kg) avec un angle tronc-cuisse similaire à la position assise (130°). La plupart des modèles existants dans la littérature ne représentent que les fessiers et cuisses, voir uniquement les fessiers. La raison est que les compressions les plus importantes dans les tissus sont situées au niveau des fesses et en particulier sous les ischions. Il a donc été décidé de ne modéliser également que cette partie anatomique. De plus cela rend le modèle plus facilement personnalisable et positionnable qu'un modèle corps entier.

Les images IRM ont été segmentées à l'aide du logiciel 3d Slicer (version 4.4.0). Les os ont été segmentés en associant partie corticale et spongieuse. Le gras a été segmenté en y associant la peau. Tous les muscles situés entre le bassin et le fémur ont été segmentés (Figure 110).

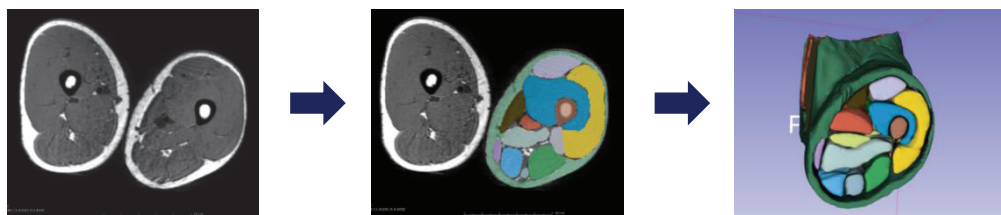


Figure 110: Segmentation des images IRM

Seulement une cuisse et la moitié du bassin ont été segmentées par hypothèse de symétrie.

Les surfaces obtenues ont été maillées à l'aide du logiciel Hypermesh. Une étude de convergence du maillage a été réalisée afin de déterminer la taille optimale du maillage. Pour cela des conditions de chargement génériques ont été appliquées au modèle. Le modèle a été chargé par gravité au-dessus d'une plaque rigide. Le poids de la partie supérieure du corps a été appliqué sur le bassin. Une simulation explicite a été lancée avec le solveur Radioss (développé par Altair). Les sorties du modèles analysées furent celles étant reliées à l'apparition de l'inconfort :

- Aire de contact à l'interface du siège
- Pression de contact moyenne
- Pression maximale
- Gradient maximal
- Contraintes internes maximales
- Déformations internes maximale

L'étude de convergence a montré que la taille de maillage optimale consistait en des éléments de taille 5 mm de côté.

### 3.2 Analyse de sensibilité

4 maillages avec plusieurs niveaux de détail ont été développés à partir des surfaces obtenues : os + tissus mous, os + tissus mous + peau, os + gras + muscles (un bloc) + peau, os + gras + muscles (différenciés) + peau.

Le niveau de détail affecte peu les sorties concernant la pression de contact (différence maximale de 28%). Par contre la différenciation des tissus mous implique d'importantes variations de contraintes dans les tissus (jusqu'à 186% de différence).

Si la différenciation des tissus mous affecte peu la pression de contact, il est intéressant d'étudier si la variation de proportion de muscle et gras affecte celle-ci. Différents maillages avec différentes proportion de gras ont été réalisés à partir du maillage de départ. Le pourcentage volumique de muscle varie de 36% à 58% conformément aux valeurs trouvées dans la littérature.

La proportion de muscle n'affecte pas l'aire de contact sur l'assise mais affecte de manière non négligeable la pression maximale. Celle-ci évolue de manière linéaire avec le volume de muscle. Plus le volume de muscle est important, plus la pression est répartie et moins le pic de pression est important. La pression maximale varie de 40 kPa à 15 kPa.

Afin d'étudier l'impact des propriétés matériau sur les sorties du modèles, l'effet des différentes lois utilisées dans la littérature a été étudié. Pour cela 3 modèles ont été développés avec chacun une loi différente comprenant les paramètres utilisés dans la littérature : une loi linéaire élastique, une loi hyper élastique d'ordre 1 (Neo Hookean) et une loi hyper élastique d'ordre 2 (Mooney Rivlin). La loi matériau a un impact non négligeable sur les sorties concernant la pression, la différence de pression maximale peut atteindre 57%. Cet impact est encore plus important concernant les contraintes internes, les contraintes peuvent être multipliées par 6 ou 8 suivant la loi matériau.

Cependant, l'impact de la loi peut être lié aux paramètres matériau utilisés. L'effet du module d'Young a été étudié avec le modèle élastique linéaire et il apparaît que la pression maximale est linéairement corrélée avec le module d'Young. Un coefficient de 0.5 a été trouvé, ainsi pour une augmentation du module d'Young de 20 kPa, la pression maximale augmente de 10 kPa. De même l'aire de contact peut passer de 450 cm<sup>2</sup> à 250 cm<sup>2</sup> pour une augmentation du module d'Young de 220 kPa.

Deux lois, linéaire élastique et hyper élastique de type Mooney Rivlin ont alors été testées avec des paramètres matériau équivalent. Les résultats sont quasi similaires concernant l'estimation de pression. Cela signifie qu'une loi linéaire élastique est suffisante pour estimer la pression. Cependant la loi linéaire élastique ne modélise pas correctement le comportement des tissus pour de grandes déformations. Ainsi lorsque des poids plus importants sont appliqués au modèle, les valeurs de contraintes divergent entre les deux modèles.

Pour conclure, le niveau de détail affecte peu l'estimation de pression à l'interface avec l'assise. La variation de l'aire de contact ou de la pression max n'excède pas 6% entre les modèles de différent niveau de détails. La proportion de muscle n'affecte pas l'aire de contact mais légèrement la pression maximum. Cela implique que la modélisation des différentes couches de tissus mous n'est pas nécessaire pour l'estimation de la pression. Cependant les propriétés matériau affectent de manière

importante la pression. Les variations entre les différents modèles peuvent dépasser les 100%. Cet effet est principalement lié aux paramètres de la loi. Par exemple, une loi élastique donne les mêmes résultats qu'une loi hyper élastique avec des paramètres équivalents. Un modèle optimal pour estimer la pression de contact peut donc être défini comme un modèle avec des tissus mous non différenciés et une loi élastique avec le module adéquat. Ce type de modèle sera utilisé par la suite. Cependant, si le modèle est dédié à l'étude des contraintes internes, une loi élastique linéaire n'est pas suffisante. Une loi hyper élastique doit être utilisée avec des paramètres choisis avec précautions étant donné leur impact sur les contraintes.

## 4. Chapitre 3 : Un modèle paramétrique du complexe fessiers-cuisse basé sur des données scan 3d : développement et validation

L'état de l'art a révélé que peu de modèles prenaient en compte la variation d'anthropométrie. Or l'anthropométrie a un impact très important sur la pression d'assise (Kyung & Nussbaum 2008). Un grand nombre d'études ont révélé les relations entre les paramètres anthropométriques (taille, poids, age, genre, IMC...) et les variables de pression (Hiemstra-van Mastrigt et al. 2017). Il est donc nécessaire d'avoir un modèle capable de prendre en compte ces paramètres anthropométriques. Un modèle paramétrique de l'ensemble cuisse-fessiers contenant les surfaces osseuses et externes (peau) a été développé. La surface des os et de la peau peut être prédite à partir de paramètres anthropométriques tel que l'IMC, la taille, le genre et la posture. Ce modèle paramétrique de surface a ensuite été utilisé pour développer un modèle EF paramétrique permettant de simuler l'interaction homme-siège pour tout type d'anthropométrie.

### 4.1 Un modèle paramétrique de l'enveloppe

Un modèle paramétrique de surface contenant la surface externe et les points osseux du bassin et des fémurs a été développé à partir de données expérimentales.

Un protocole expérimental a été réalisé sur 36 sujets pour recueillir les surfaces externes et les points osseux. La surface externe a été scannée grâce à un laser à main (Nikon, Tokyo, Japon). La personne était positionnée sur un dispositif spécial permettant d'avoir un angle au niveau du bassin correspondant à la position assise. Les points osseux ont été obtenus à l'aide d'un dispositif de palpation comprenant des marqueurs réfléchissants dont la position était enregistrée à l'aide d'un système de capture du mouvement Vicon. Les surfaces ont été post traitées de manière à obtenir des surfaces segmentées, symétrisées et ordonnées avec le même maillage. Les points osseux ont été associés aux surfaces à l'aide d'un repère commun.

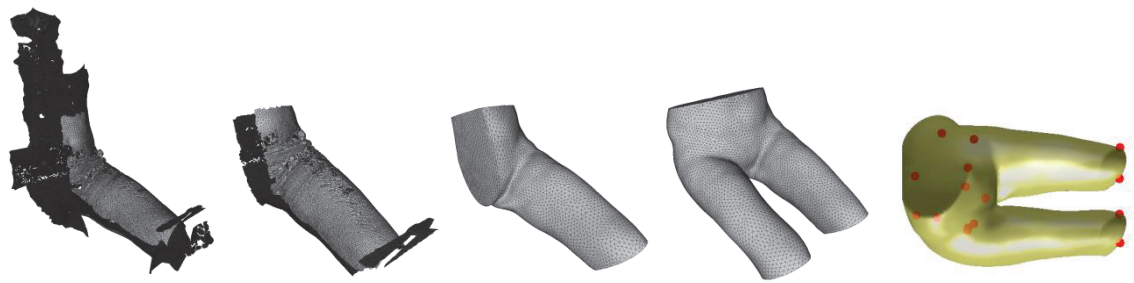


**Figure 111: Traitement des surfaces.** De gauche à droite: surface brute, surface brute après segmentation, déformation du maillage template sur le scan, symétrisation, association des points osseux

Une analyse en composante principale a alors été réalisée sur les données ordonnées. Elle a permis d'exprimer les données dans une base orthogonale où chaque direction (composante principale) représente la plus grande variation. Pour chaque composante principale, une régression multi variée a été utilisée pour prédire comment le score de la composante principale associé varie en fonction des paramètres anthropométriques et de posture (IMC, taille, genre, angles). La surface externe et les points osseux ont pu être alors prédits à partir de ces paramètres.



**Figure 112: Influence de l'IMC , de l'angle du fémur et de la taille.** Les prédictions pour la moyenne (rouge), la moyenne + 2 std (bleu) et la moyenne - 2 std (vert) sont comparé pour chaque prédicteur

Une procédure de « leave-one-out » a alors été effectuée pour évaluer la précision de la prédiction des surfaces et des points osseux. La régression sur l'analyse en composante principale a été effectuée à partir de  $n-1$  sujet, la surface externe et les points osseux des  $n$  extra sujets ont été prédits en utilisant cette régression. Cette procédure a été répétée de manière itérative jusqu'à ce que chaque sujet ait été considéré comme un extra sujet.

Une erreur moyenne de prédiction de la surface externe de  $26.6 \pm 9.3$  mm a été trouvée. Cette erreur est un peu supérieure aux modèles paramétriques développés précédemment. Par exemple Kim et al. (2016) a calculé une erreur entre  $11.98 \pm 6.59$  mm and  $12.90 \pm 6.88$  mm en fonction de la position pour leur modèle paramétrique de l'épaule. Bd et al. (2017) a trouvé une erreur quadratique moyenne de  $9.5 \pm 2.2$  mm pour leur modèle paramétrique de l'enfant et une erreur de  $17.35 \pm 3.43$  mm pour la prédiction du 95<sup>ème</sup> percentile.

Une procédure de « leave-one-out » a également été réalisée pour la prédiction des points osseux. Une erreur moyenne de  $21.7 \pm 6.2$  mm a été trouvée pour la prédiction des points osseux sur les 36 sujets. Cette erreur est légèrement supérieure à celle trouvée par Nerot et al. (2016) qui a prédit les point osseux de la colonne à partir de la surface externe et a trouvé une erreur résiduelle de 12.5 mm

ou 14.7 mm en fonction de la méthode. Des distances invariantes prédictes ont également été comparés à ces distances mesurées. Par exemple, une erreur moyenne de la prédiction de la largeur du bassin de  $19.2 \pm 17.2$  mm a été trouvée. Cette prédiction est meilleure que celle trouvée par Reed et al. (2009) qui a trouvé une erreur de 27 mm pour la prédiction de la largeur du bassin d'un enfant de 6 ans.

La limitation principale de cette étude est le nombre limité de sujet. Un échantillon plus important permettrait de développer un modèle spécifique pour chaque genre. En effet, la variation de forme diffère selon le genre. Notre modèle contient des données des deux genres mélangées. Néanmoins, grâce à la variabilité importante entre les sujets, des régressions avec de fortes corrélations entre les composantes principales et les paramètres anthropométriques ont été trouvées, permettant de représenter de manière précise la variation anthropométrique.

## 4.2 Prédiction de la surface des os

Un modèle paramétrique permettant de prédire la peau et les repères osseux a été développé. Cependant, pour développer un modèle EF du complexe cuisse-fessiers, les surfaces osseuses sont nécessaires. La surface osseuse d'un maillage template doit donc être déformée pour correspondre aux repères osseux prédicts. Deux méthodes ont été testées pour ajuster la surface osseuse aux repères osseux. Une méthode de krigeage permettant de déformer par interpolation une surface à partir de points de contrôle a été réalisée. Les points de contrôle de ce krigeage ont été les repères osseux. Une méthode se basant sur un modèle en composante principale développé dans une étude antérieure à partir de données de scan d'os cadavériques a été également réalisée. Le modèle en composante principale permet de prédire la surface osseuse à partir des repères osseux.

A partir d'une procédure de « leave-one-out », cette dernière méthode a pu être évaluée. Une erreur moyenne de  $5.7 \pm 1.6$  mm a été trouvée. Le même échantillon de données a été utilisé pour évaluer la méthode de krigeage. Une erreur moyenne de  $12.53 \pm 3.22$  mm a été trouvée avec le krigeage. La méthode basée sur le modèle en composante principale a donc été plus précise.

La validité de la prédiction à parti des repères osseux a été réalisée mais la prédiction de la surface à partir des paramètres anthropométriques n'a pas pu être effectuée en raison de l'absence de données concernant la géométrie osseuse des sujets.

## 4.3 Modèle EF paramétrique

A partir de la prédiction des surfaces osseuses et externes, un maillage volumique doit être développé afin d'avoir un modèle EF permettant de simuler l'interaction de la personne avec le siège. Pour cela un maillage volumique template est déformé par krigeage vers les deux surfaces (interne et externe) prédictes. Le template correspond au modèle optimal décrit précédemment.

Les modèles correspondant à 13 personnes ont été développés à partir de leurs données anthropométriques. Une étude expérimentale permettant d'enregistrer les forces de contact ainsi que les positions de la personne en position assise a été réalisée. Une configuration correspondant à un

siège d'avion Z301 a été réalisée avec chacun de ces sujets. La pression de contact au niveau de l'assise constituée d'une mousse correspondant au siège a été enregistrée à l'aide d'une nappe de pression.

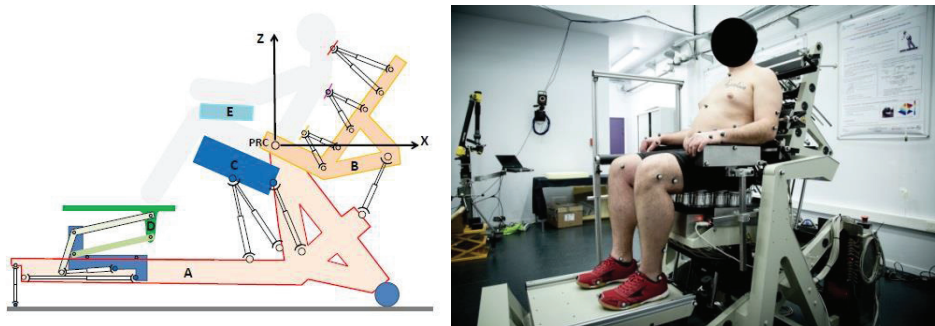


Figure 113: Siège expérimental permettant de reproduire la configuration et de mesurer les forces de contact

Des simulations correspondant à cette configuration pour chacun de ces sujets ont été réalisées avec le modèle correspondant. Le modèle a été positionné à l'aide de la position enregistrée par capture du mouvement. La force d'assise enregistrée a été appliquée au modèle.

Les pressions ainsi simulées ont été comparées avec les pressions mesurées. Si les valeurs absolues montrent des erreurs importantes (au maximum : 62% pour la pression moyenne, 33% pour la pression maximale, 37% pour l'aire de contact, 58% pour le gradient max), les résultats montrent une bonne capacité du modèle à simuler l'influence des paramètres anthropométriques. Les relations entre l'anthropométrie (taille et IMC) et les valeurs de pression de contact (pression moyenne, pression maximale, aire de contact et gradient maximal) étaient similaires entre les résultats de simulation et expérimentaux. L'aire de contact a été sous-estimée, ce qui entraîne une sur-estimation de la pression moyenne. Ces erreurs sont probablement liées à deux facteurs. Le premier est probablement lié aux propriétés matériaux qui devaient être trop rigides. Le module élastique choisi n'était sûrement pas approprié et devrait être spécifique au sujet. Pour obtenir une meilleure estimation des valeurs de pression, une étude paramétrique pourrait être réalisée sur les paramètres matériaux des 13 sujets. La seconde erreur proviendrait d'une erreur de positionnement du modèle. Le modèle a été positionné à partir de la position des marqueurs. Les artefacts liés aux mouvements des tissus mous peuvent être importants, en particulier pour les sujets avec un IMC important. La position estimée pourrait donc être loin de la position réelle.

Néanmoins, l'objectif de ce modèle paramétrique n'était pas de simuler un cas spécifique avec un sujet spécifique mais de pouvoir simuler un large spectre de configurations et d'anthropométrie.

## 5. Chapitre 4 : Couplage modèle multi-corps et modèle EF

Le modèle EF paramétrique développé a besoin de conditions aux limites pour être positionné et chargé. Le but de cette thèse étant de développer un outil numérique permettant de simuler un cas virtuel, il doit être possible d'utiliser cet outil sans aucune donnée expérimentale. Une méthode a été développée afin de prédire les conditions aux limites à appliquer au modèle EF pour éviter le recours aux données expérimentales. Cette méthode utilise un couplage entre un modèle multi-corps et le

modèle EF. Cette méthode associant deux approches de modélisation a deux avantages : 1/ de fournir des conditions aux limites réaliste au modèle EF et 2/ de prédire la totalité des facteurs mécanique liés à l'inconfort. Comme expliqué précédemment, les simulations EF permettent de prédire la pression de contact ou les déformations des tissus alors que les simulations multi-corps permettent de calculer l'activité musculaire et les pressions inter discales.

## 5.1 Méthode de couplage

Afin d'associer les deux modèles, le modèle multi-corps (MC) doit être mis à l'échelle du modèle EF pour lui correspondre. Pour cela le bassin est transformé à l'aide d'une fonction intégrée au logiciel Anybody : la fonction RBF (Radial Basis Function) qui met à l'échelle le bassin afin de faire correspondre certains repères osseux (points prédis positionnés précédemment) aux dimensions voulues. Le fémur est transformé à l'aide d'une homothétie pour correspondre à la longueur voulue. Les autres segments sont transformés par homothétie pour correspondre aux différentes mesures anthropométriques prises sur le sujet. Le modèle MC est ensuite positionné dans le siège à l'aide de contraintes géométriques définies à des points de contact entre la personne et le siège. Une cinématique inverse, puis une dynamique inverse et une optimisation des efforts musculaires permet ensuite d'estimer les efforts dans les articulations. Le modèle EF est alors positionné pour correspondre à la position du modèle MC. Les forces et moments estimés par Anybody au niveau de L5/S1 et de l'articulation du genou sont alors appliqués au modèle EF. Une simulation EF est lancée avec le solveur EF RADIOSS. A la fin de la simulation, la nouvelle position des os est extraite et utilisée pour repositionner le modèle MC. Une nouvelle dynamique inverse est lancée avec le modèle MC. La boucle est ainsi répétée jusqu'à ce que les positions du bassin et fémur convergent (Figure 114).

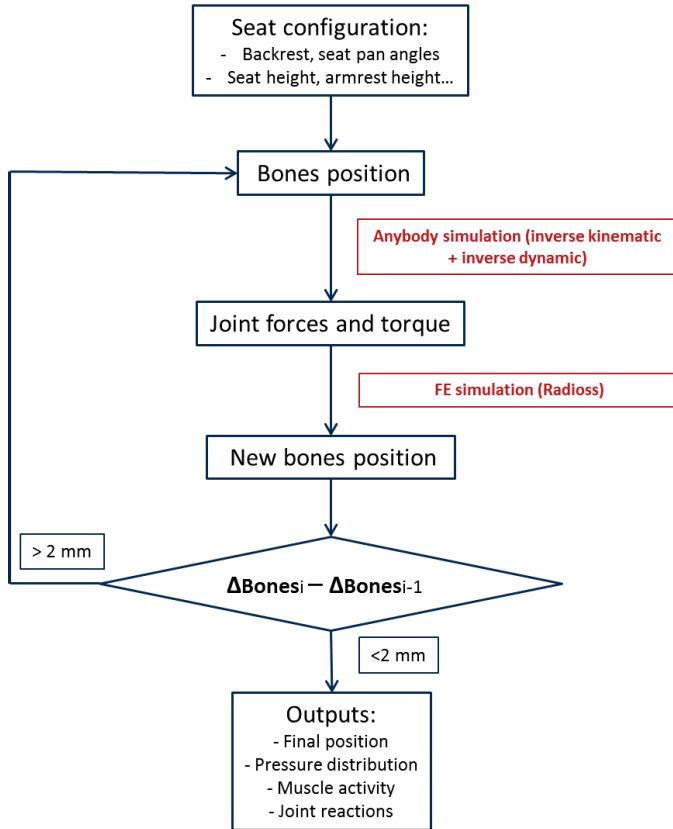


Figure 114: Processus de couplage

## 5.2 Validation

L’expérimentation décrite précédemment a été simulé avec 6 personnes choisis parmi les 13 précédentes. Le premier objectif était d’évaluer la capacité de la méthode de couplage à bien estimer la distribution de pression. Les pressions simulées et mesurées ont été comparées. Le deuxième objectif était d’étudier la capacité du couplage à corriger la position des os. L’hypothèse a été faite que le couplage corrigerait la position estimée à partir des marqueurs, en particulier la position des genoux. La position estimée par le couplage diffère de celle mesurée expérimentalement pour deux raisons : la position estimée à partir des contraintes géométriques dans Anybody diffère par rapport à l’expérimentale et le couplage modifie ensuite la position. Trois différentes simulations ont donc dû être effectuées pour chaque sujet :

- Méthode avec couplage : Simulation sans données expérimentales avec coulage
- Méthode sans couplage : simulation avec les conditions aux limites définies par l’initiale position estimée par Anybody
- Méthode expérimentale : simulations avec conditions aux limites définies à partir des données expérimentales

Toutes les simulations avec couplage ont convergées avant 10 itérations.

En comparant les pressions simulées avec le couplage et celle simulées avec les données expérimentales, il apparait que le couplage améliore la prédition de la pression. L’erreur moyenne de la pression moyenne sur les 6 personnes était de  $8.8 \pm 9.9\%$  avec la méthode de couplage alors qu’elle

était de  $46 \pm 24\%$  avec les données expérimentales. Cette différence est due à un grand écart de positionnement des os entre les deux méthodes. La différence d'angle bassin-cuisse peut atteindre  $70^\circ$  entre les deux méthodes. Etant donné que la méthode de couplage estime mieux la pression, on peut supposer que le couplage améliore la prédition de posture par rapport à l'expérimental. Quand on compare les résultats de la méthode de couplage avec la méthode sans couplage mais avec la même position initiale, la différence est moins importante (différence angle bassin-cuisse de maximum  $10.5^\circ$ ). Cependant il apparaît que le couplage améliore la prédition de la pression. L'erreur moyenne de pression moyenne sur les 6 sujets était de  $37.9 \pm 29\%$  sans le couplage et de  $8.8 \pm 9.9\%$  avec le couplage. Ainsi on peut dire que le couplage améliore globalement la posture et la prédition de pression. Cela peut se vérifier qualitativement sur la distribution de pression sur la Figure 115.

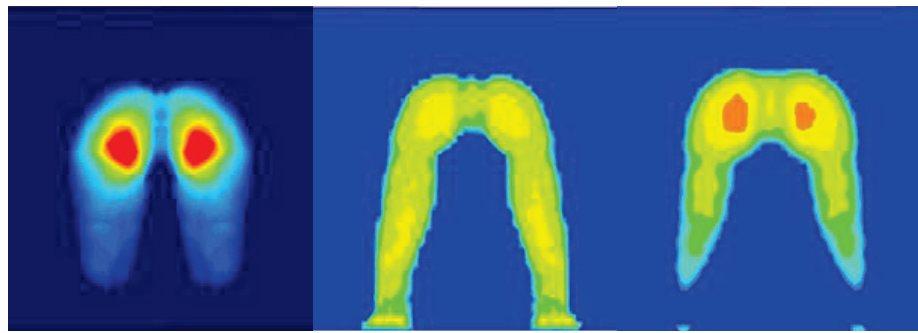


**Figure 115: Exemple de distribution de pression ( de gauche à droite: mesurée expérimentalement, simulée sans couplage, simulée avec couplage)**

Si cette méthode de simulation avec couplage semble corriger la position des os, un certain nombre d'incertitudes persistent. Tout d'abord, la position initiale a été estimée grâce à une cinématique inverse qui dépend de lois de couplage pour les angles articulaires comme le « spine rythm » pour les angles des vertèbres et le rythme thorax-bassin-pelvis-cuisse pour la position du pelvis. Ces lois de couplage n'ont pas été validées mais ont une forte influence sur la position. Deuxièmement, les conditions aux limites appliquées au modèle EF (forces et moments articulaires) dépendent de la dynamique inverse et de l'estimation des forces musculaires qui dépend du critère d'optimisation. Le choix de ce critère et son influence sur les résultats n'a pas été étudié. De plus, les forces articulaires dépendent aussi de l'estimation des forces de contact qui dépendent de la formulation de ces forces. L'influence des points de contact, de leur nombre et de leur disposition n'a pas été étudiée. Une étude de sensibilité des résultats à tous ces paramètres devrait être conduite dans le futur.

## 6. Chapitre 5 : Comparaison des déformations internes simulées

### avec des données IRM

Les sorties du modèles étudiées jusqu'ici étaient principalement les valeurs de pression or nous avons vu que celles-ci n'étaient pas forcément corrélées au chargement des tissus sous-cutanés (Oomens et al. 2003). Les déformations des tissus internes sont la source première de l'inconfort à cause de la compression des vaisseaux sanguins et des nerfs (Reed et al. 1994). Nous savons qu'à

partir de certaines valeurs de contraintes, le flux sanguin est limité (Chow & Odell 1978). Plusieurs études ont également relié les déformations à la nécrose des cellules dans les muscles (Breuls et al. 2003; Gefen et al. 2008). Pour mieux comprendre l'impact du siège sur le corps et les phénomènes menant à l'inconfort, il est important d'étudier ces déformations internes. Les modèles EF permettent de simuler ces déformations, cependant la capacité du modèle à estimer ces déformations doit être validée en confrontant les résultats à des observations expérimentales. Parmi tous les modèles développés pour l'étude de ces déformations, très peu on décrit un processus de validation de ces déformations. Dans la première (Todd & Thacker 1994), les déformations ont été étudiées dans un seul plan et dans une position couchée. Dans la deuxième (Makhsous et al. 2007), le chargement appliqué était éloigné du chargement d'assise. Enfin dans la dernière étude ayant comparé les déformations simulées et observées (Al-Dirini et al. 2016), le chargement d'assise n'était pas connu et seulement une configuration a été étudiée.

L'impact de l'assise en termes de déformation a donc été étudié dans plusieurs configurations à l'aide d'images IRM et comparés aux simulations EF.

## 6.1 Collecte de données IRM

Un IRM ouvert situé à Manchester (Paramed, Genova, Italy) a été utilisé pour recueillir les données d'un sujet male d'1m64 et de 68 kg. L'IRM ouvert a permis d'effectuer des acquisitions en position assise. 4 configurations ont été effectuées :

- Une position sans chargement afin de développer le modèle avec les tissus mous en position non chargée
- Une position de référence correspondant à un siège d'avion avec support d'assise rigide
- Une position correspondant à la position de référence mais avec une mousse positionnée sur le support d'assise
- Une position impliquant plus de forces de cisaillement en inclinant l'assise

## 6.2 Développement du modèle EF

Un nouveau modèle EF a été développé à partir de la segmentation des images de la configuration initiale sans chargement. Deux maillages ont été développés : un maillage homogène avec tous les tissus mous assemblés en un seul composant et un modèle détaillé séparant les muscles des tissus adipeux.

## 6.3 Simulations

Les différentes configurations effectuées dans l'IRM ont été simulées avec les deux modèles. Pour cela les os ont été positionnés conformément à leur position dans l'IRM, l'angle bassin cuisse a été modifié par simulation et le bassin a été ré orienté pour que sa position par rapport au plan d'assise soit conforme. La force de contact n'étant pas mesurable dans l'IRM, l'expérience a été reproduite en laboratoire sur un siège expérimental afin de pouvoir mesurer la force sous l'assise. L'inter variabilité de la force globale sous l'assise pour une même configuration étant faible, il peut être considéré que la

force mesurée en laboratoire était conforme à celle de l'IRM. Pour simuler les configurations, cette force d'assise a été appliquée au modèle.

## 6.4 Résultats

Différents plans ont été définis afin d'évaluer les déformations. Un plan ayant la normale dans le plan de symétrie du bassin et parallèle au plan d'assise et dont l'origine est située au niveau de l'ischion a été défini. Deux autres plans parallèles à celui-ci mais décalés vers l'arrière du bassin ont également été définis. Les différentes épaisseurs de tissus ont alors été mesurées dans ces plans.

Les surfaces des différentes couches de tissus ayant été segmentées dans les différentes configurations, il a été possible de calculer la différence entre la surface simulée et la surface segmentée utilisant la distance de Hausdorff du logiciel Meshlab.

Les déformations mesurées sont élevées (jusqu'à 82.1%), notamment lors de la configuration rigide. Les déformations sont plus importantes dans les tissus adipeux (maximum de 82.1%) que dans les muscles (maximum de 49.1%). Les déformations les plus importantes se situent sous l'ischion. La mousse réduit légèrement les déformations, notamment au niveau de l'ischion, mais les augmentent sur les bords extérieurs des fessiers. La mousse implique une réduction des déformations dans le gras et une augmentation dans les muscles.

Les déformations observées ont été comparées aux simulations des deux modèles. Pour le modèle détaillé, dans la plupart des plans d'observation, l'erreur de prédiction de déformation de la surface externe ne dépasse pas 25%. Par contre, de grandes disparités ont été observées sur la prédiction de la déformation du muscle. Ainsi selon la location, l'erreur peut varier de 3.9% à 1112%. L'erreur la plus importante était localisée sous les ischions dans les deux configurations. Cependant en regardant de manière globale, l'erreur sous le sacrum était bien plus importante que sous les ischions. Il a été observé que l'erreur était moins importante dans la configuration d'assise rigide que dans la configuration avec mousse. La distance moyenne entre la surface externe simulée et segmentée sur les images était de 4.7 mm pour l'assise rigide et 5.3 mm pour l'assise en mousse. Pour le modèle homogène les erreurs de déformations ont été très faibles pour la configuration rigide (entre 0 et 3.8%). L'erreur était légèrement plus importante avec la mousse mais toujours en dessous de 20%. La distance moyenne entre la surface externe segmentée et simulée était plus faible pour la configuration rigide (4.3 mm) que pour la configuration mousse (5.6mm) (Figure 116). Ces erreurs étaient dans le même ordre de grandeur qu'avec le modèle détaillé.

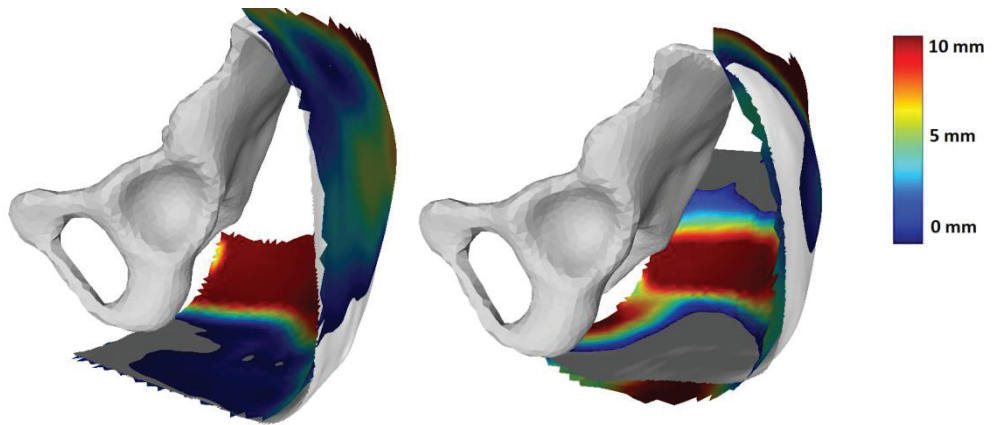


**Figure 116: Distance entre la peau segmentée et simulée pour la configuration rigide et mousse avec le modèle homogène**

Les valeurs de déformations observées sur l'assise rigide sont dans l'ordre de grandeur des valeurs décrites dans la littérature. Al-Dirini et al. (2015) a mesuré des déformations moyennes sur 6 sujets de 38.1 % dans le muscle et de 11.8% dans le gras au niveau de l'ischion. Linder-Ganz et al. (2007b) a également mesuré les déformations sur 6 personnes assises sur un plan rigide et trouvé des déformations dans le muscle comprises entre 36 et 55%. Ces valeurs sont supérieures au seuil à partir duquel la nécrose des cellules apparaît. Selon Gefen et al. (2008) ou Gawlitza et al. (2007), les cellules ne peuvent tolérer 50% de déformations sur une période d'une heure seulement.

Le modèle a montré une bonne capacité à simuler les déformations globales des tissus mous dans les deux configurations. Le modèle homogène a montré une bonne estimation des déformations des tissus mous, erreurs inférieures à 20%. La distance moyenne entre la surface simulée et segmentée était de 4.3 mm et 5.6 mm pour respectivement les configurations rigide et mousse. Ces erreurs sont inférieures à celle calculée par Makhsoos et al. (2007) qui a trouvé une erreur moyenne sur la position de 30 points de repères de 6.2 mm. Cela veut dire que les propriétés matériau définies à partir de la littérature pour les tissus mous homogènes peuvent être considérés comme valides pour simuler les déformations des tissus mous dans ce type de configuration, au moins pour ce type de morphologie. Le modèle détaillé a révélé des erreurs légèrement plus importantes, en particulier pour les déformations internes. Néanmoins le modèle estime bien les déformations globales dans la configuration rigide (erreur en dessous de 13%) et l'erreur moyenne entre les surfaces simulées et segmentées du muscle ou de la peau était comprise entre 4.5 mm et 5.7 mm. Ces résultats sont dans le même ordre de grandeur que ceux trouvés par Al-Dirini et al. (2016) qui a mesuré une erreur moyenne de 4.7 mm. Ces résultats signifient que les paramètres matériau pour le gras et les muscles peuvent être considérés comme valides pour ce type de configuration et que la prédiction des déformations internes par le modèle est validée.

La principale limitation de cette étude a été le fait que les forces de contact n'ont pas pu être mesurées dans l'IRM mais sur une configuration répliquée dans le laboratoire. Si la force d'assise globale ne varie pas énormément entre deux configurations identiques (maximum de 6% pour la force normale et 17% pour les forces de cisaillement), l'erreur entre la force mesurée dans le laboratoire et la force réelle dans l'IRM pourrait avoir un impact sur les résultats de la simulation.

Enfin, seulement un sujet a été étudié. La morphologie et la proportion de muscle et gras dans le corps a un impact important sur les déformations des tissus (Al-Dirini et al. 2015). L'influence de ces paramètres anatomiques devrait être étudiée.

Des travaux futurs pourraient se concentrer sur l'étude de l'impact de la morphologie en répliquant la même méthodologie avec différents sujet ayant différents niveau d'IMC et de pourcentage de gras. L'impact des caractéristiques de la mousse pourrait aussi être étudié. Enfin, des travaux pourraient être conduits sur l'impact des forces de cisaillement en trouvant un moyen efficace de mesurer les cisaillements dans l'IRM.

## 7. Conclusion

Cette thèse avait pour objectif de développer un outil numérique permettant d'évaluer l'inconfort induit par un siège d'avion. L'outil développé comprend une modèle EF paramétrique qui permet d'obtenir la géométrie à partir de paramètres anthropométriques telles que la taille, l'IMC, le genre ainsi que des paramètres posturaux tels que les angles articulaires. Ainsi tout type d'anthropométrie peut être simulé. Une méthode de couplage avec un modèle MC existant a été développés afin d'avoir un outil de simulation n'ayant besoin d'aucune données expérimentales. Cet outil peut ainsi simuler tout type de configuration assise où le modèle de siège est disponible. Les sorties de la simulation sont : la pression à l'interface de l'assise avec toutes les valeurs qui lui sont associées (pression maximale, pression moyenne, gradients...), les forces de cisaillement, les déformations internes, les contraintes internes, les efforts musculaires dans le corps entier, les efforts articulaires dans les disques intervertébraux. Les critères existants peuvent être ensuite utilisés pour apprécier la qualité ergonomique du siège en fonction des valeurs de ces sorties.

### 7.1 Principaux résultats

Une étude de sensibilité sur la composition du modèle et les paramètres matériaux a permis de mettre en évidence les points suivants :

- Pour l'estimation de la pression à l'interface de l'assise :
  - o la distinction des différents tissus mous n'est pas nécessaire
  - o Une loi élastique linéaire est suffisante
  - o Les paramètres matériaux ont un impact non négligeable
- Pour l'estimation des déformations internes :
  - o La distinction des tissus mous est nécessaire
  - o Une loi hyper élastique est nécessaire
  - o Les paramètres matériaux ont un impact non négligeable

Le développement du modèle EF paramétrique a permis de montrer que :

- Des paramètres anthropométriques globaux tels que la taille et l'IMC permettent de prédire de manière précise la surface externe ainsi que les points osseux avec le modèle développé

- Les résultats ne sont pas meilleurs avec des paramètres locaux

La simulation sujet-spécifique de configuration expérimentale donne les résultats suivants :

- Le modèle EF paramétrique permet de bien simuler l'effet de l'IMC ou de la taille sur les valeurs de pression
- Des écarts constants importants sont observés entre l'expérimental et la simulation. Ces écarts sont probablement dû à une erreur de positionnement à cause de la mauvaise fiabilité des marqueurs

La méthode de couplage développé a permis de montrer que :

- Il est possible d'associer un modèle MC à un modèle EF afin d'apporter les conditions aux limites au modèle EF et ainsi simuler une configuration sans aucune donnée expérimentale
- Les résultats (pression) prédits par ce couplage sont conforme à l'expérimental et plus précis qu'avec une méthode utilisant les données expérimentales
- La position prédite par Anybody à partir de contraintes géométrique semble correcte (meilleur que celle donnée par les marqueurs)
- Le couplage permet d'améliorer la prédition de la posture, en particulier au niveau des genoux
- La position des os a un fort impact sur la prédition de la pression

L'étude des déformations sous IRM a mis en évidence les points suivants :

- Les valeurs de déformations sur une assise rigide dépassent les seuils de nécrose des cellules